

**MECHANICAL PROPERTIES
OF GRANULAR AGRO-MATERIALS
AND FOOD POWDERS FOR INDUSTRIAL PRACTICE**

Part I
**Characterization of mechanical properties
of particulate solids for storage and handling**

Marek Molenda, Józef Horabik

Edited by
Józef Horabik, Janusz Laskowski



Centre of Excellence for Applied Physics in Sustainable
Agriculture AGROPHYSICS



Institute of Agrophysics Polish Academy of Sciences



Agricultural University of Lublin



EU 5th Framework Program QLAM-2001-00428



EC Centre of Excellence AGROPHYSICS
Centre of Excellence for Applied Physics
in Sustainable Agriculture
QLAM-2001-00428

Reviewed by: Prof. Jarosław Frączek

ISBN 83-89969-35-1

© Institute of Agrophysics PAS, Lublin 2005

Edition: 180 copies

Project of cover: Wanda Woźniak
Computer edition: Joanna Sykut

Printed by: Alf-Graf, ul. Kościuszki 4, 20-006 Lublin, Poland

CONTENT

PREFACE	5
BASIC NOTATION	6
1. INTRODUCTION	7
2. CONTINUUM MECHANICS APPROACH	9
2.1. The plastic flow rule	9
2.2. Plastic model with hardening and softening	10
2.3. Elastic-plastic models of Ghaboussi and Momen and of Lade	14
3. MICROSTRUCTURAL APPROACH. DEM MODELLING	17
3.1. Geometric structure of granular medium	17
3.2. Anisotropy of seed layer	20
3.3. Microstructural models	28
3.4. Distinct Element Method	30
3.5. Model of micropolar continuum	34
3.6. Localization of shear deformation	36
4. CLASSIFICATION OF GRANULAR MATERIALS	38
5. DENSITY OF GRANULAR MATERIALS	40
5.1. Bulk density	40
5.2. Density of consolidated material	42
6. COMPRESSIBILITY AND ELASTICITY	43
7. STRENGTH PARAMETERS	50
7.1 Methods and apparatus	50
7.1.1. Direct shear test	50
7.1.2. Triaxial compression test	53
7.2 Factors influencing angle of internal friction of cereals	55
7.2.1. Moisture content of the material	55
7.2.2. Bulk density	56
7.2.3. Time of consolidation	57
7.2.4. Method of sample deposition. Anisotropy of packing	57
7.2.5. Surface properties of particles	59
7.2.6. Formation of shear bands	59
7.2.7. Correction of change in sample cross-section area	62
8. FLOW FUNCTION	63
9. COEFFICIENT OF FRICTION	65
9.1. Theories of dry friction	65
9.2. Experimental methods	67

9.3. Factors influencing the coefficient of friction	70
9.3.1. Moisture content	70
9.3.2. Surface roughness	71
9.3.3. Normal pressure	73
9.3.4. Velocity of sliding	74
9.3.5. Wear in	74
9.3.6. Frictional vibrations, slip-stick effect	74
10. PRESSURE RATIO	75
10.1. Yielding at the silo center	75
10.2. Yielding at the silo wall	76
10.3. Experimental procedures	78
10.4. Factors influencing the pressure ratio	79
10.4.1. Friction force mobilization	80
10.4.2. Packing structure	81
10.4.3. Moisture content	82
10.4.4. Grain shape and surface roughness	82
10.5. Concluding remarks	83
11. AIRFLOW RESISTANCE	84
11.1. Effects of density, moisture and packing	84
11.2. Laboratory testing	86
11.3. Ergun's equation	87
12. FLOW RATE THROUGH ORIFICES	88
13. INDICES OF STRENGTH AND FLOWABILITY USED BY PROCESS TECHNOLOGY	89
13.1. Quality determination	90
13.1.1. Peschl rotational split level shear tester	91
13.1.2. Johanson's apparatus and indices	92
13.1.3. Jenike & Johanson powder quality tester	96
13.1.4. Uniaxial tester of POSTEC	97
13.2. Carr Indices	98
13.3. In-line control of structure of granular products	99
13.4. Tendencies in development of applications	101
14. REFERENCES	103
15. SUMMARY	111
16. APPENDIX – Physical Properties of Grain and Food Powders	112

PREFACE

In recent decades granular materials have gained great interest of both industrial specialists and researchers. Growing competition on the global market, combined with an increase in the scale of operations, enforced producers to use raw materials and final products in granular form that is relatively easy for storage, handling and processing. On the other hand, after fairly complete description of solid, liquid and gaseous states of matter, scientists turned their attention to granular materials. With their unique behaviour, some researchers postulate to consider this group of materials as a separate state of matter. Research and technology developments made from the sixties of the twentieth century resulted in a substantial progress in science and technology in the field.

This work deals with some aspects of the mechanics of granular materials. It is focused on the materials of biological origin used in agro and food technology. The main features of agro and food materials that make them different from mineral materials are strong influence of moisture content on mechanical behaviour and high deformability of granules. These differences bring about certain peculiar behaviours and necessity of adjustments of models of material, experimental techniques and technological solutions.

While presenting this book, our purpose was to focus attention of the reader on what we believe is important for understanding of the mechanical behaviour of granular materials of biological origin. Selection of the presented material was based on direct professional experience of the authors. The main theoretical approaches – from the origins of soil mechanics to micropolar theory and DEM modelling have been addressed. A review of commonly applied experimental methods and material parameters has been presented. Finally, a catalogue of material parameters drawn from laboratory testing of the authors was attached for reference as well as for comparison with results of other laboratories. This “Mechanical Properties of Granular Agro- Materials and Food Powders for Industrial Practice” is composed of two volumes. Part I presents mainly issues relevant for storage and handling, while Part II addresses questions of grinding and agglomeration.

We kindly acknowledge support given by the European Commission that made this publication possible.

Authors

BASIC NOTATION

c – cohesion [kPa];
 d – particle diameter [m];
 D – shear cell diameter [m];
 E – modulus of elasticity [MPa];
 f – flow function;
 H – height [m];
 i – flow index;
 k – pressure ratio;
 L – length [m];
 ΔL – displacement [mm];
 m – mass [kg];
 N – normal force [N];
 p – pressure [MPa];
 Q – volume flow rate [$\text{m}^3 \text{h}^{-1}$];
 R – radius [mm];
 R_h – Hausner Ratio;
 t – time [s];
 T – tangent force [N];
 V – volume [m^3];
 w – moisture content [%];
 γ – bulk unit weight [kN m^{-3}];
 $\varepsilon_1, \varepsilon_2, \varepsilon_3$ – principal strains;
 ε_v – volumetric strain;
 μ – friction coefficient;
 ν – Poisson's ratio;
 φ – angle of internal friction [deg];
 Φ – angle of repose [deg];
 ρ – bulk density [kg m^{-3}];
 $\sigma_1, \sigma_2, \sigma_3$ – principal stresses [kPa];
 σ_c – unconfined yield strength [kPa];
 σ_r – consolidation reference stress [kPa];
 τ – shear stress [kPa].

1. INTRODUCTION

Granular materials are substances made up of many distinct solids (“grains”) that have been present in human activity since very early history in forms such as cereal grains or construction materials. Granular materials are important constituents in numerous industrial processes. Such industries as: chemicals, cosmetics, pharmaceuticals, biotechnology, ceramics, food, energy, paper/wood, metallurgy, cement, glass, minerals, consumer products, plastics strongly depend on granular materials. A single shift in conditions can drastically change performance of a process in those industries. Following growing industrial use of granular materials a number of branches of engineering evolved devoted to understanding how to deal with these materials, among them powder technology, soil mechanics, geotechnology, foundation engineering, earthquake engineering, erosion control and mining engineering. The most important technologies of process engineering involving granular materials as listed at ‘Powder, bulk solids’ portal are: pneumatic conveying, transport, size reduction, spheroidization, screening, coating, mixing (blending), segregation, product consistency, weighing, metering, packaging and bagging, storage, stratification, dust collection, instrumentation and control, feeding, quality control. Each of the above applies specific equipment. For example a group of particle enlargers and formers constitute of: briquetters, coaters, compactors, conditioners, dedusters, densifiers, disc pelletizers, drum flakers, drum pelletizers, encapsulators, extruders, flakers, fluid bed agglomerators, granulators, instantizers, kneaders, laboratory mixing agglomerators, pelletizers, pinmixers, powder coaters, powder presses, rewetting agglomerators, roller presses, rotary agglomerators, rotating pans, screens, spheroidizers, spray agglomerators, spray congealers, tablet coaters, tablet presses, vibratory agglomerators.

As compared to liquid granular material reveal three distinct differences in mechanical behavior:

- Granular materials are characterized by higher than zero angle of internal friction that in the case of liquids is zero. As a result of that static pressure in liquids is not dependent on direction, while in granular material pressure may vary with direction of measurement. Static granular material may carry shear stress, while liquid cannot. Therefore the surface of static liquid is flat, while the free surface of static granular material has conical shape.
- In granular material tangent stress under condition of shear load does not depend on velocity of deformation, but depends on the mean stress. In liquid shear stress depends on velocity of deformation (as an effect of viscosity), but does not depend on pressure.

- Numerous granular materials when consolidated reveal cohesion that allows to maintain shape enforced under load. Ratholes or channels may be formed in granular materials but not in liquids.

No fundamental mechanical model is currently available to describe behaviour of granular materials. The lack of precise description of material behaviour results in serious practical problems. Unpredictability leads to clogged chutes and catastrophic failures of industrial silos. Mechanical properties of materials stored in silos influence pressures exerted on the walls and flow patterns developing during discharge. Variation in raw material properties may result in a lack of reliability and repeatability of final product properties that may cause high costs in food industry, but may be disastrous in the case of pharmaceutical product. In pharmaceutical industry uniform mixing of medicinal components may be critical, as well. Considering that granular materials are so widespread and their use in industry increasing further understanding of how these media behave can have a profound impact on economy worldwide. Research in this area that has been intensively conducted in last 40 years had important implications for manufacturing and new processes.

Background for the recent development in granular mechanics and technology has been given by results of investigations of Andrew Jenike presented in „Gravity flow of bulk solids” published in 1961 [74]. Although at that time it was clear that most of processing industries dealt with flow of granular materials Jenike’s book was the first comprehensive study of the subject. The fact that the work appeared at that time stemmed from the progress in theory of plasticity and in techniques of numerical calculations that had taken place in former fifteen years [74]. Jenike adopted testing technique and some concepts of soil mechanics but his creative input was substantial in that he analyzed granular material under 100 to 1000 lower load. In such conditions some effects that were never observed in soil mechanics got great importance. One example is curvature of the envelope of Mohr circles in (σ, τ) coordinates with no meaning in soil mechanics and of crucial importance for determination of flowability of granular material.

For Jenike silo technique was natural field of application of the theory where he contributed significantly. After 40 years of work in numerous laboratories specialists achieved agreement in some questions and a set of national and international codes of practice as in the case of silo design: American ACI 313-91 [1] and ASAE EP433 [4]; Australian AS 3774 [10], Polish PN-B-03254 [135], and European Eurocode 1 [50]. Usually code of practice are contains standard procedures for determination of mechanical properties of stored granular materials.

The earliest approach of scientists for predicting behaviours of bulk solids was continuum theory that looks at a volume of material as a whole, as a solid

body or a liquid. Continuum approach led to solutions numerous problems of technology but it failed in the cases where interactions of grains were important. Thus, the opposite extreme alternative is to model every single grain, which is what the discrete element method (DEM) does. This modelling technique requires extensive and costly computations so current solutions are limited to two-dimensional models of systems not exceeding 10000 particles. Other more popular approaches applied are: statistical mechanics, fluid mechanics, kinetic theory micropolar medium and finite element method. Specific questions in interest of science are, to quote several: *granular flows, granular compaction, segregation, convection, avalanches, surface waves, collisions and friction, inelastic collapse, jamming and fluctuations, energy flows, strength properties, anisotropy of packing, stress fluctuation*. The findings are published in journals like Powder Technology, Powder Handling and Processing, Geotechnique, Acta Mechanica, Granular Matter, International Journal for Analytical and Numerical Methods in Geomechanics, BIT Numerik Mathematik, and the International Journal of Solids and Structures.

The presented work contains brief description of the most popular theoretical approaches, presents popular methods and equipment for determination of material parameters and typical or interesting examples of experimental results.

2. CONTINUUM MECHANICS APPROACH

2.1. The plastic flow rule

The common feature of granular materials that distinguish them from other materials is the negligible value or total absence of tensile strength. Subjected to the isotropic stress, the materials are characterized by considerable compressibility and variable resistance to shearing related to precompaction applied. The high practical significance of mechanical effects taking place in granular materials resulted in the creation of numerous theoretical models and experimental methods for the investigation of yielding of such materials [32, 35, 39, 165].

Plastic strain of granular material can take place under the effect of both isotropic and deviatoric stress. Isotropic stress causes only the compaction of a material, while deviatoric stress can cause both compaction and dilation of the material, depending on the earlier stress path, as well as shear strain without volume change referred to as the critical states.

The theory of plastic yielding is based on the assumption of the existence in space of the stress of plastic potential $G(\sigma_{ij})$. The existence of the potential has not been proven through deduction. Therefore, the assumption has to be treated as an axiom of the theory of plastic yielding, and its correctness has to be confirmed experimentally [15]. The plastic flow rule is a term applied to the relation between

the tensor of plastic strain increments or the plastic strain rate and the tensor of stress during yielding:

$$\dot{\varepsilon}_{ij}^p = \lambda \frac{\partial G(\sigma_{ij})}{\partial \sigma_{ij}}, \quad (2.1)$$

where:

$\dot{\varepsilon}_{ij}^p$ – tensor of plastic strain rate,
 λ – non-negative coefficient.

The above relation means that coaxiality of the stress and strain rate tensors has been assumed, which is an expression of isotropy of the material during yielding. The plastic flow rule has the form of a potential rule. This means that the tensor of plastic strain rate is normal to the surface representing the potential G . The plastic potential G is frequently taken to be identical with the yield condition F which is the limiting states of stress that must be reached for plastic strain to occur, $F \equiv G$. In such a case we speak about so-called associated flow rule:

$$\dot{\varepsilon}_{ij}^p = \lambda \frac{\partial F(\sigma_{ij})}{\partial \sigma_{ij}}. \quad (2.2)$$

The plastic potential for an ideally plastic material can be chosen in various manners, and associated or non-associated flow rule can be constructed. Such relations, however, are never completely in agreement with the results of experimental studies and usually cover only a certain aspect of yielding (e.g. dilatation or steady flow without volume change). In reality, the principal directions of the tensors of stress and of strain rate are not coaxial, and the dilatation of the material as predicted by the models is much greater from that observed experimentally. The process of plastic strain of granular materials is more realistically approximated by models including material hardening and softening [118].

2.2. Plastic model with hardening and softening

Models of plastic flow with material hardening and softening attempt to predict overall change of the material state from any initial state to any other final state or to critical state when material yield without volume change. Special attention is paid in the models to important role of density ρ , which is treated as hardening parameter [45]. It is assumed that the material has no single yield condition but a whole family of such conditions:

$$F(\sigma_{ij}, \rho) = 0. \quad (2.3)$$

Density ρ is strictly related to volumetric deformation and dependent on the major principal stress $\rho(\sigma_1)$. The most important contribution in the development of the model of granular material with hardening and softening is that by Roscoe [143]. In the model, for the particular values of density ρ we obtain, in the plane (τ, σ) , yielding conditions separating the plastic states of the material from its elastic or rigid states. As higher density is related to higher strength, the yield condition is a monotonically increasing function of density. For a fixed density ρ the yield condition represents in the stress space an enclosed surface that, in the case of a cohesionless material, passes through the origin of the system of coordinates whose axis of symmetry is the axis of isotropic stress. In axial-symmetric state of stress the yielding condition can be written in the system of coordinates (p, q) :

$$F(p, q, \rho) = 0, \quad (2.4)$$

where:

$$\begin{aligned} p &= \frac{1}{3}(\sigma_1 + 2\sigma_2), \\ q &= \sigma_1 - \sigma_2, \\ \sigma_1 \neq \sigma_2 &= \sigma_3. \end{aligned}$$

In figure 2.1 the critical line separates the area of compaction where plastic strain is accompanied by an increase in density $\rho > \rho_1$ and therefore expansion of the yield curve from the area of dilation in which strain is accompanied by volume increase of the material, decrease in density $\rho < \rho_2$ i.e. in effect shrinking of the yield curve. The change in density is defined by the law of mass conservation:

$$d\rho = \rho d\varepsilon_p, \quad (2.5)$$

where:

$$\begin{aligned} d\varepsilon_p &= \frac{dV}{V} = d\varepsilon_1 + 2d\varepsilon_2, \\ d\varepsilon_q &= \frac{2}{3}(d\varepsilon_1 - d\varepsilon_2). \end{aligned}$$

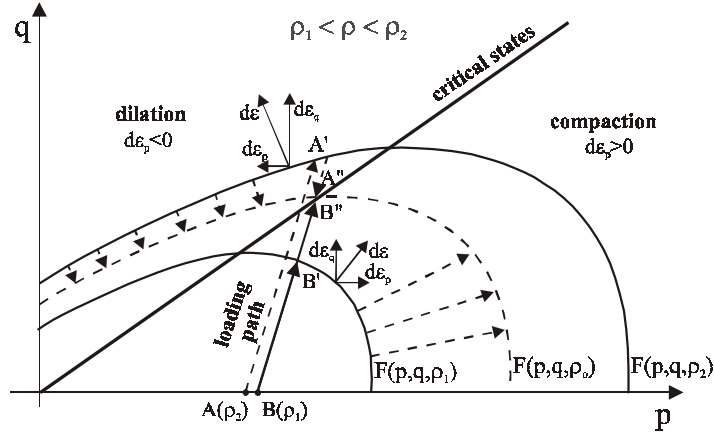


Fig. 2.1. Yield curves with compaction and dilation regimes

The critical line represents the state of stress in the material that causes yielding without changes in density, therefore corresponds to steady flow. The above model comprises hardening, softening, or flow in the critical state of stresses. The hardening or softening are determined by the sign of the partial derivative $\partial F/\partial p$. If the following relations occur in the process under study:

$$\begin{aligned} F(p, q, \rho) &= 0, \\ dF(p, q, \rho) &= 0, \end{aligned} \quad (2.6)$$

then the yield condition is fulfilled. If we also have the inequality:

$$\frac{\partial F}{\partial p} dp + \frac{\partial F}{\partial q} dq > 0, \quad (2.7)$$

which means that the angle between the direction of stress increment (dp, dq) and the direction of the normal to the yield curve is less than 90° and

$$\frac{\partial F}{\partial p} > 0, \quad (2.8)$$

then, on the grounds of the assumption of coaxiality of the principal stresses and strain increments, the increase of volumetric deformation is positive ($d\varepsilon_p > 0$). In such a case material hardening takes place. Density increases ($d\rho > 0$), and the yield curve expands. Such plastic strain is called stable strain. In this case the flow rule presents a unique description of plastic strain of the material.

In a case when the partial derivative equals zero:

$$\frac{\partial F}{\partial p} = 0 \quad (2.9)$$

the strain increment $d\varepsilon_q$ tends to infinity, and increase of volumetric strain $d\varepsilon_p$ is indeterminate. This is the case of critical yielding. The material is in the state of steady flow at constant material density. Therefore, neither hardening nor softening of the material take place.

In the case of the inequality of:

$$\frac{\partial F}{\partial p} < 0 \quad (2.10)$$

it follows from the flow rule that the increase in the volumetric strain is negative ($d\varepsilon_p < 0$), and therefore density decreases ($d\rho < 0$) and material softening takes place. The material yields, and the yield curve shrinks due to the decreasing density ρ :

$$\frac{\partial F}{\partial \rho} d\rho > 0. \quad (2.11)$$

As the total differential of the yield condition $F(p,q,\rho)$ equals zero:

$$\frac{\partial F}{\partial p} dp + \frac{\partial F}{\partial q} dq + \frac{\partial F}{\partial \rho} d\rho = 0, \quad (2.12)$$

therefore, taking into account relation (11), vector (dp, dq) must be pointed into the interior of the initial yield curve:

$$\frac{\partial F}{\partial p} dp + \frac{\partial F}{\partial q} dq < 0. \quad (2.13)$$

This is a case of experimentally observable unstable yielding with softening.

Stable or unstable behaviour of a material can be observed at the same density of the material but at different stress paths. The model predicts stable and unstable behaviour of material also for the case of the same stress path but different initial densities. The model with density controlled hardening and softening does not describe correctly all the mechanical processes that take place in granular materials. It provides a unique description only for the stress paths on which compaction of the material occurs. This substantiates the adoption of the associated flow rule. The model does not describe accurately the transition of the material from stable state to steady flow in critical state, nor does it uniquely describe unstable states of the material.

Density hardening is an example of isotropic hardening, that is such a process in which the yield curve expands uniformly, while retaining its shape.

There are also hypotheses of anisotropic hardening, assuming that in the course of plastic strain the yield curve does not change its shape and size, but moves as a rigid object towards the increase of plastic strain [167]. Such a hardening is called kinematic hardening. The yield condition in an advanced stage of the process of kinematic hardening of the material can be described by means of the function:

$$F(\sigma_{ji} - \alpha_{ij}) = 0, \quad (2.14)$$

where tensor α_{ij} represents the displacement of the yield condition, and therefore the kinematics of the hardening.

2.3. Elastic-plastic models of Ghaboussi and Momen and of Lade

Among the more advanced elastic-plastic models that find a broader application for granular materials of plant origin, we should mention the models of Ghaboussi and Momen, and that of Lade, applied by Zhang *et al.* [175] for the description of the behaviour of wheat grain in bulk in triaxial stress state. In those models the strain increment $d\varepsilon_{ij}$ is the sum of the elastic strain increment $d\varepsilon_{ij}^e$ and the plastic strain increment $d\varepsilon_{ij}^p$:

$$d\varepsilon_{ij} = d\varepsilon_{ij}^e + d\varepsilon_{ij}^p. \quad (2.15)$$

The modulus of elasticity E_u is a non-linear function of the minor principal stress σ_3 :

$$E_u = k_e P_a (\sigma_3 / P_a)^l. \quad (2.16)$$

where:

- k_e – elastic modulus number,
- l – elastic modulus exponent,
- P_a – atmospheric pressure.

Ghaboussi and Momen adopted the Drucker-Prager yield condition for a non-cohesive material (fig. 2.2):

$$F(\sigma_{ij}) = I_2 - Y^2 I_1^2 = 0, \quad (2.17)$$

where Y is the yield constant, and the plastic potential of the same shape as the yield condition additionally including isotropic and kinematic hardening:

$$G(\sigma_{ij}, \alpha_{ij}, \kappa) = 0, \quad (2.18)$$

where:

- α_{ij} – kinematic hardening tensor,
- κ – parameter of isotropic hardening.

The eight-parameter model of Ghaboussi and Momen contains 3 parameters describing elasticity, 3 parameters of kinematic hardening, and 2 parameters of isotropic hardening. The model describes correctly all phenomena typical for isotropic as well as kinematic hardening, and it describes especially well the anisotropy of the material, hysteresis in the load-unload cycle, and the evolution of the hysteresis loop in the course of multiple loadings.

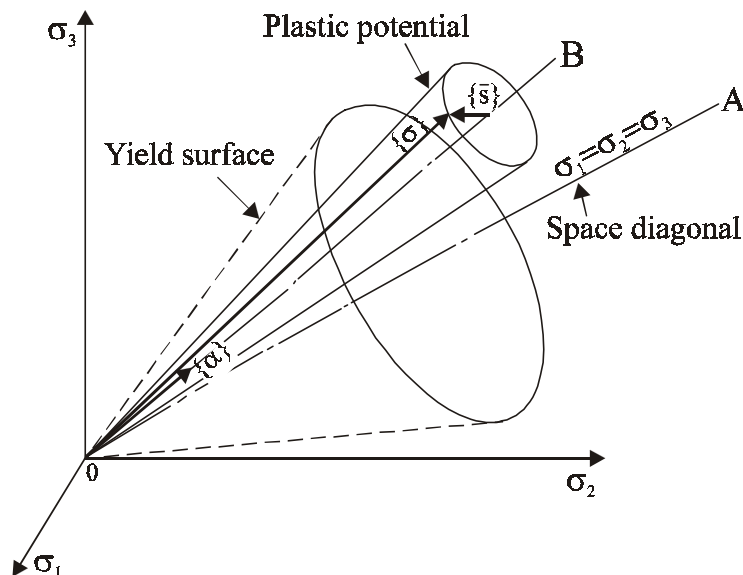


Fig. 2.2. A schematic of yield and plastic potential surfaces in the principal stresses space [175]

In turn, the model of Lade, also applied by Zhang *et al.* [175] for the description of wheat grain during loading, assumes that the plastic strain increment $d\varepsilon_{ij}^p$ is the sum of two independent components: the plastic strain increment related with the compaction of the material $d\varepsilon_{ij}^c$ and the plastic strain increment related with the dilation of the material $d\varepsilon_{ij}^d$:

$$d\varepsilon_{ij}^p = d\varepsilon_{ij}^c + d\varepsilon_{ij}^d. \quad (2.19)$$

The division of the plastic strain increment into two independent components entails the necessity of adopting also two independent yield functions and two flow rules. For the description of the behaviour of wheat Zhang *et al.* [175] adopted the following yield functions F_c and F_d , and plastic potentials G_c and G_d :

$$F_c = I_1^2 + 2 \cdot I_2 - P_a \cdot (W^c / C \cdot P_a)^{1/4}, \quad (2.20)$$

$$F_d = (I_1^3 / I_3 - 27) \cdot (I_1 / P_a)^m - a e^{-bW^d} \cdot (W^d / P_a)^{1/4}, \quad (2.21)$$

$$G_c = I_1^2 + 2 \cdot I_2, \quad (2.22)$$

$$G_d = I_1^3 - (27 + \eta \cdot (P_a / I_1)^m) \cdot I_3, \quad (2.23)$$

where:

- a, b, c, m, q, η – material constants,
- I_1, I_2, I_3 – first, second and third invariant of stress tensor,
- P_a – atmospheric pressure,
- W^c, W^d – collapse and expansive plastic work.

The yield functions F_c , responsible for irreversible compaction of material, represents in the space of principal stresses a concave surface with axis of symmetry lined with the axis of isotropic stresses. This condition confirms the known rule that a granular material compacts the easiest under the isotropic stress. In the plastic potential G_d , responsible for material expansion, the material constant η represents the slope of the plastic potential surface, and the exponent m represents the curvature of the meridian of the surface.

Figure 2.3 presents examples of the application of the models of Ghaboussi and Momen and of Lade for the approximation of the experimental stress-strain relations obtained during tests of monotonic loading of wheat grain samples in triaxial compression apparatus. The presented comparison shows that the model of Lade more accurately approximates the course of the stress-strain relation during monotonic

loading. However, it is inferior to the model of Ghaboussi and Momen in the case of description of the behaviour of materials with hysteresis under the conditions of cycling loading. Nevertheless, its simplicity and mathematical coherence make it a highly useful tool for modeling the plastic flow of granular materials.

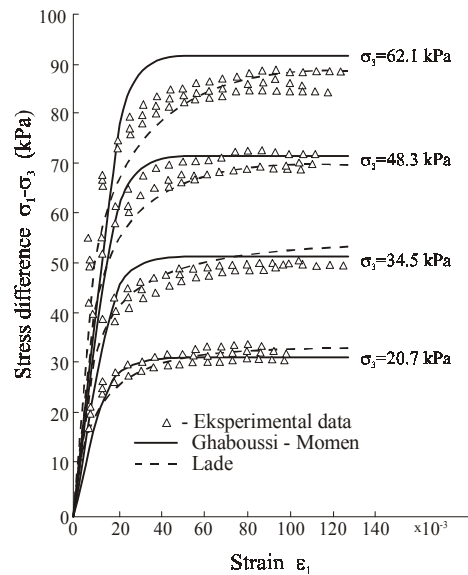


Fig. 2.3. Comparisons of calculated and measured stress-strain relations in triaxial compression tests of wheat grain samples [175]

3. MICROSTRUCTURAL APPROACH. DEM MODELLING

3.1. Geometric structure of granular medium

The results of geotechnical studies have shown that natural sand deposits formed under the effect of gravity are usually anisotropic. Allen [2] proved that in the course of sand deposit formation grains of sand tend to orient themselves so that their long axes are parallel to the horizontal plane. The result of this is the formation of deposits with a high degree of geometric arrangement of particles. Oda [126] became interested in the effect of the anisotropy of a deposit on its mechanical properties. He conducted a series of laboratory tests on sand samples. The author showed that knowledge of the structure of particle packing is necessary for the determination of the stability of non-cohesive soils subjected to external loads. Mechanical phenomena, such as the anisotropy of response to loading, stress-strain relations, strain hardening, strength and porosity, turned out to be dependent on the structure of packing [127-129]. Ever since those experiments it has been known that two samples of the same sand with the

same porosity need not have identical mechanical properties. The author distinguished two elements of the packing structure: 1) spatial orientation of the long axes of non-spherical granules (characterized by two parameters) and 2) packing density.

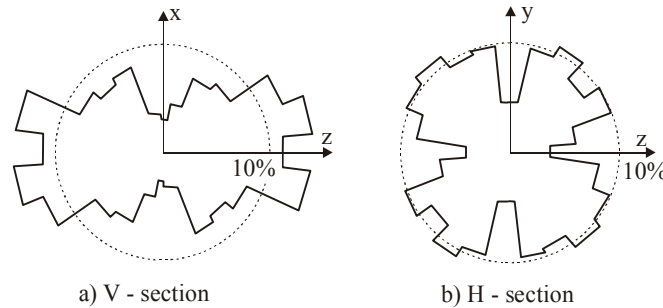


Fig. 3.1. Distribution of density of probability of angle of inclination to horizontal line of long axis of sand grains [129]

Figure 3.1 [127] presents the density distribution of probability of sand grains long axis inclination angle. The sample was formed by pouring sand into a mould filled with water, then compacted by tapping on the walls of the mould. V-section is the vertical section and H-section is the horizontal section of the sample. In the vertical section, the density of probability in the horizontal direction is considerably higher, while in the horizontal section no distinct orientation of long axes of the granules is observed. The manner of characterizing the geometric structure of a granular material illustrated in figure 3.1 has been later frequently used by other researchers, especially in the case of 2D models.

Konishi *et al.* [83] made an elasto-optical study of biaxial deformation of 2D systems of particles in the form of rods with oval cross-section. The authors recorded force values at various strain stages while taking elasto-optical photographs. They estimated the effect of anisotropy related to the sample forming method, friction between the particles, and their form on the response of the material to mechanical loading. They used particles with two section forms and three size classes. The length ratio of the long to short axes of the elliptical cross-section was 1.1 in the first group, and 1.4 in the second. The dimension of the long axis of the cross-section ellipse in the first group was 14.8, 9.9 and 6.3 mm, and in the second – 16.0, 10.7 and 7.1 mm. To examine the effect of interparticle friction two series of measurements were performed; one with non-lubricated particles with internal friction angle of 52° and another with particles lubricated with talcum, for which the internal friction angle was 26° . Samples were poured into a cuboid mould with different angles θ of mould bottom inclination to the horizontal. The sample, compressed horizontally with a constant force, had freedom to deform vertically. Measurements included vertical loads as well as vertical and

horizontal deformation of the sample. Elasto-optical photographs show that the load is transmitted by columns of particles oriented in the direction of maximum compressive stress. The points of contact around the columns transmit only a limited amount of the load applied, but ensure stability of the columns that transmit most of the load. The distribution of forces obtained is highly similar to that presented earlier by Drescher and De Josselin de Jong [44] in their work concerned with verification of the theoretical model of granular medium flow.

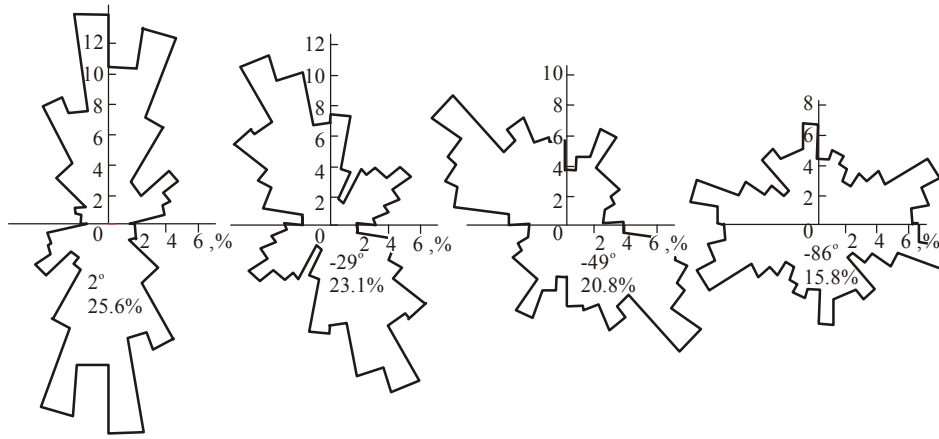


Fig. 3.2. Distribution of probability density of angle of contact normal directions in the assembly of rods of cross section (ratio of length of axes 1.4 [83])

Konishi *et al.* [83] applied the distribution of unit normal directions at contact points for the description of the packing structure of particles. Figure 3.2 presents the obtained distributions of contact normal directions for the particular variants of the experiment in an undeformed sample. The authors adopted an approximation of the distribution of normal directions by means of an ellipse. The long axis of the ellipse in undeformed state is perpendicular to the plane of deposit pouring. The effect is more pronounced in the case of flatter particles and in the case of lubricated particles that display higher anisotropy. The numbers in figure 3.2 represent the direction of the long axis of the ellipse (higher) and the degree of anisotropy (lower). The parameters were calculated according to the relation [130]:

- long axis direction:

$$\bar{\beta} = \frac{1}{2} \arctg(A/B), \quad (3.1)$$

- degree of anisotropy:

$$M = \sqrt{A^2 + B^2} * 100, \quad (3.2)$$

where:

$$A = \int E(\beta) \sin \beta d\beta ,$$

$$B = \int E(\beta) \cos \beta d\beta ,$$

$E(\beta)$ – distribution of probability density.

With progressing deformation, some of the contacts disappear and new ones come into existence. The distribution of contact normal directions changes. The main axes of the ellipses that describe the distribution rotate so that more contact normals assume a direction close to that of the maximum compressive stress. This tendency is more pronounced for spherical particles than for flatter particles. Kanatani [80] proposed the characterization of the spatial distribution of particles by means of the packing tensor. He performed a quantitative estimation of the distributions of contact normal directions obtained by Konishi *et al.* [83]. Figure 3.3 presents the experimental distributions and Kanatani's approximations [81] up to the fourth order, for material prior to loading and subjected to a load.

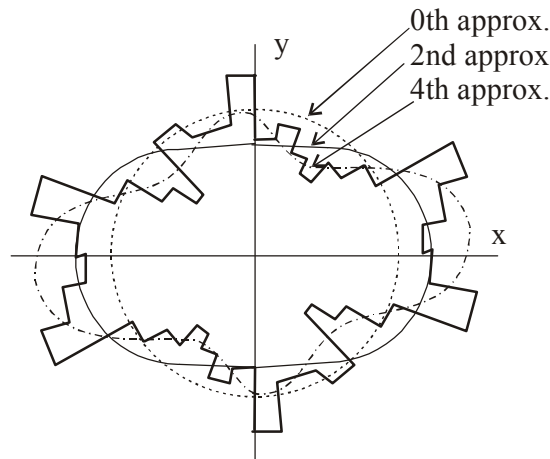


Fig. 3.3. Probability density distribution of angle of inclination of contact normals and their approximations [81]

3.2. Anisotropy of seed layer

The literature results described above induced us to undertake studies, at the Institute of Agrophysics, PAS, Lublin, on the effect of the anisotropy of a seed sample on the angle of internal friction [107]. Selected for the studies were seeds of wheat, barley, rye, as well as rapeseeds. The seed of the species chosen represent shapes varying from the spherical (rape seeds) to a strongly elongated

ellipsoid (rye). The seed moisture varied from 10.5% to 12%, and in the case of rapeseed it was 8%.

To achieve a specific orientation of seeds in the sample the researchers made use of the phenomenon of the formation of an angle of natural repose and the effect of grains arranging themselves usually with the long axis towards the generatrix of the cone formed by the seeds. The method of sample preparation for the triaxial compression test is illustrated in figure 3.4. Grain was poured with a steady flow from the funnel through a rectangular outlet of 8 x 24 mm in size into a rubber diaphragm placed in a two-part cylindrical mould. The funnel, placed at the wall of the mould, was lifted up as the mould was filled with grain, so that the outlet hole was always positioned about 20 mm above the top of the freely formed surface of grain poured. After complete filling of the mould, the cylindrical top cover of the sample was fixed in place. Next, vacuum was generated within the grain sample, which gave the sample rigidity of shape, and that permitted its placement inside a pressure chamber without risk of disturbing the spatial structure of the medium created in the course of sample formation. The angle between the freely formed surface of poured grain and the base of the sample was varied by tilting the mould away from the vertical in the course of grain pouring. As grains tend to orient themselves so that their long axis is parallel to the generatrix of the cone of natural repose, varying the tilt of the mould with relation to the vertical resulted in a change of the preferred spatial orientation of the grains with relation to the sample-related system of reference.

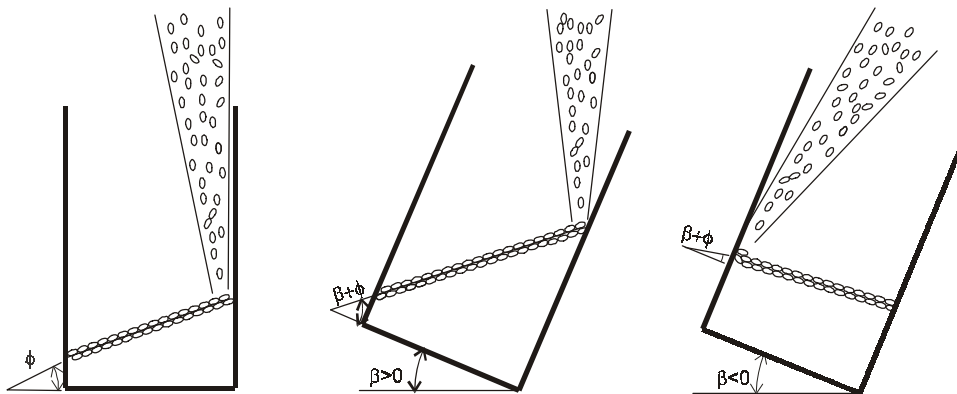


Fig. 3.4. The method of sample preparation for the triaxial compression test

For further tests six values of sample inclination were chosen: $\beta = -20^\circ, -10^\circ, 0^\circ, 10^\circ, 20^\circ$ and 30° (fig. 3.4). The angle of natural repose of the grain was about 20° . Additionally, for purposes of comparison, grain was poured into a vertical mould

($\beta = 0^\circ$), positioning the outlet hole of the funnel along the sample axis of symmetry and not close to the mould wall as before. Every time the same quantity of grain filled the whole volume of the mould, therefore every time the same density of the medium was obtained.

To estimate the degree of arrangement of the long axes of the grains, the samples prepared according to the method described above were flooded with polyester resin. Once the resin was set, the samples were cut along horizontal and vertical planes. The sections obtained were used to determine the measure of grain arrangement after [129], in accordance with the formula:

- preferred angle of inclination of long axes of grains with relation to chosen system of coordinates:

$$\bar{\theta} = \frac{1}{2} \operatorname{arctg} \left(\frac{\sum_{i=1}^n \sin 2\theta_i}{\sum_{i=1}^n \cos 2\theta_i} \right), \quad (3.3)$$

- intensity of parallel orientation of the long axes

$$V \cdot M = \sqrt{\left(\sum_{i=1}^n \sin 2\theta_i \right)^2 + \left(\sum_{i=1}^n \cos 2\theta_i \right)^2} \cdot \frac{100}{n}, \quad (3.4)$$

where:

n – number of measurements,

θ_i – the angle of inclination of the long axis of a given grain with relation to the adopted system of reference.

The value of the expression $V \cdot M$ varies within the range from 0 to 100%. The value of 0% corresponds to totally random orientation of the long axes of the grains, while 100% represents ideally parallel orientation of the long axes of the grains. For angle $\beta = 20^\circ$ and for the vertical sample section, the measures had values of $\theta = 38^\circ$, $V \cdot M = 65\%$, respectively, and therefore the sample was characterized by considerable anisotropy.

The effect of spatial orientation of grains of three cereals and of rape on the angle of internal friction was examined with the triaxial compression method and with the direct shear method. The methods were chosen due to their popularity in experimental studies on the mechanics of granular materials. It was assumed that

comparison of the two methods would permit formulation of conclusions on their applicability in studies on agricultural materials.

The procedure of sample preparation for the direct shear test was identical as in the case of the triaxial compression test. In the direct shear tests five levels of normal load σ were applied, equal to the values of stress σ_3 in the triaxial compression test. The speed of mutual displacement of two sample halves was 1.3 mm s^{-1} . Each variant of the experiment was repeated three times.

A preliminary study of the effect of sample preparation, performed with the method of triaxial compression on rye seeds within an expanded range of the angle of sample inclination $\beta = -40^\circ, -20^\circ, 0^\circ, 20^\circ$ and $+40^\circ$, permitted the conclusion that the manner of grain pouring into the mould had a significant effect on the mechanical characteristics obtained. The highest values of strength were obtained for grain samples poured into vertical mould. Those samples were also characterized by the highest uniformity of deformation. As a rule, no distinct plane of shear was observed. The sample swelled uniformly, assuming barrel shape. The behaviour of samples poured into mould tilted from the vertical by an angle β was totally different. Such samples lost the uniformity of deformation much sooner, and a clearly defined shear plane was formed. With increasing value of angle β , the maximum value of the ratio of main stresses decreased. A marked orientation of the shear plane occurred regularly in every experiment. On the basis of the obtained maximum values of principal stresses ratio σ_1/σ_3 , the value of the angle of internal friction φ was calculated on the basis of the Coulomb-Mohr yield condition. Figure 3.5 presents the

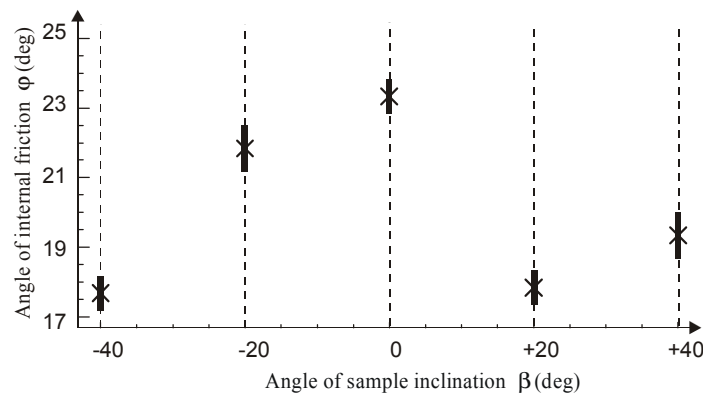


Fig. 3.5. The values of the angle of internal friction φ of rye samples for various values of angle β of mould inclination from the vertical

values of the angle of internal friction for various values of angle β of mould inclination from the vertical. The highest values of the angle of internal friction were obtained for the case of samples poured into vertical mould, and especially when

grain was poured into the mould along the axis of symmetry. With increasing angle of sample inclination β , the angle of internal friction φ decreased significantly.

According to the Coulomb yield criterion, the slip plane is inclined at the angle $\alpha = \pm(\pi/4 + \varphi/2)$ to the plane of the higher main stress. Figure 3.6 presents the theoretical slip planes and the plane of free surface of grain sample, inclined to one of them at angle γ_1 . Figure 3.6a refers to the triaxial compression test at sample inclination angles β : $10^\circ, 20^\circ$ and 30° , while figure 3.6b refers to angles β : $0^\circ, -10^\circ$ and -20° . While in the case of an isotropic medium there are many possible orientations of the slip plane, in the case of an anisotropic material the slip plane is determined by the direction of the lowest strength.

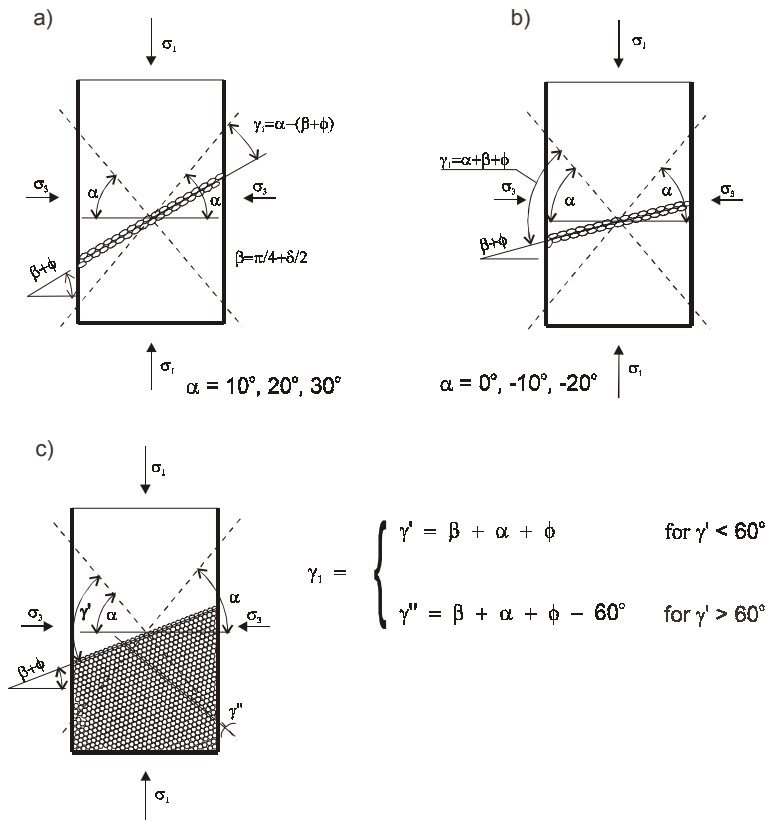


Fig. 3.6. Sample of granular material in triaxial compression test: a), b) non-spherical grains, c) spherical grains

In a material composed of spherical granules there may occur anisotropy of concentration of normal directions to the points of grain contact. In a hexagonal structure, the normal directions to the points of contact are mutually inclined at 60° ,

and therefore the angle of inclination of the normal directions to the slip plane is described by the equations presented in figure 3.6c.

Figure 3.7 presents the stress condition realized in the direct shear apparatus. Point P in the Mohr graph illustrates the values of normal stress σ and maximum tangential (shear) stress τ measured in a horizontal shear plane. Point P is not identical with point T – the point of tangency of the Coulomb-Mohr yield criterion of strength with the Mohr circle [150]. Therefore, the plane in which the Coulomb-Mohr yield criterion is fulfilled does not coincide with the horizontally enforced shear plane, but is inclined to it at the angle $\delta/2$. The angle of long granule axis preferred inclination γ_2 was referred not to the plane in which the Coulomb-Mohr yield criterion is fulfilled, but to the horizontal shear plane.

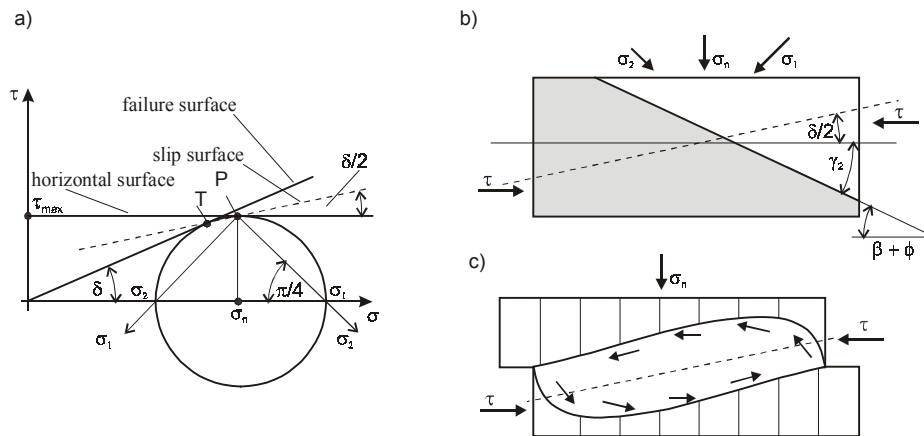


Fig. 3.7. Sample of granular material in direct shear test: a) diagram of Mohr for state of stress in the sample, b) orientation of preferred direction of long axis of grains against theoretical slip plane γ_2 , c) image of deformation of the sample

The results of the measurements are presented in figure 3.8 as graphs of the relation of the angle of internal friction ϕ to the angle of slip plane inclination to the direction of grain long axes or to the normal direction of the normals at contact points. The closest agreement of the relations $\phi(\gamma_1)$ and $\phi(\gamma_2)$ was obtained in the case of rapeseed. In both the tests performed on rapeseed the maximum of the angle of internal friction, $\phi = 29^\circ$, occurred at similar values of the angles $\gamma_1 \approx \gamma_2 \approx 35^\circ$. Considering the fact that the plane of the higher main stress σ_1 is inclined to the slip plane at an angle $\alpha = \pi/4 + \phi/2$ it is easy to note the agreement of the obtained maximum of the angle of internal friction with the results obtained by Oda [126-128]. The author found that in the course of non-dilatational hardening of granular material the normal directions to the points of contact concentrate around the direction of the major principal stress, and that the direction gradually rotates with increasing tangential (shear) stress. The main

axes of the ellipse characterizing granule packing tend towards a position coaxial with the directions of the principal stresses.

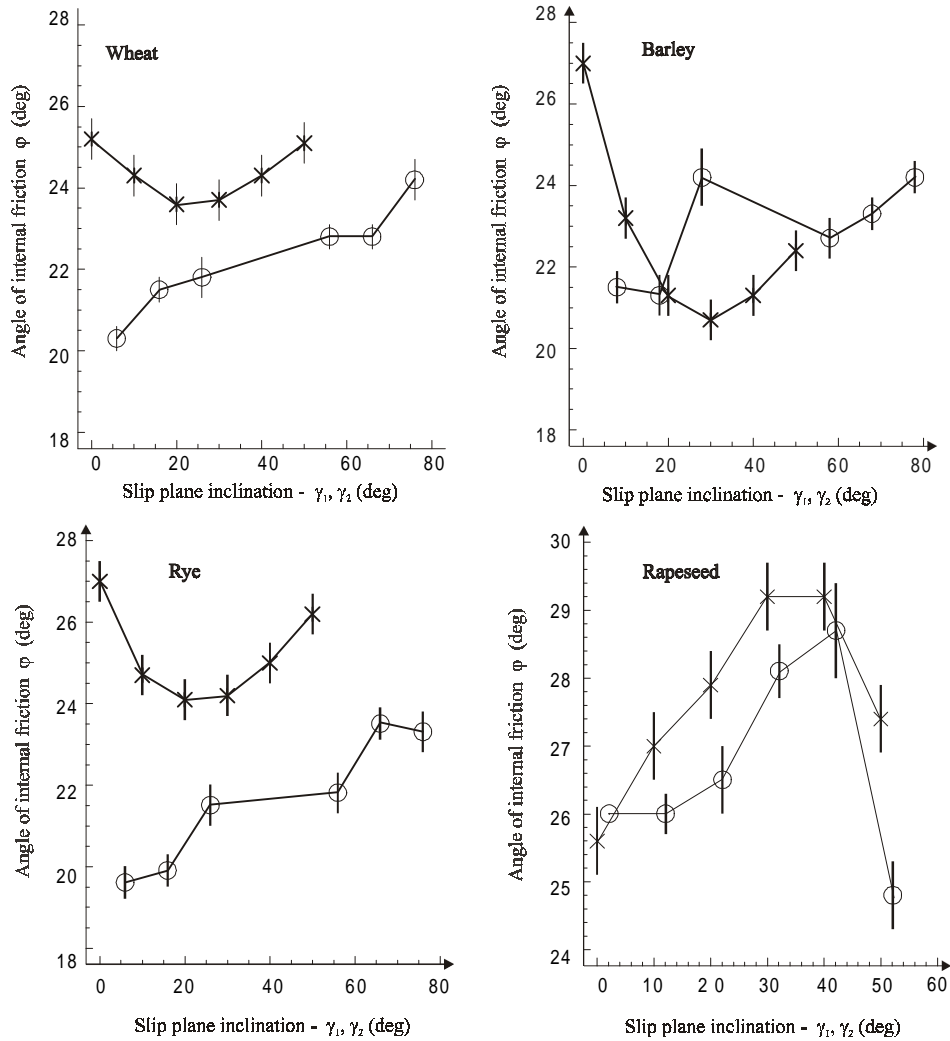


Fig. 3.8. Influence of the angle of slip plane inclination γ_1 and γ_2 on the angle of internal friction φ in direct shear test \times and triaxial compression test \circ

In the case of non-spherical grains, a different relation was observed between the angle of internal friction and the angle between the direction of granule long axis orientation and the direction of slip for the tests of triaxial compression and of direct

shearing. In the triaxial compression test, the angle φ increased with increasing values of angle γ_1 – of granule long axis inclination to the slip plane. The trend was observed for all the cereal species under study. The relation $\varphi(\gamma_2)$ obtained in the direct shear test had an approximately parabolic form, with a minimum for the angle $\gamma_2 \approx 25^\circ$. The divergence between the relations $\varphi(\gamma_1)$ and $\varphi(\gamma_2)$ results from differences in the mechanisms of sample deformation in the tests compared. In the triaxial compression test, the slip plane forms freely, conforming to the state of stress and to the structure of the material, while in the direct shear test the slip direction is forced. In the latter test, the process of shearing is additionally complicated by the non-uniform state of deformation and by the anisotropy of the material; the displacement and the rotation of individual grains are forced. Figure 3.7c presents schematically the two components of the shearing process under macroscopic observation. The minimum of the angle of friction φ obtained with the method of direct shearing should be interpreted as the result of optimum spatial distribution of grains under conditions of forces direction of sample shearing.

The results of the experiments described above permit the formulation of several methodological remarks concerning the measurement techniques. Due to the relatively large dimensions of the grains, it is recommended to increase the size of samples with relation to those routinely used for soils. It appears that the sample dimensions used in the studies presented here (triaxial sample: $D = 150$ mm, $H = 300$ mm, direct shear test sample: $D = 210$ mm, $H = 120$ mm) are sufficient. Especially worthy of recommendation for measurement of the angle of internal friction is the triaxial compression method, though in the case of spherical granules the less complex direct shear test yields similar results. The recommendation of the triaxial compression method is also supported by the fact that the method has been frequently used for the determination of theoretical and empirical parameters of models describing the stress-strain relation. The method was used by Zhang *et al.* [173] and by Li *et al.* [94] for the determination of parameters of the elasto-plastic model adapted by the authors for the description of the stress-strain relation in wheat grain. In that model, formulated by Lade [92] for cohesionless sand, the total increase of strain caused by increase in stress equals the sum of three components: increase in elastic strain, increase in plastic strain caused by normal stress, and increase in plastic strain caused by stress deviator. The values of model parameters determined in the triaxial compression test permit an accurate description of the response of a medium to other loading conditions. For the description of anisotropy and hysteresis in the stress-strain relation in the case of multiple loading of wheat grain, Zhang *et al.* [173] used an elasto-plastic model that included the density and kinematic hardening of the medium. The determination of the values of the parameters of the model also involved the application of the triaxial compression test. Likewise, the method of triaxial compression was applied by Zhang and Jofriet

[176] for the determination of parameters of an elasto-plastic model describing the stress-strain relation for soybeans and corn.

3.3. Microstructural models

A granular material is a discontinuous random system of elementary granules. The description of phenomena occurring in such a medium can be sought on the grounds of statistical mechanics of media with discrete structure [140]. The microstructural approach undertakes an attempt at deriving general laws governing the behaviour of a granular material on the basis of interactions between individual granules [165]. This approach originates from molecular dynamics which is based on the description of movement of each particle of a system. Applied here are the laws of mechanical equilibrium, with the requirement that the laws be fulfilled by all the elements of the system. Macroscopic behaviour of granular material is strictly related with interactions taking place on the micro scale. The correlation between the solution and the initial orientation of the granules caused that in the beginning the method permitted only a qualitative description of the processes under consideration.

Micromechanical models derive the description of macroscopic variables – stress and strain, from analysis of microscopic variables – deformation and displacement of individual grains of the medium and distribution of forces at the points of contact between the grains. It is assumed also that the macroscopic scale of length (the whole deposit of granular material) is several orders of magnitude greater than the microscopic scale of length (a single granule of the medium).

The fundamental relation between the macroscopic stress (averaged over the deposit volume V) and the distribution of the microscopic variables: forces f^C at the points of contact between granules and vectors of normal directions l^C is obtained by averaging, for all the points of contact between the granules, the products of vectors f^C and l^C :

$$\bar{\sigma}_{ij} = \frac{1}{V} \sum_{C \in V} f_i^C l_j^C. \quad i, j = 1, 2, 3 \quad (3.5)$$

This relation is based on the virtual work theorem. The total work performed by the microscopic forces at the contact points of grains is equal to the work performed by the macroscopic stress [32], assuming also that the distribution of forces f^C and of normal vectors at the points of contact between grains l^C are known. In figure 3.9 vector l^C connects the centres of granules A and B contacting each other at point C : $l^C = X^B - X^A$. Granule A acts on granule B with force $f^{AB} = -f^{BA} = f^C$. A similar relation can be derived for macroscopic strain with displacement and rotation of individual granules [33].

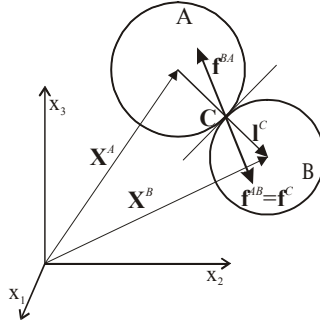


Fig. 3.9. Force and normal direction at contact point of grains

In this approach every elementary contact point of the granules of the medium has an individual contribution to the expression $f_i^C l_j^C / V$. The mean value of the stress tensor $\bar{\sigma}_{ij}$, averaged for a highly numerous system of particles, is an adequate measure of the stress tensor σ_{ij} in the sense of the mechanics of continuum. Determination of the stress tensor on the basis of the equation (3.5), however, requires the knowledge of the force vectors and the normal directions for all the granules of the material. An equivalent method for the determination of the mean stress tensor is based on the knowledge of the probability distribution of the microscopic variables instead of on the consideration of the force vectors and normal directions at the contact points of the particular granules. In such a case the macroscopic stress is determined from the integral expression [14]:

$$\bar{\sigma}_{ij} = N_1 \int_0^{2\pi} P(\theta) \bar{f}_i(\theta) l_j d\theta, \quad (3.6)$$

where:

- $\bar{f}_i(\theta)$ – i -th component of average force at contact points oriented at angle θ ,
- N_1 – number of contacts per unit of surface area,
- $P(\theta)$ – probability distribution.

Another simplification consists in considering only the average values of the product $\overline{f_i^C l_j^C}(\theta_g)$ within identified domains of the granular material, comprising domains of granules with a certain similarity of packing structure, instead of analyzing the full probability distribution of the macroscopic variables. Macroscopic stress is determined in a manner analogous to that in formula (3.6), on the basis of mean values of the variables considered for the whole domain [14]. The size of the domains is intermediate between the size of the granules and the size of the deposit of the material.

A different approach to the description of interactions between the granules of a granular material has been presented by Gózdź and Pietrow [56] who applied a formalism close to that of quantum mechanics. The formalism permits the creation of a more coherent description of irregularly distributed granules of a medium than is possible in the classical micro-mechanical approach operating with distribution of forces at the contact points of the granules. The basic element of the description is the Hamiltonian operator representing the energy of the system and the interactions between the granules. Another element of the description are vectors of states represented by functions related to the shape and size of granules and to mass distribution. The introduction of strain operators acting on the vectors of states of individual granules ultimately gives the global strain of the whole medium [57].

3.4. Distinct Element Method

Common popularity has been attained by the Distinct Element Method (DEM) developed by Cundall and Strack [39]. The method is used for modelling mechanical processes in granular materials on the basis of elementary interactions between the grains. The method consists in approximated solution of the equation of motion for each grain of the material. The motion takes place as a result of propagation through the material of a disturbance initiated under boundary conditions. The calculation procedure is based on the assumption that during a very short time step Δt acceleration and speed are constant, and the disturbance of motion of a single grain does not reach further than to the nearest neighbours. This is the key assumption of the method that permits the description of nonlinear interactions occurring among a large number of elements without excessive requirements concerning the calculation memory power. In this approach all the forces acting on a given granule are considered – those resulting from gravity, from interactions with neighbouring granules, and those resulting from the boundary conditions [12]. Then, on the basis of Newton's second law of dynamics, the acceleration of the granule is determined. Integration in time permits the determination of the new velocity and position.

The deformation of individual grain is considered to be infinitely small compared to the deformation of the whole medium. Therefore, it is usually assumed that the grains are rigid and their deformation at the contact points is modelled through their overlapping. The displacements in the normal direction ΔL_n^C , tangential direction ΔL_s^C , and those resulting from grain rotation ΔL_ω^C (fig. 3.10) are considered separately. Modelling of interactions between grains usually involves viscoelastic contact in the normal direction (η_n, k_n) and visco-elastic-frictional contact (η_s, k_s, μ_s) in the tangential (shear) direction (fig. 3.11). Elasticity models the accumulation of energy in the contact points of the granules, and viscosity and dry friction model the dissipation of energy. The forces of cohesion are neglected.

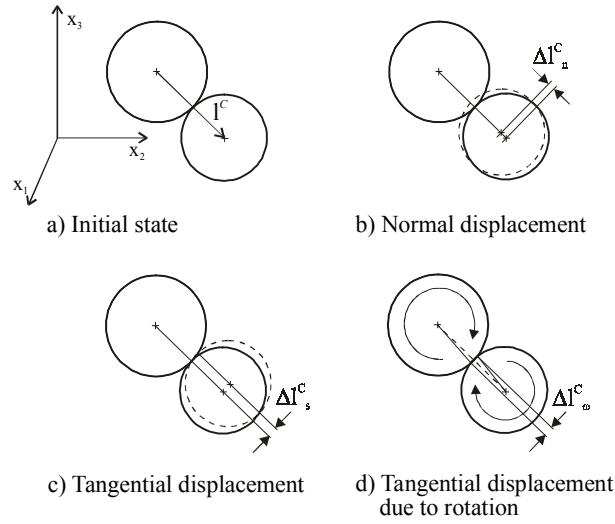


Fig. 3.10. Normal, shear and rotational shear displacements at contact point of grains

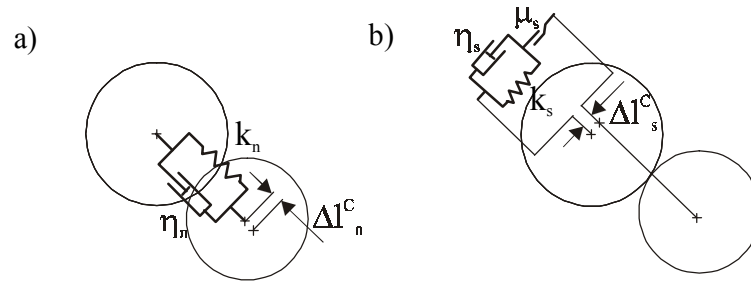


Fig. 3.11. A typical model of contact force between two grains: a) a linear, damped spring element in the normal direction, and b) a linear, damped spring element with a sliding friction in the tangential direction

Differential equations of displacement (x) and rotation (ω) of an individual granule of the material, including the visco-elastic contact between granules [39, 103, 146]:

$$m\ddot{x} + \eta\dot{x} + kx = 0, \quad (3.7)$$

$$I\ddot{\omega} + \eta R^2 \dot{\omega} + kR^2 \omega = 0,$$

are approximated with the incremental equations:

$$m[\ddot{x}]_t = -\eta[\dot{x}]_{t-\Delta t} - k[x]_{t-\Delta t}, \quad (3.8)$$

$$I[\ddot{\omega}]_t = -\eta R^2 [\dot{\omega}]_{t-\Delta t} - kR^2 [\omega]_{t-\Delta t},$$

where:

- I – moment of inertia,
- k – coefficient of elasticity,
- m – mass,
- R – radius,
- Δt – time increment,
- η – viscosity.

In equations (3.8) for the determination of acceleration at time $t = t$ values of position and velocity at time $t = t - \Delta t$ are used. In turn, the position and velocity at time $t = t$ are determined through numerical integration of the equations of motion. The cycle, repeated a number of times, permits the description of the motion of all the granules in the system one by one: the forces determined on the basis of the adopted model of interactions at the contact points of the granules are substituted in the equation of motion, which permits the determination of successive values of position and velocity.

The rapid development of computer calculation techniques permitted the realization of computer simulations of a variety of processes occurring in granular materials, such as: dynamic effects in silos, mixing, segregation gravitational discharge from silos [85, 103, 147, 172].

The numerous examples of simulations indicate the universal applicability of the method. Figure 3.12 presents a comparison of computer simulations of glass balls and rice grain discharge performed by Sakaguchi *et al.* [146] with the results of experimental studies. The authors obtained very close convergence of the theoretical and experimental results thanks to the inclusion of the rolling friction into the grains rotation, apart from interactions in the normal and tangential directions.

Masson and Martinez [103] obtained good agreement of computer simulations made according to the DEM method with results of calculations based on the methods of mechanics of continuum. The DEM method proved to be especially useful in the analysis of relations between micro-sopic parameters (contact rigidity, surface roughness, contact friction coefficient) and the spatial distribution of forces in the contact points, anisotropy, and distribution of porosity.

The concept of Sakaguchi *et al.* [146] of introducing of rolling friction in the DEM method, was then expanded by Iwashita and Oda [72] who proposed the Modified Distinct Element Method (MDEM). The modification consists in the inclusion of interactions taking place in the contact surface of elementary granules of the material, as opposed to the classical method which reduces the interactions to the consideration of resultant forces applied at the contact points. The substitution of contact surface for the contact points of the granules introduces a significant quality change that permits a deeper analysis of the contribution of granule rotation in the

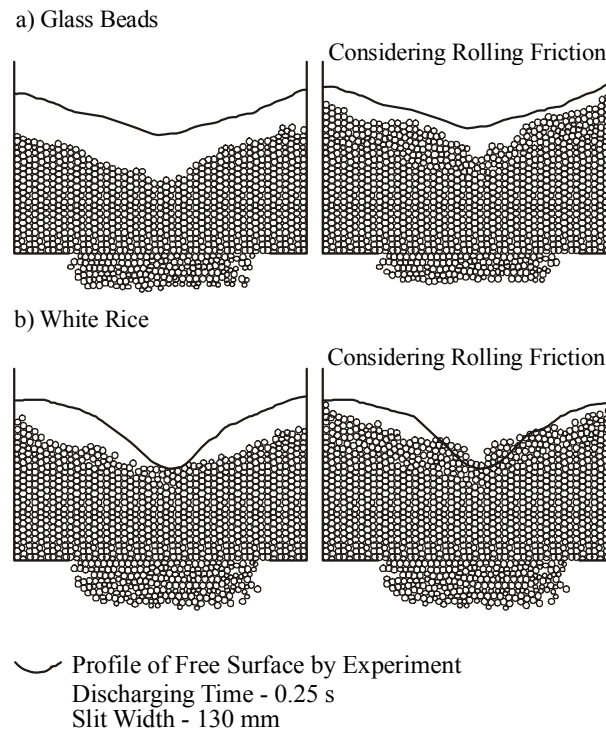


Fig. 3.12. Comparison between simulation and experimental results [146]

formation of macroscopic deformation, and especially the explanation of the mechanisms of dilation of the material. In classical theories of granular material, the dominant role in the occurrence of dilatation has been attributed to mutual displacement of the granules. In the micro-structural approach, the source of dilation was sought in the mutual rotation of the granules. However, the reduction of the interactions to the consideration of forces solely in the contact points of the granules permits mutual rotation of granules without mobilizing the resistance to motion at the points of contact, e.g. through the rotation of neighbouring granules in opposite directions (fig. 3.13 a). Such rotation of granules does not lead to dilation. In reality, granules have rough surface, and the contact surface area is limited. Substituting the contact points with contact area (fig. 3.13 b), the authors included the equations of rotational motion in a form analogous to the equation of linear motion in tangential direction (visco-elastic element and dry friction). Like in the case of tangential displacement, the frictional element in rotational motion is activated when the force moment M is greater than friction resistance. Computer simulations made by Iwashita and Oda [72] showed that the modified method creates quite new possibilities of interpretation.

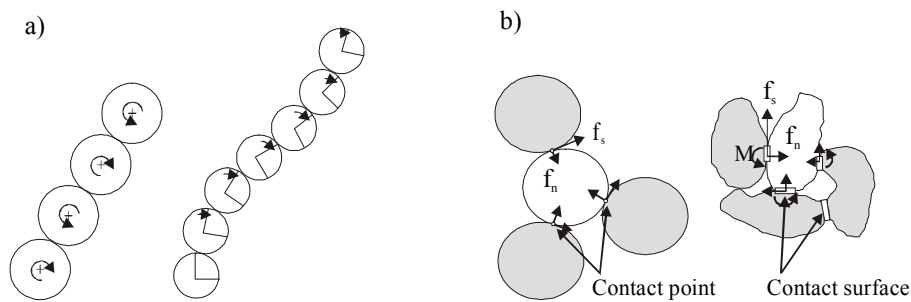


Fig. 3.13. Idealization of contact behaviour in MDEM by Iwashita and Oda [72] a) two mechanisms of particle rotation, b) contact points (DEM) and contact surfaces (MDEM) behaviour

The accuracy of representation of the simulated processes increases as the models are equipped with more and more precise values of the moduli of elasticity, rigidity, micro-hardness, roughness, of contact friction coefficient, and damping coefficients.

3.5. Model of micropolar continuum

The model of micropolar continuum includes rotation into the kinematics of material. The starting point is the derivation of the field of displacement $\mathbf{u}(\mathbf{x}, t)$ and rotations $\omega(\mathbf{x}, t)$ vectors (fig. 3.14). Deformation of infinitesimal element of the material occurs as a result of superposition of displacement and rotations.

Interaction between elements of the structure of material on elementary surface dS takes place not only through the force vector, but also through the couple force vector. An elementary area of the material is affected not only by force stresses, but also by couple stresses. The theory of non-symmetrical elasticity was formulated by the brothers E. and F. Cosserat. At present the theory draws considerable attention from researchers, and one of the areas of its application is the mechanics of granular materials [79].

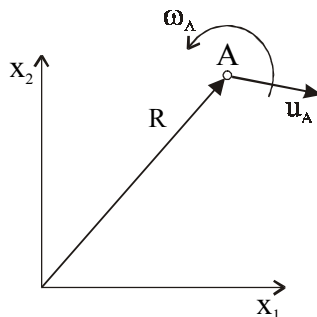


Fig. 3.14. Displacement and rotation in a micropolar continuum

The micropolar elasto-plastic constitutive model of a granular material with isotropic hardening and softening differs from the classical theory of plasticity by the presence of rotations, couple stresses, and a characteristic length corresponding to the mean grain diameter. Due to the introduction of rotations into the kinematics, each material point in the 3D case has three translational and three rotational degrees of freedom, while in 2D and in axis-symmetrical cases two translational and one rotational degree of freedom. The gradient components of the rotation cause curvatures that are associated with the couple stresses. This makes the stress and strain tensors non-symmetric, and the constitutive equation contains the characteristic length. The micropolar elasto-plastic model in Mühlhaus's approach [119] was formed by the extension of the non-associated elasto-plastic flow rule of Drucker-Prager with isotropic hardening and softening by the Cosserats' rotations, curvatures, couple stresses, and mean grain diameter. As a result, the micropolar model includes the characteristic length and at the same time retains the essence of the continuous medium. The constitutive model of granular materials formulated by Mühlhaus contains a number of constants and of material functions that have to be determined experimentally. These include the modulus of elasticity, Poisson constant, cohesion, dependence of internal friction angle on plastic strain, dependence of dilatation angle on plastic strain, mean grain diameter, and micropolar constants.

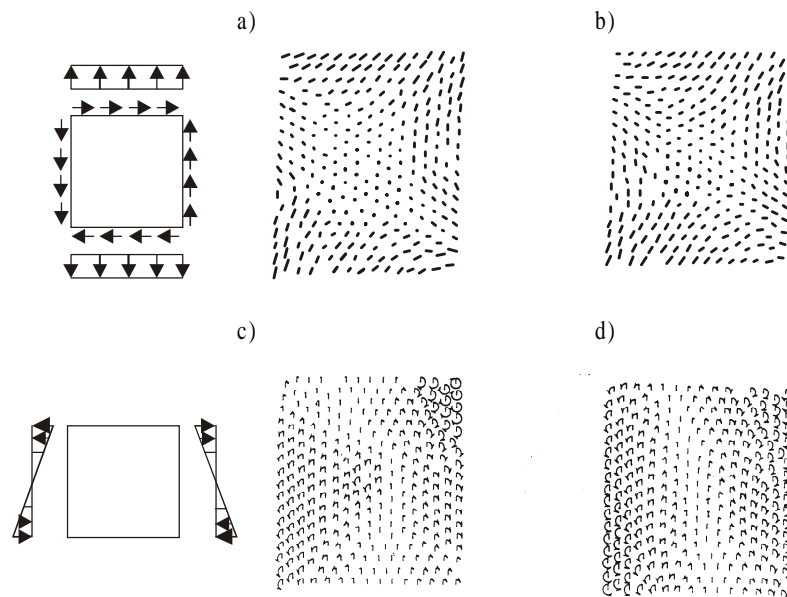


Fig. 3.15. Comparison of the particle displacement (a, b) and rotation (c, d) fields obtained from the discrete method (a, c) and the continuum method (b, d) for the case of loading by (a, b) normal and shear stress (c, d) couple stresses [32]

The micropolar model yields results that are convergent with those obtained with the distinct element method. Comparison of the fields of displacement and rotation of the material, determined with the two methods for the case of loading of a random system of spheres with normal and tangential stresses and with couple stresses, performed by Chang and Liao [32], confirms the good agreement of the solutions of both the methods (fig. 3.15). However, the methods differ in their areas of practical application. Models basing on the formalism of the mechanics of continuum provide a convenient and practical method of solving problems concerning a large number of granules. The model of micropolar medium combined with the finite element method constitutes then an effective tool for the description of even highly complex processes occurring in practice [160]. Limitations of microstructural models analyzing the motion of each individual granule of the medium result from the computational capacity. Nevertheless, the models provide deeper knowledge on the mechanisms of stress transmission and on the occurrence of deformations on the level of interactions between individual granules [72].

3.6. Localization of shear deformation

In the course of numerous operations performed on granular materials, non-dilatational strain of the material is localized within a small area of the material. The reasons for this lie both in external conditions of the operations performed, and in the mechanical properties of the granular material. In the final stage of the shear process, when the stress is close to the critical stress state, strain usually loses its initial uniformity and a clearly defined shear band forms, separating the areas of rigid movement of the material (fig. 3.16). Deformation is mainly localized within the shear band formed. This phenomenon is commonly observed in silos with rough walls, during so-called mass flow, when between the silo wall and the flowing material there forms an intermediate (boundary) layer of granular material. It is in that layer that shearing of the material occurs, as well as dilation causing silo overload. It is assumed that the thickness of the boundary layer of a granular material, in which shear takes place, is constant and does not depend on the dimensions of the silo [120, 177]. This would imply that with increasing dimensions of the silo the effect of the boundary layer on dynamic overload of the silo decreases. Analysis of the scale errors resulting from generalization of results of stress distribution in model scale studies onto real size objects indicates a significant contribution of the processes taking place in the shear band to the level of the errors [120, 124, 125].

The theory of the Cosserat brothers, including in the equations of medium motion the displacements and rotations of granules, permits the analysis of stress and strain distribution along the shear band thickness [119]. Inclusion of granule rotations in the theory introduces into the equations of medium motion the dimension of a single

granule as a natural consequence of the principle of conservation of momentum. The introduction in the material model of the grain size, i.e. a value with the dimension of length, permits the obtaining of a non-zero thickness of the shear band. For granule rotations to contribute to the deformation of the material, the change of average stress on a distance equal to the size of a granule should be large enough for a moment of force to appear, greater than the rolling friction [119].

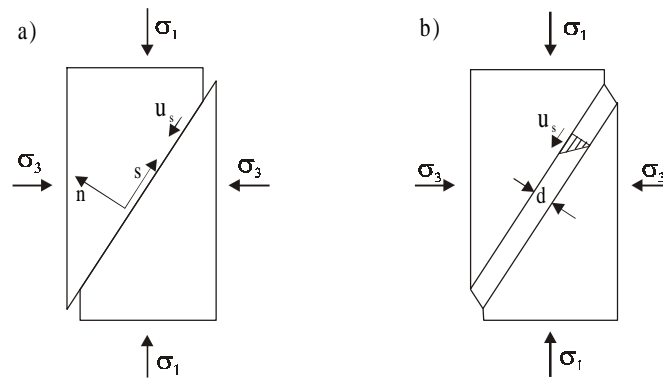


Fig. 3.16. Shear band: a) classical theory of plasticity approach, b) microstructural approach

Similar conclusions are arrived at through considerations conducted on the grounds of the microstructural approach, and from realized on their basis simulations of the behaviour of granular material in successive stages of deformation, made according to the MDEM method mentioned earlier. Iwashita and Oda [72] proved that in the course of density hardening there gradually forms a certain structure of granule contact points combining into chains along which a larger part of the main shear stress is transmitted (fig. 3.17a). In the course of the process, granule contacts formed earlier disappear to be replaced by new contacts. Due to this, the axis of the chain follows the direction of the major principal stress. Between the chains, elongated pores parallel to the chains are formed, which makes the material to become anisotropic (fig. 3.17b). Such a structure gradually becomes less and less stable, as there appears a shortage of points of support along the direction of the minor principal stress. The process leads to the exhaustion of the strength of the material. From that moment the microstructure undergoes a gradual restructuring through buckling of the long load bearing columns formed before. Limitations of the chain buckling leads to the localization of strain. As a result of the process, the well known shear band is formed. Due to the buckling of the force bearing columns, pores between the columns expand, resulting in a sudden increase in porosity. Column buckling leads to considerable rotation of the granules. A strong gradient of rotation appears, localized within the narrow space of the shear band.

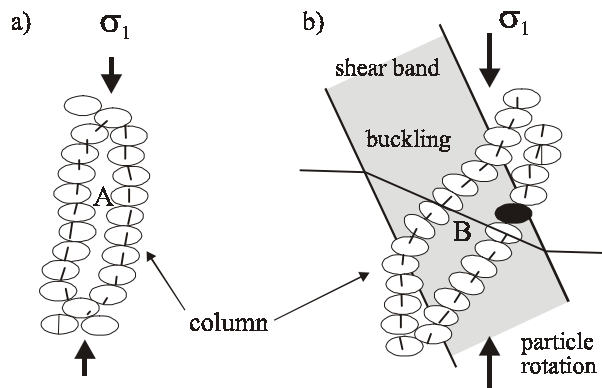


Fig. 3.17. Model of shear band formation according to Iwashita and Oda [72]

4. CLASSIFICATION OF GRANULAR MATERIALS

The concept of granular material covers a very broad class of materials, beginning with pharmaceuticals, cement and aspiration dust – through agricultural products, like e.g. cereal grain – food products, like flour, sugar, powder milk – to mineral raw materials, like e.g. gravel, stones and coal. For a variety of technological operations highly important is the wide array of such physical properties as bulk density, granulation, friction coefficient, hardness, moisture, explosiveness, sorptive and thermal properties. This creates the need for a coherent classification of such materials, to avoid the risk of errors and misunderstandings resulting from the omission of some material characteristic important for a given process. The properties of granular materials vary within a very broad range, depending on the origin of a material, the processes of production and processing applied, and on external factors and conditions. At present, two systems of classification of granular materials are most commonly used – CEMA and ISO [71]. The CEMA classification comprises bulk density, grain size, flowability, abrasiveness, and a number of other mixed characteristics. The ISO classification [71] is rather abbreviated – it comprises particle form, flowability, and several characteristics related to material transport and handling.

The popular division of granular materials according to the mean grain size D includes the following classes [169]:

- dusty (e.g. aspiration dusts, fertilizer lime) $D \leq 0.05\text{mm}$,
- powder (e.g. flour, fine meal) $0.05 < D \leq 0.5\text{ mm}$,
- granular (e.g. cereal grain) $0.5 < D \leq 10\text{ mm}$,
- nodular (e.g. gravel, wood chips) $10 < D \leq 50\text{ mm}$,
- lumpy (e.g. coal) $50 < D \leq 300\text{ mm}$,
- massive (e.g. unsorted stones) $D > 300\text{ mm}$.

Classification of materials according to the shape or form of grains, adopted by ISO [71], is as follows:

- sharp-edged, with three dimensions similar,
- sharp-edged, with one of the three dimensions clearly greater than the other two,
- sharp-edged, with one of three dimensions clearly smaller than the other two,
- round-edged, with the three dimensions similar,
- round-edged, with one of three dimensions clearly greater than other two,
- fibrous, stringy, curly, linked.

The hardness of granular materials is most frequently assessed using the 10-grade Mohs scale. The particular grades of the scale correspond to the following: 1 – talcum, 2 – gypsum, 3 – calcite, 4 – fluorite, 5 – apatite, 6 – orthoclase, 7 – quartz, 8 – topaz, 9 – corundum and 10 – diamond. In this scale, cereal grain falls between grade 1 and 3 of hardness.

Abrasiveness of granular materials is their ability to damage surfaces of equipment with which they are in contact as a result of movement over the surfaces. The degree of abrasiveness is related to the hardness, shape and size of the material grains. Chattopadhyay *et al.* [34] list four grades of abrasiveness of granular materials:

- mildly abrasive,
- moderately abrasive,
- extremely abrasive,
- very sharp, gouges soft materials like rubber.

Flowability of granular materials is related to grain size and shape, surface properties, moisture, temperature, adhesion, cohesion, and mainly on consolidation time. ISO proposes a classification of materials according to their flowability that is based on the flow function ff introduced by Jenike [76]. The function will be discussed in detail in chapter 8. Chattopadhyay *et al.* [34] supplemented that classification with two extreme categories, proposing a division comprising six classes of materials:

- fluidlike flooding
- very free flowing $ff > 10,$
- free flowing $10 > ff > 4,$
- average flowing $4 > ff > 2,$
- poor flowing $2 > ff,$
- sluggish/interlocked.

In the case of agricultural materials and food powders, apart from the classifications mentioned above attention should be paid also to a number of additional features, such as:

- friable, easily degradable,
- freezing,
- hygroscopic,
- toxic properties,
- flammable,
- explosive,
- very dusty,
- decomposes, deteriorates in storage.

The tendency of certain materials to freeze may constitute a serious problem during winter and demand for heating equipment. Explosive powders require the application of suitable construction materials, protective devices, and following fire prevention rules. In some cases wetting of transported material is applied.

5. DENSITY OF GRANULAR MATERIALS

Density, that is mass divided by volume, is one of the fundamental parameters of granular materials. Knowledge of the exact value of the density of a deposit of granular material is very important for numerous practical applications. The density of a material has a significant effect on its mechanical characteristics. It is one of the three basic parameters, along with the friction coefficient and the pressure ratio, that are used in the determination of granular material pressure against the structure of the bin or silo. It is also necessary for accurate estimation of container capacity.

With relation to their bulk density, granular materials are classified as:

- light (peat, sawdust, bran, cereal meal, dried plant material) $\rho < 600 \text{ kg m}^{-3}$,
- medium (cereal grain, fertilizers, soil) $600 < \rho \leq 1100 \text{ kg m}^{-3}$,
- heavy (mineral raw materials, sand, gravel) $1100 < \rho \leq 2000 \text{ kg m}^{-3}$,
- very heavy (minerals, stone) $\rho > 2000 \text{ kg m}^{-3}$.

5.1. Bulk density

A popular method for the determination of the bulk density is based on measurement of the mass of a granular material poured freely into a cylindrical container of constant volume, typically 0.25 or 1 dm³ [22, 137–138]. The values of bulk density of typical agricultural materials presented in Table 5.1 differ significantly from the density of those materials in silos [22, 31]. That density is a function of moisture, pressure, degree of contamination, manner and rate of filling, and falling height of the grain [135]. Cereal grain density usually varies within a relatively broad range, depending on the species and cultivar, manner of bin or silo filling, height of deposit, degree of contamination of the grain, and other factors.

Tapped density provides information on the susceptibility of a granular material to compaction through vibrations. The relevant standard provides for a measurement consisting in bringing a known mass of a granular material to the lowest volume possible through the application of vibrations of constant amplitude and frequency [138]. The tapped density of cereal grain is higher than the bulk density by several percent, and in some cases even by over twenty percent [159].

Chang *et al.* [31] showed that distributed filling of silo increases the density of granular material by from 5.1 to 9.2% as compared to filling from centrally located spout of conveyor. Stephens and Foster [155] observed increases in density of the order of 3 to 5% above the bulk density values in condensed filling from spout of a conveyor, and 7% in the case of distributed filling. Versavel and Britton [166] showed that density depends on the falling height, the degree of contamination, and on the filling rate. The researchers noted a considerable increase in density, of the order of 8-10%, and in the case of high filling rates a decrease in density. Similar relations were found by Schott and Britton [150] in laboratory studies. With increasing grain falling height the kinetic energy of the grain increases, which increases the packing density of the material [116]. That effect disappears above a certain height, due to increasing aerodynamic drag during the free fall of the grain.

Table 5.1. Bulk density, porosity and specific gravity of grain [3]

Grain	Bulk density (kg m^{-3})	Moisture (%)	Porosity (%)	Specific gravity (kN m^{-3})
Barley	618	9.7-10.7	39.5-57.6	12.1-13.3
Rape	669	6.5-6.7	38.4-38.9	11.0-11.5
Maize	721	9-15	40.0-44.0	11.9-13.0
Linseed	721	5.8	34.6	11.0
Oat	412	9.4-10.3	47.6-55.5	9.5-10.6
Rice	579	11.9-12.4	46.5-50.4	11.1-11.2
Rye	721	9.7	41.2	12.3
Soy	772	6.9-7.0	33.8-36.1	11.3-11.8
Wheat	772	9.8	39.6-42.6	12.9-13.2

In view of the wide range of variation and considerable number of factors affecting density, attempts are made at developing methods for the determination of „apparent density” that would correspond to the density of a material in a silo. Therefore, it is necessary to search for general rules applicable to the determination of the actual density of granular media in containers that would be common for as extensive a class of materials as possible. Basing on experimental results obtained so far it is recommended to estimate the density of a granular material in a silo by assuming an average density increase of 6% with relation to the density value determined from the mass of 1 hectolitre [22]. It appears, however, that application of more accurate methods for the prediction of density of granular material deposit is a necessity.

5.2. Density of consolidated material

The density of granular material is a monotonically increasing non-linear function of pressure. The function most frequently used for the description of the relation is a power, exponential or logarithmic function. Gu *et al.* [59] made a detailed analysis of empirical relationships used, determining for each the range of pressure values for which a given function best describes the change in density.

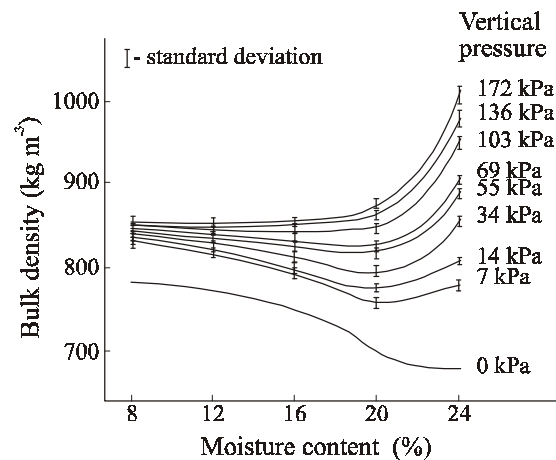


Fig. 5.1. Bulk density values for wheat as a function of moisture content and pressure [161]

In the case of materials of plant origin, another parameter – apart from pressure – that significantly affects the density of a deposit is the moisture content of the material. Thompson and Ross [161] made an in-depth study of the density of wheat grain deposit within the range of pressures from 0 to 170 kPa. They found that within the grain moisture range from 8% to 12% a half of the change in the density of the medium was attributable to reorientation of the grains, and the other half their elastic deformation. Increase in the grain moisture caused an increase in the contribution of deformation of the grains in the change of the density of the medium. At grain moisture level of 24% the contribution of deformation of the grains was about 70% of the change in density. For vertical pressure values below 100 kPa the authors found a distinct minimum of density at grain moisture levels within the range of 20-24%. With increasing pressure, the minimum shifted slightly towards lower values of moisture (fig. 5.1). The authors described the relation with a non-linear function. A similar course of the relation was determined – for corn – by Clower *et al.* [36] and by Loewer *et al.* [96]. The curve marked with the symbol 0 kPa in figure 5.1 presents bulk density decreasing with increasing grain moisture content.

Eurocode 1 [50] recommends direct application of bulk unit weight of granular materials, determined experimentally under uniaxial compression, for the calculation of pressure. It is also recommended to use the value of vertical pressure that will exist in the bottom part of the silo as the consolidation pressure. If the information is not available, pressure value of 100 kPa is recommended for use as reference pressure. Bulk unit weight determined in this manner is used for the determination of the upper limit of load. A sample of the material tested is placed in a cylindrical container with diameter D that is greater than the maximum grain size by a factor of at least 40. Height H of the sample should be in the range of $0.3-0.4D$. After the filling of the container, without any vibration and application of compacting loads, the upper surface of the sample is loaded with normal force generating the reference pressure σ_r (corresponding to maximum vertical pressure p_v or to 100 kPa). Then the top plate of the apparatus is rotated three times by 10° right and left for additional compaction of the material. Bulk unit weight is determined as the quotient of the weight of consolidated sample and its volume (Tab. 5.2).

Table 5.2. Bulk unit weight γ of consolidated granular materials according to Eurocode 1 [50]

Granular material	Bulk unit weight γ (kN m ⁻³)
Barley	7.0-8.0
Flour	6.5-7.0
Maize	7.0-8.0
Soybeans	7.0-8.0
Sugar	8.0-9.5
Wheat	7.5-9.0

6. COMPRESSIBILITY AND ELASTICITY

Granular materials in storage get compacted under their own weight and/or under external loads. Compaction increases through a change in packing and through deformation of the grains. The resultant strain ϵ_p is the sum of reversible deformation ϵ^e , caused by the elastic deformation of grains and thus disappearing with the removal of the load, and of the permanent deformation ϵ^p related to the change of mutual orientation of grains:

$$\epsilon_p = \epsilon^e + \epsilon^p. \quad (6.1)$$

Figure 6.1 presents the curve of cyclic loading of wheat grain sample under the conditions of uniaxial compression. Irrespective of the type of material tested

(cereal grain, sand, soil), the stress-strain curves display qualitative similarity [70, 94, 114]. The wide hysteresis loop during the first loading (curve 0AB) is dominated by plastic deformation with less contribution of elastic strain. During repeated loading of the sample, at a load value below the previous maximum, the material is stiffer than before (curve BC), while after exceeding the maximum value of the previous loading (section CD) the stiffness of the material decreases and the material behaves as if never subjected to loading. The behaviour of the material along the curve sections AB, BC, DE can be described by the modulus of elasticity K and along the curve 0ADG by the modulus of compressibility E_i . The values of the moduluses are strain dependent.

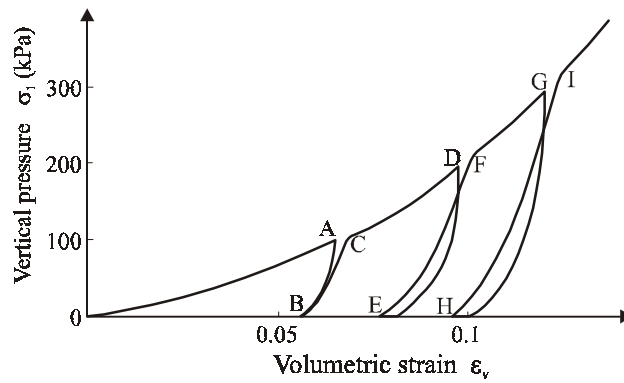


Fig. 6.1. Stress-strain relation during loading-unloading cycles of wheat grain in uniaxial test

Zhang *et al.* [174] determined the modulus of volumetric elasticity K and the modulus of plasticity H_o of wheat grain in bulk in the triaxial compression test at constant value of minor principal stress σ_3 from the following power relations:

$$K = K_o P_a (\sigma_3 / P_a)^A, \quad (6.2)$$

$$H_o = B P_a (\sigma_3 / P_a)^C, \quad (6.3)$$

where:

- A – exponent of the modulus of elasticity,
- B – constant of the modulus of plasticity,
- C – exponent of the modulus of plasticity,
- K_o – constant of the modulus of elasticity,
- P_a – atmospheric pressure,
- σ_3 – minor principal stress.

The modulus of compressibility E_i was determined on the basis of the resultant material strain, sum of reversible (elastic) and irreversible (plastic) strain [174]:

$$\frac{1}{E_i} = \frac{1}{K} + \frac{1}{H_o}. \quad (6.4)$$

Examples of experimental values for wheat grain are presented in Table 6.1 [174].

Table 6.1. Modulus of compressibility, elasticity and plasticity of wheat grain [174]

Minor principal stress (kPa)	Modulus of compressibility E_i (MPa)	Modulus of elasticity K (MPa)	Modulus of plasticity H_o (MPa)
20.7	3.3	8.8	5.3
34.5	4.5	11.1	7.7
48.3	6.4	13.6	12.1
62.1	7.9	16.2	15.3

Volumetric elasticity of granular material is closely related to the elasticity of individual grains. Modulus of elasticity of seeds of individual plant species varies within a broad range. In the case of wheat, Young modulus determined for cylindrical samples cored from the grain endosperm falls within the range of 0.2-3 GPa depending on the cultivar [55] (figure 6.2). With increasing grain moisture, Young modulus decrease to stabilize at moisture levels above 22% [41]. Modulus of elasticity depends on the protein content and on the type of endosperm [84]. For vitreous grains, the values of the modulus are about 30% higher than for mealy grains [58, 171].

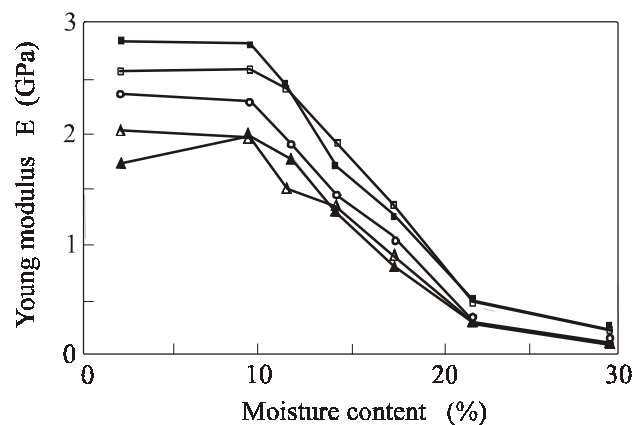


Fig. 6.2. Young modulus of wheat endosperm as influenced by moisture content [55]

Multiple wetting and drying of grain causes internal cracks in the grain endosperm structure, which reduces the values of modulus of elasticity even by 40% [171]. In the case of corn kernels, modulus of elasticity decreases with increasing moisture, from 600 MPa at moisture content of 10% to 50 MPa at moisture of 35% [86]. Modulus of elasticity of rape seeds at moisture content of 6-8% is about 40 MPa, and with increasing seed moisture drops to the level of several MPa [158]. Modulus of elasticity of pea seeds falls within the range of 100-400 MPa depending on the cultivar and the seed moisture content [43].

Direct linking of the modulus of volumetric elasticity of a granular material with the elastic properties of elementary grains by means of a quantitative mathematical formula is extremely complicated. Theoretical studies are usually focused on the search for general conditions that would permit the determination of modulus of volumetric elasticity of a system of elastic granules. Walton [168] derived the relationship of effective modulus of volumetric elasticity of a random system of spheres K on the basis of elastic reactions taking place within the area of elementary contact:

$$K = K_1 E^{\frac{2}{3}} |p|^{\frac{1}{3}} \quad (6.5)$$

where:

$$K_1 = \frac{1}{6} \left(\frac{3v^2 N_t^2}{\pi^2 (1-v^2)^2} \right)^{\frac{1}{3}},$$

$$v = \frac{4\pi R^3 n}{3V},$$

E – Young modulus,

K_1 – material parameter,

n – number of granules in volume V ,

N_t – mean number of contacts per individual granule,

p – pressure,

R – radius,

V – volume,

v – solid fraction,

ν – Poisson constant.

For the description of the stress-strain relation within the area of elementary contact of the bodies he applied the Hertz formula that is commonly used for the case of contact of an elastic sphere with flat rigid surface [104, 105 162].

Relating the modulus of elasticity of a material deposit with the Young modulus and Poisson coefficient of the granules of the medium and with the average pressure and the material packing parameters permits correct physical interpretation of elastic reactions in a bulk of granular material. Studies by Horabik and Molenda [65] showed that the Hertz formula permits also the description of the behaviour of grain within a broad range of moisture content (fig. 6.3). At the current stage of the research, the application of the relation derived by Walton for a big number of bodies like granular plant material permits only qualitative analysis of the phenomenon.

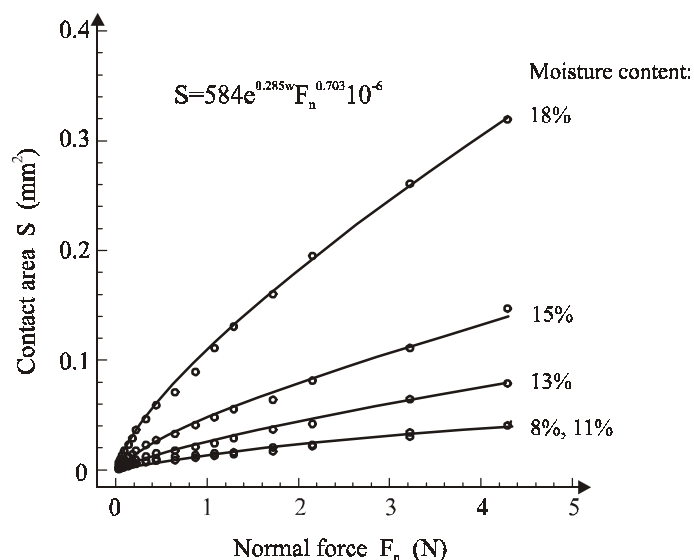


Fig. 6.3. Contact area of wheat grain with smooth surface as influenced by moisture content and normal load [65]

Granular material volumetric elasticity has a very strong influence on the pressure transmitted by the granular material onto the structure of the container or silo [98, 99]. For the purpose of solving practical problems, an empirical value of modulus of elasticity of granular material in bulk is usually adopted, constant for a given range of pressure values [139, 148]. In the case of granular materials of plant origin, the value of the modulus is strongly related to moisture content. Stasiak and Molenda [154] showed that the modulus of elasticity of wheat grain, determined under the conditions of uniaxial compression at the vertical pressure of 100 kPa and grain moisture content of 10% was 22 MPa, and at grain moisture content of 20% decreased to 11 MPa, while Poisson constant ν did not depend on grain moisture and oscillated around 0.2. Modulus of elasticity of corn kernels in bulk determined by Frontczak and Metzger [53] in uniaxial compression test at

vertical pressure within the range of 100-240 kPa decreased from 14 MPa to 6 MPa at moisture content increasing from 7% to 23.5%.

The Eurocode 1 [50] recommends to use two different values of modulus of elasticity: loading and unloading effective elastic moduli. Loading modulus describes compressibility (eq. 6.4) while unloading modulus describes elastic reaction of material (eq. 6.2). The unloading effective elastic modulus is usually much higher than the loading modulus. In assessments where use of a low elastic modulus may be deleterious to the structure (e.g. thermal differentials), the unloading modulus should be used. Where the high value of elastic modulus of the solid leads to safe design of the structure (e.g. in thin-walled rectangular silos) the loading modulus should be used.

Elastic parameters presented in the Appendix were determined using a model describing the total vertical strain in granular materials under loading developed by Sawicki [148]. The model equation is based on the elasto-plastic approach and assumes that during loading both reversible (elastic) and irreversible (plastic) strains develop in the sample. Plastic ε_z^p and elastic ε_z^e strains develop in the material during loading:

$$\varepsilon_z = \varepsilon_z^e + \varepsilon_z^p \quad (6.6)$$

$$\varepsilon_z = D_1 \ln(1 + D_2 \sigma_{z0}^\alpha) + \frac{\sigma_{z0}}{E} \left(1 - \frac{2\nu^*}{1-\nu^*} \right) \quad (6.7)$$

where:

ε_z - total vertical strain,

ε_z^p - plastic vertical strain,

ε_z^e - elastic vertical strain,

σ_{z0} - mean vertical pressure on the top cover,

E - modulus of elasticity,

ν^* - equivalent of Poisson's ratio for loading $\nu^* = K_o / (1 + K_o)$,

K_o - slope of straight line $\sigma_x = K_o \sigma_z$,

D_1, D_2, α - model parameters.

K_o , which is used to calculate the Poisson's ratio equivalent ν^* during loading, is the ratio of the horizontal stress σ_x and vertical stress σ_{z0} during consolidation of the sample. During this phase of compression the horizontal deformation which is the sum of plastic and elastic horizontal strains, is zero ($\varepsilon_x = \varepsilon_x^e + \varepsilon_x^p = 0$). D_1 and D_2 are compaction coefficients. Originally Sawicki [148] assumed the value of the exponent α to be equal to 3/2, but in examination of Stasiak and Molenda [154] the value of α was treated as a variable to obtain a better fit of the experimental results to the model curve.

Two phases of the unloading can be observed (see figure 6.4). The first phase is characterized by a purely elastic deformation and was used in the determination of elastic constants, the modulus of elasticity E and Poisson's ratio ν . The second stage of unloading is characterized by both elastic and plastic deformations. It was assumed that the material reversible response is governed by Hooke's law:

$$\varepsilon_x^e = \frac{1}{E} [(1-\nu)\sigma_x - \nu\sigma_{z0}] \quad (6.8)$$

$$\varepsilon_z^e = \frac{1}{E} [\sigma_{z0} - 2\nu\sigma_x] \quad (6.9)$$

During the first phase of unloading (path BC) granular material exhibits a linear relationship which is characteristic for elastic deformation. Assuming that $\varepsilon_x^e = 0$ from (Eq. 6.8) $\sigma_x/\sigma_{z0} = (\nu/1-\nu)$ is obtained and applying the assumption that $\varepsilon_z = \varepsilon_z^e$ to (Eq. 6.9) ε_z may be expressed as below:

$$\varepsilon_z = \frac{\sigma_{z0}}{E} \left(1 - \frac{2\nu^2}{1-\nu} \right) \quad (6.10)$$

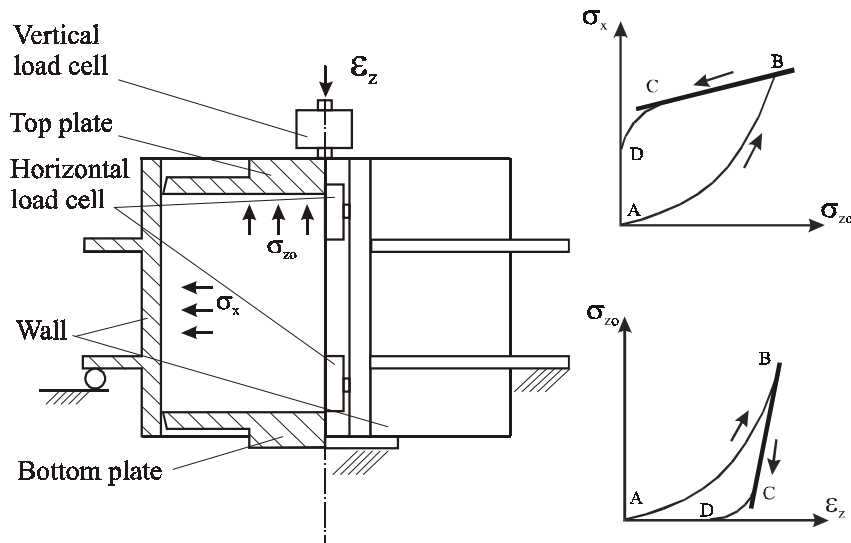


Fig. 6.4. Uniaxial compression tester and determination of modulus of elasticity [154]

Elastic constants were determined using experimental results measured during the linear phase of unloading. The ratio of horizontal stress σ_x to vertical stress σ_{z0} was assumed constant (elastic state of stress) and the slope of the straight portion

of the curve defined by A , where $A = \sigma_x / \sigma_{z0} = \nu / (1 - \nu)$ was determined. Values of A for different granular materials were estimated using linear regression procedure applied to experimental values of stresses (see figure 6.4). Knowing A , values of Poisson's ratio ν were calculated as:

$$\nu = \frac{A}{1 + A} \quad (6.11)$$

Values of modulus of elasticity E were estimated using relationship $\varepsilon_z(\sigma_{z0})$ (Eq. 6.10) with experimental values of ε_z and σ_{z0} , and ν determined as described above.

The apparatus utilized was an uniaxial tester whose walls were formed by two semicircular halves cut along the axis (see figure 6.4). The two semicircular halves were connected with four load cells installed in pairs on the two connection lines, restoring cylindrical shape of the wall. Bottom and top plates of the chamber transmitted the vertical load through the load cells. The experimental setup allowed for the determination of mean lateral pressure σ_x , mean vertical pressure on the bottom σ_z , and the mean vertical pressure acting on the top plate σ_{z0} . The surface of the cylinder walls was smooth while the surfaces of the top and bottom plates were rough.

During testing the granular material was poured into the test chamber, without vibration or any other compacting action. The test sample was 80 mm high and 21 cm in diameter. The bedding was loaded in compression to the reference vertical stress, σ_{z0} of 100 kPa using a universal testing machine at a constant loading rate of 0.35 mm min⁻¹. The displacement of the sample was measured using an inductive transducer having an accuracy of 0.01 mm. Loading was followed by unloading which took place at the same speed of deformation until σ_{z0} of 0 kPa was reached.

7. STRENGTH PARAMETERS

7.1. Methods and apparatus

Two test methods are recommended by Eurocode 1 [50] for the estimation of strength parameters (angle of internal friction φ and cohesion c): direct shear test and triaxial compression test.

7.1.1. Direct shear test

For this test reference may be made to the ASTM D6128 [9], but the parameters derived following that standard are not identical with those defined in Eurocode 1. The test apparatus is a cylindrical shear cell as shown in figure 7.1.

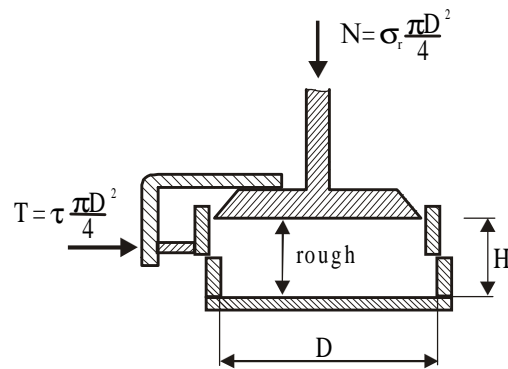


Fig. 7.1. Jenike shear cell

The up-to-date method of testing flow properties is based on the concept of Jenike, first published in 1961. The apparatus consists of the lower ring, the upper ring and the base. The chamber of the apparatus, comprised of the lower and upper ring, is filled with a sample of granular material. The lid is loaded with vertical force N and horizontal force is applied on a bracket attached to the lid. Shear tests performed with identically consolidated samples under different normal loads give maximum shear forces T for every normal force N . Ratios of forces N and T to the shear cell cross-section area give normal stress σ and shear stress τ . Characteristic of τ versus σ (see fig. 8.2) represents the maximum shear stress that a sample can support under a certain normal stress and is called yield locus. Material bulk density ρ is the parameter of the yield locus. With an increase in normal consolidation stress, bulk density increases and the yield locus moves upwards. Each yield locus terminates at a point E in the direction of increasing normal stress σ . The conditions of point E are called steady state flow, that is the flow with no change in bulk density and stresses.

The original procedure of the shear test was as follows:

1. A prescribed mass of material was placed into the compartment of the apparatus;
2. Vertical consolidation reference pressure, σ_r , was applied for a prescribed period of time;
3. Sample was sheared until an asymptotic value of frictional force (steady flow) was approached, thus values of σ_r and τ_a stresses at the terminus of yield locus were determined;
4. Steps (1) and (2) were repeated;
5. Sample was sheared until 95% of an asymptotic value of frictional force was achieved;

6. Vertical consolidation reference pressure, σ_r , was released to zero;
7. Vertical pressure, σ_{z1} , was applied for a period of static holding;
8. Sample was sheared under pressure, σ_{z1} , until the end of the prescribed shear path;
9. Steps (4) to (8) were repeated for vertical pressures of σ_{z2} and σ_{z3} , and thus three points on the yield locus were obtained.

The Jenike method allows the determination of: cohesion c , angle of internal friction φ and effective angle of internal friction δ (see $\varphi = \varphi_1$ and $\delta = \varphi_1$ in fig. 7.2).

Eurocode 1 [50] recommends using a simplified Jenike method (including consolidation and shearing of the sample) for the determination of strength parameters (fig. 7.2). The shear cell diameter D should be at least 20 times the maximum particle size and not less than 40 times the mean particle size. The height H should be between 0.3 and 0.4 D . The maximum particle size is limited to ensure that interaction of material with the cell wall will not influence the measured property. The sample should be poured into the test cell, without vibration or other compacting forces, and the consolidation stress σ_r applied. A top plate should be rotated clockwise and anticlockwise about the vertical axis several times through an angle of at least 10 degrees to consolidate the sample.

The Eurocode 1 shearing procedure is as follows:

1. The reference stress σ_r should be approximately equal to the vertical stress in the stored material.
2. Shearing of the sample should be carried out at a constant rate of approximately 0.04 mm min^{-1} .
3. To calculate strength parameters of granular material maximum shear strength τ should be used that developed at or before the horizontal displacement had reached the value of $\Delta L = 0.06D$.
4. At least two tests should be carried out as defined in (5) and (6) below.
5. The first sample should be sheared under a normal load causing the reference stress σ_r to obtain the failure shear stress τ_a .
6. The second sample should first be preloaded under a normal load causing the stress σ_r and just brought to shear failure as for the first sample. Shearing should be stopped and the applied shear load reduced to zero. The normal load on the second sample should then be reduced to a value causing approximately half the consolidation stress ($\sigma_b = \sigma_r/2$) and sheared again to obtain the failure shear stress τ_b .

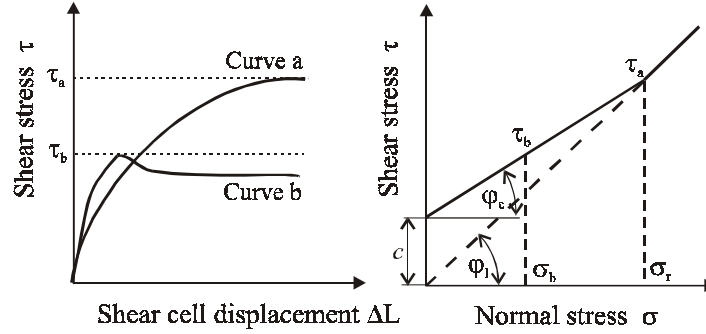


Fig. 7.2. Determination of shear strength parameters

Two parameters of the material – cohesion c and angle of internal friction φ should be used to define the effects of a stored solid's strength on silo pressures after the silo has been filled. The loading angle of internal friction φ_1 for the stored solid should be calculated as:

$$\varphi_1 = \arctan(\tau_a/\sigma_r). \quad (7.1)$$

The cohesion c that develops in the stored solid under the reference stress σ_r should be calculated as:

$$c = \tau_a - \sigma_r \tan \varphi_c \quad (7.2)$$

in which:

$$\varphi_c = \arctan \frac{\tau_a - \tau_b}{\sigma_r - \sigma_b}, \quad (7.3)$$

where:

φ_c is the unloading internal friction angle for an over-consolidated material. The value of cohesion c depends strongly on the consolidation stress, so cannot be regarded as a fixed property of the solid. For a cohesion-less material (where $c = 0$), frictional strength should be described only by the angle of internal friction φ_1 that is equal to φ_c .

As an alternative to direct shear test, Eurocode 1 recommends triaxial compression test for the estimation of frictional strength parameters of granular material.

7.1.2. Triaxial compression test

Determination of strength parameters of wheat at five levels of moisture content of 10, 12.5, 15, 1.5 and 20% was performed using direct shear and triaxial compression tests. The parameters were determined following Eurocode 1 with a cylindrical shear box, 210 mm in diameter and with 80 mm bedding height. The sample was

poured into the box without vibration and the reference stress of 100 kPa was applied. A top plate was rotated backwards and forwards three times through an angle of ten degrees to consolidate the sample. Following consolidation, the sample was sheared under normal stress equal to reference stress, at the rate of 10.8 mm min^{-1} . Second sub-test was performed for consolidation reference stress of 100 kPa and test load value of normal stress of 50 kPa. Three replications were performed. Triaxial compression tests with a sample 15 cm in diameter and 30 cm high were conducted on wheat to compare results with the results of direct shear test. Comparison of angles of internal friction of wheat obtained in direct shear test and those obtained in triaxial compression test is shown in figure 7.3.

Mean values for five levels of moisture content taken as one sample were not significantly different except the values for 10% of m.c. To obtain such an agreement of the results of two testing methods, the procedures had to be modified. In the case of direct shear test the shear deformation was extended up to 0.10 of sample diameter instead of 0.05 as recommended by Eurocode 1. In the case of triaxial compression test the sample was compacted by tapping during filling, up to a density equal to that of the sample in direct shear test. No clear explanation may be given for the discrepancy of results of direct shear test and triaxial compression test at 10% of grain moisture content. The probable reason is difference in the mechanism of deformation in the two tests combined with distinctly lower (than at higher levels of moisture content) grain-on-grain coefficient of friction.

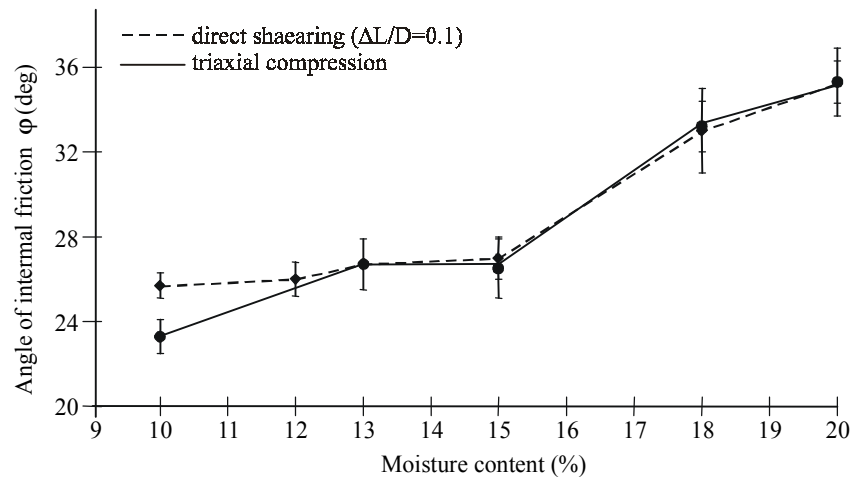


Fig. 7.3. Mean values and 95% confidence intervals of the angle of internal friction of wheat determined with the direct shear test and the triaxial compression test

7.2. Factors influencing angle of internal friction of cereals

7.2.1. Moisture content of the material

Grain moisture content has deep influence on the mechanical properties of grain in bulk [67] as it modifies surface properties of seed-coat as well as the properties of kernel endosperm. Changing moisture content of grain influences shear stress-strain characteristics, and consequently the determination of strength parameters: the angle of internal friction φ and the cohesion c . Figure 7.4 presents data obtained in direct shear test for wheat of moisture contents of 12, 20 and 22%.

The results show that for wheat at 10% of m.c. (fig. 7.4 a) experimental curves stabilized or attained maximum below the 0.05 $\Delta L/D$ level of strain required by Eurocode 1. An increase in grain moisture content resulted in an increase in shear path to attain a stable level. In the case of grain of 20% moisture content (fig. 7.4 b) and 100 kPa of normal pressure the test curve stabilized at a stress level clearly above the 0.05 of the sample diameter. For grain moisture content of 22% (fig. 7.4c) shear stress stabilized only for the two lowest levels of normal stress and for strain of approximately equal to 0.05 $\Delta L/D$ that precluded determination of the strength parameters. These results show that to determine strength parameters of wet grain an extension of shearing path up to 0.10 of sample diameter is necessary.

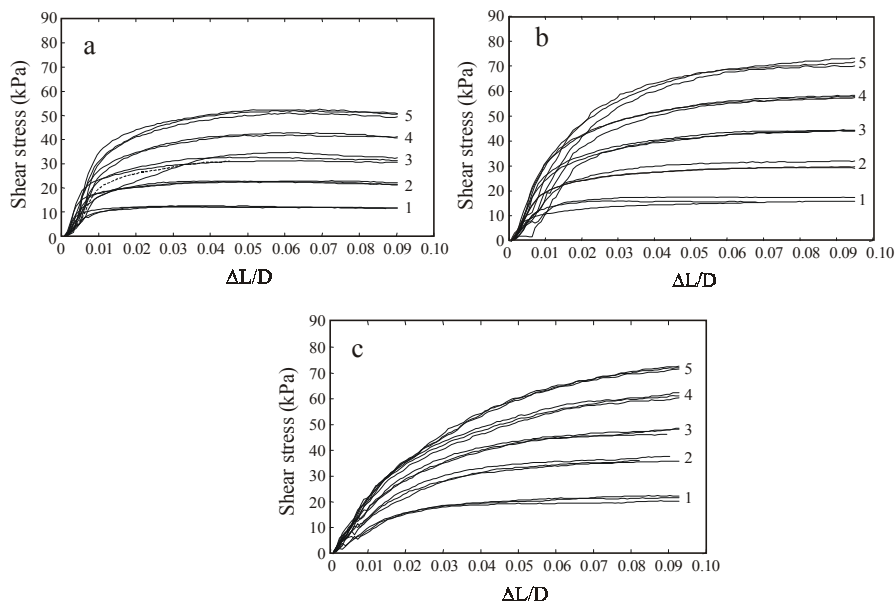


Fig. 7.4. Shear stress τ versus ratio of displacement to the sample diameter $\Delta L/D$ for wheat of moisture contents of : a) 12%, b) 20% and c) 22%, for normal stress σ_n of: 1-20 kPa, 2-40 kPa, 3-60 kPa, 4-80 kPa and 5-100 kPa

7.2.2. Bulk density

Stress-strain behaviour of granular material depends on the bulk density of the sample. Dense samples dilate during shear test while loose samples decrease in volume. In dense samples shear stress attains a peak value, and with continuing shear displacement it drops back to a lower ultimate value and remains at that constant level during further shear. In the loose state most granular materials tend to decrease in volume when subjected to shear under constant normal load. For such samples shear stress gradually increases until it reaches ultimate value. Thereafter, with increasing displacement it remains stable. The density at which material is sheared without change in volume is termed, after Cassagrande [30], *the critical density*.

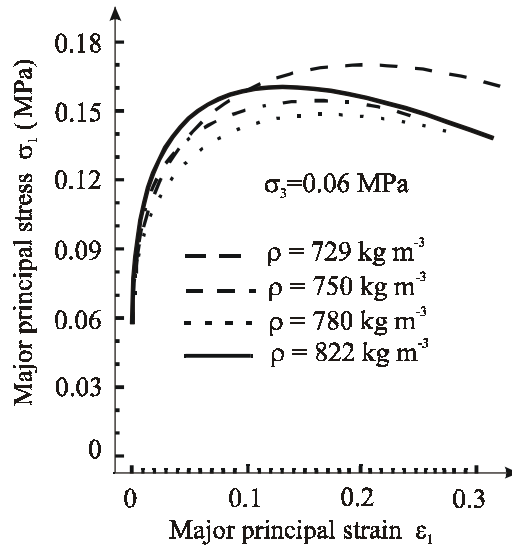


Fig. 7.5. Relationships of stress versus strain obtained in triaxial compression test for wheat grain of moisture content of 13% and four levels of bulk density

Figure 7.5 illustrates relationships between axial total stress and axial strain in triaxial compression of wheat grain of 13% in moisture content at four levels of bulk density [101]. The graphs show that increase in density ρ resulted in a quantitative change in material properties. For denser samples higher were both the maximum value of σ_1 and the maximum value of axial strain ϵ_1 . For the sample of bulk density of 822 kg m^{-3} the axial stress reached maximum value $\sigma_{1\text{max}}$ for ϵ_1 of 0.1. For the sample of the lowest density (of 729 kg m^{-3}) the stress $\sigma_{1\text{max}}$ was attained at ϵ_1 of 0.22, thus at the strain about four times higher than ϵ_1 of 0.06 recommended by Eurocode 1.

7.2.3. Time of consolidation

The time of consolidation is one of the most important factors influencing mechanical properties of powders. For example, a long period of storage of powders in bags or in silo can lead to caking when the material becomes nearly solid, causing serious problems in handling. In the case of food powders moisture is the most severe factor causing caking. In order to determine the effects of time of consolidation, the sample has to be compressed for the prescribed period of time before the shear test is performed.

Figure 7.6 shows the results of determination of strength parameters of wheat meal following Eurocode 1 procedure. The sample was sheared immediately after consolidation by twists or remained under reference load for additional two hours. Time consolidation resulted in an increase of the angle of internal friction from $31^{\circ} \pm 4^{\circ}$ to $43^{\circ} \pm 2^{\circ}$. After the time consolidation, the sample usually returns to its original state if no chemical or physical changes have taken place. In such a case the material may be used for the measurement of the next point of the $\sigma(\tau)$ characteristic. This may be verified by running normal instantaneous test procedure. If any change in strength properties occurs after the time consolidation, this points out to chemical or other irreversible changes and a new sample should be taken for determination of the next point of the characteristic.

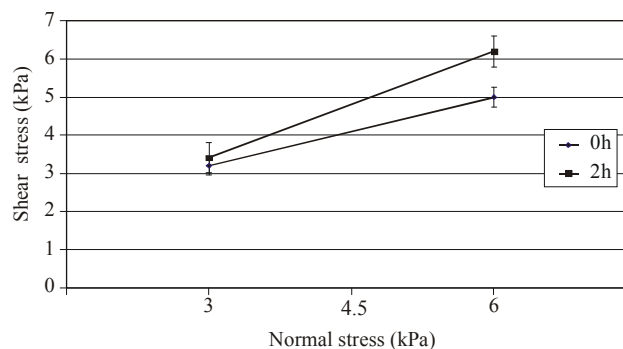


Fig. 7.6. Shear stress versus normal stress relationship from direct shear test for wheat meal without time consolidation and consolidated for two hours

7.2.4. Method of sample deposition. Anisotropy of packing

The angle of natural repose Φ and the phenomenon of grains lying nearly along the generatrix of the formed cone was used for producing the preferred grain orientation. Rye grains were poured through a funnel into the shear box inclined to horizontal at an angle β as shown in figure 3.1. The outlet of the funnel was placed

near the box wall and lifted along the wall generatrix so that the outlet was constantly approximately 20 mm above the surface of gathered grains. The grain was allowed to slide down the surface of natural repose to the front side of the box. Any change in the angle of inclination of the shear box to the horizontal resulted in a change of preferred inclination γ of long axes of grains to the bottom of the box.

Examination of an influence of the angle of preferred grain orientation on the shear stress-strain characteristic was performed under the normal pressure of 100 kPa. Samples were prepared so that the preferred orientation of grain formed angles, γ , of inclination to the shearing direction of: 0, 10, 20, 30 and 40 degrees. To preserve the packing structure of the bedding no additional consolidation was applied. The angle of preferred orientation of grains was found to influence strongly the stress-strain characteristics as shown in figure 7.7. The strongest was the sample with γ of 40° showing maximum shear stress τ_{\max} of approximately 50 kPa, while the lowest τ_{\max} of approximately 30 kPa was found in the case of $\gamma = 0^\circ$. The probable reason for the observed difference of behaviour is the distribution of contact normals.

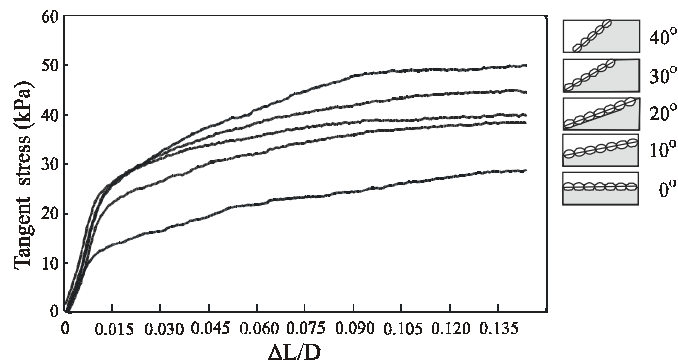


Fig 7.7. Relationships of shear stress versus ratio of displacement to the sample diameter $\Delta L/D$. Samples of rye with an angle of preferred inclination of kernels long axes to horizontal ranging from 0 to 40 degrees

Oda [126] suggested that, for a two dimensional system, the distribution of contact normals may be approximated by an ellipse. The major axis of such an ellipse is initially oriented normal to the bedding plane. The preferred orientation of the long axes of the particles is parallel to the bedding plane. In the process of biaxial deformation the distribution of the contact normals changes so that a greater number of contact normals tend to orient themselves in the direction of contact force.

Testing with grain samples deposited in various ways and subsequently consolidated by twisting (as recommended by Eurocode 1 [50]) did not show any differences in stress-strain characteristics, and consequently in obtained values of

the angle of internal friction. This result shows that the consolidation procedure of Eurocode 1 erased all stress history similarly to pre-shearing to steady-state as recommended by Jenike [74].

7.2.5. Surface properties of particles

The inter-particle friction is an obvious component of shear strength and in 1960's and 70's attempts were undertaken to find a relationship of the two effects. Rowe [144] suggested that the primary task was to separate the strength component of particle structure from that of inter-particle friction. This author derived relationships of strength limits for loose and dense sands that gave "quite close" agreement over the range of the angle of inter-granular friction φ_{μ} from 17° to 39° for cohesion-less soils. Apart from φ_{μ} and density, Rowe considered measurement technique for the stress state of deformed sample and found that for dense sands triaxial compression and direct shear gave similar results. Fedá [51] summarized results of efforts undertaken up to 1975. No substantial progress in theoretical description of internal friction took place after that time. The structural component (or packing structure) of internal friction remains difficult to describe and monitor, but these days may be treated by DEM. Analysis of force distributions in three-dimensional granular assemblies performed by Blair *et al.* [20] regarded the significance of inter-particle friction. The authors varied the coefficient of static friction between grains in such a way that for rough beads it was three times higher than for smooth ones. The resultant force distributions for rough beads were not significantly different from the distributions for the smooth beads. The tests have shown that particle deformation is the key factor for intergranular force distribution. Results of Blair *et al.* show that the phenomenon of internal friction still remains far from a conclusive description.

7.2.6. Formation of shear bands

Granular materials are deformed in many ways during processing. For a small strain the deformation is usually uniform. For a larger strain the deformation localises into a narrow region of shearing band. This region separates almost rigid blocks of a granular material. An effective rupture zone called a boundary layer or shear zone forms along the rough or corrugated wall in a silo with plug flow when friction between wall and grain is higher than internal friction of grain [119]. There is always a shear zone of a width equal to a few particle diameters in which the velocity changes rapidly from that in the bulk to that at the wall. The thickness of the boundary layer was found to be dependent on the granular material. Zhang *et al.* [177] examined shear zones in wheat sliding against corrugated steel surface. The lower boundary of the shear zone was estimated at 4.5 mm below corrugation peaks

and the upper boundary was 18.5 mm above the corrugation peaks. The dilation in the boundary layer resulting from shearing during discharge gives rise to an overpressure. The overpressure is independent of silo scale causing a decrease in the relative overpressure with increased silo size.

The shear zone in granular material has recently become the object of wider interest of researchers. The determination of the thickness of the shear zone is important for the estimation of forces transferred from the granular material to the structure. The thickness of the shear zones depends on the wall roughness, the grain diameter, the specimen size and the boundary value problem considered [160]. The relation between shear band thickness and grain size has profound implications for investigations of progressive failures within granular solids. According to direct experimental observations of Roscoe [143], the width of shear bands is about 10 times the average grain diameter. Investigations concerning the shear band formation are mainly based on computer simulations or theoretical modelling. The thickness of fully developed shear band was found to be approximately 16 times the mean grain diameter. Only a few researchers investigated experimentally the formation of the shear band in bulk of grain [109, 122, 177].

Triaxial compression tests [64] were performed to obtain information on the displacement distribution of particles inside the shear band. The sample was 30 cm high and 15 cm in diameter. The volume of the sample was divided into 30 cylindrical regions using two different colours of seeds: stained and not stained mustard seeds. Each region was 3 cm high and 3 cm thick. In the vertical direction the sample was divided into three cylindrical coaxial regions by inserting two cylindrical moulds of diameters of 3 cm and 9 cm into the sample mould. Layers of seed of 3 cm in height were poured into each of the three cylindrical regions of the sample. Ten layers of stained and not stained seed were poured into each column of the sample. Vertical cross-section of the sample of triaxial compression at $\varepsilon_1 = 0.17$ with the deformed meshes indicated is shown in figure 7.8. Orientation angle of the shear zone α and its thickness were also indicated in figure 7.8. The shear zone was oriented at an angle of:

$$\alpha = \frac{\pi}{4} + \frac{\varphi}{2} \quad (7-4)$$

with the horizontal axis (direction of the minor principal stress σ_3) as predicted by the Mohr-Coulomb theory where φ is the angle of internal friction.

Average value of the angle of internal friction for stained and not stained seed was 26° . Distributions of displacement across the shear band, at axial strain ε_1 of 0.1 and 0.17, are shown in figure 7.9 and 7.10. Vectors connecting the line of original and deformed mesh represent the distribution of displacement across the

shear band. Vertical component of the vector, u_{η}/D , represents the shear displacement, ΔL_s , (related to grain diameter D) and horizontal component represents the normal displacement, ΔL_n . The thickness of the shear band was determined from the width of the ramp in the η direction [64]. The thickness of the fully developed shear band was found to be 15 times the average grain diameter.

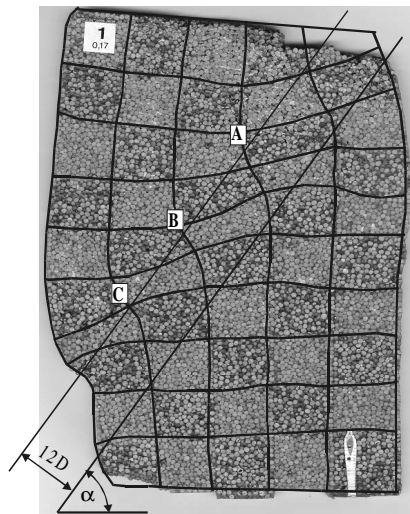


Fig. 7.8. Cross-section of mustard seeds sample deformed in triaxial compression test showing localization of deformation as shear band

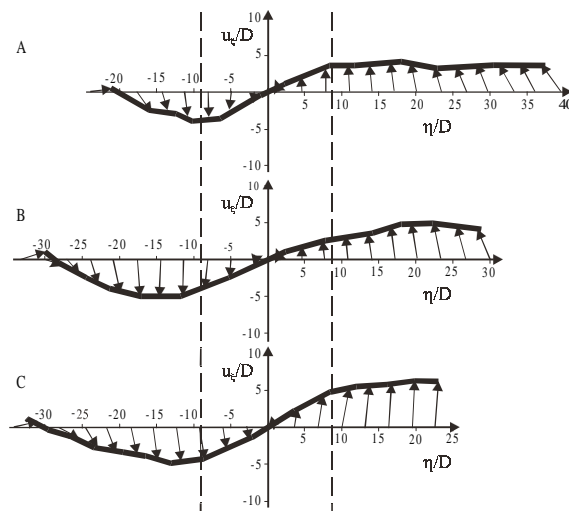


Fig. 7.9. Displacement distribution across shear band $\varepsilon_1 = 0.1$ [64]

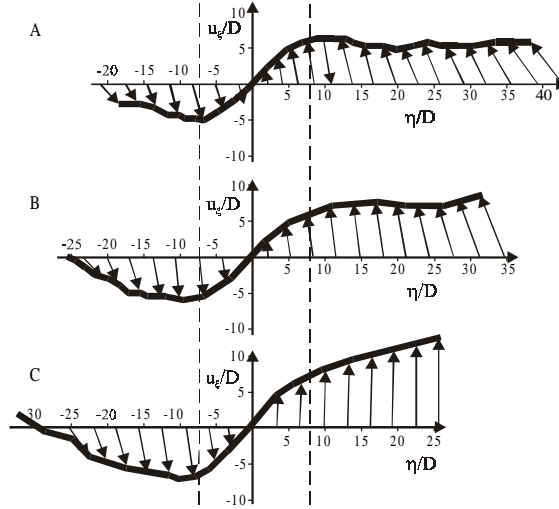


Fig. 7.10. Displacement distribution across shear band $\varepsilon_1 = 0.17$ [64]

7.2.7. Correction of change in sample cross-section area

Increase in moisture content of grain results in an increase in susceptibility of grains to deformation. Grain bedding of higher moisture content requires larger displacement to attain critical state than dry grain. As a result, the surface area of cross-section of the sample perpendicular to σ_1 increases as well. This in turn leads to an increase in measurement error of the angle of internal friction because σ_1 is calculated as a ratio of vertical force and undeformed cross-section area of the sample [101]. Correction was introduced to account for change in the sample cross section area. Assuming that volume of the sample remains constant during the test:

$$V = H(1 - \varepsilon_1)S_1 = HS = \text{const.} \quad (7.5)$$

mean surface area S_1 of cross-section of deformed sample may be expressed as a function of strain ε_1 :

$$S_1 = \frac{S}{1 - \varepsilon_1} \quad (7.6)$$

Mean surface area obtained in this way was used to determine the corrected value of higher principal stress σ_{1k} :

$$\sigma_{1k} = \sigma_3 + \frac{S(\sigma_1 - \sigma_3)}{S_1} = \sigma_3 + (\sigma_1 - \sigma_3)(1 - \varepsilon_1), \quad (7.7)$$

that was used for the determination of the angle of internal friction.

8. FLOW FUNCTION

In the early 1960s the angle of repose was used as an index of flowability of granular material. In 1961 [74] Jenike published his best known work in which he proposed direct shear test for estimation of flowability, while his analytical method provided a physical interpretation of test results. After Jenike's recommendation, shear testing to determine the flow function has been widely accepted by researchers and practitioners and still remains in use. The concept of flow function may be explained by a theoretical experiment as follows. Let us consider a cylindrical sample of material compacted under major principal stress, σ_1 , in a container with frictionless walls (see fig. 8.1). After completing the compaction, the container is removed and the vertical compressive load required to just crush the sample is measured; that is equal to the unconfined yield strength of the material, σ_c .

Contrary to the conditions of the shear test, steady state flow cannot be reached during consolidation, thus the Mohr circle will be smaller. As a result, both density ρ_b and unconfined yield strength σ_c will be smaller compared to the yield locus obtained in direct shear testing for strength. The experiment may be repeated for several values of consolidating pressure and pairs of σ_1 , σ_c are obtained. A plot of σ_1 against σ_c is termed the flow function for the considered material. The slope of the linearized flow function:

$$ff = \sigma_1 / \sigma_c \quad (8.1)$$

is termed flowability.

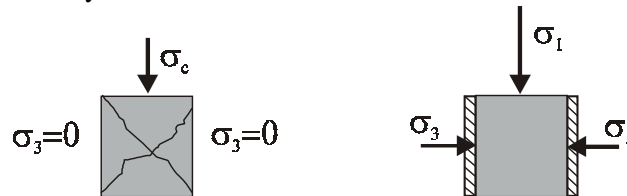


Fig. 8.1. Unconfined yield strength σ_c .

In reality the test as illustrated in figure 8.1 would be very difficult to perform for materials of low cohesion, as a majority of industrial granular materials are. In practice shear tests are used to determine the flow function. The characterization of flowability of granular materials by shear testing began with the theory and apparatus proposed by Jenike [74]. Since that time several other methods were proposed, but analysis of results of shear test remained essentially unchanged. Yield loci are determined as shown in figure 8.2 [151, 163].

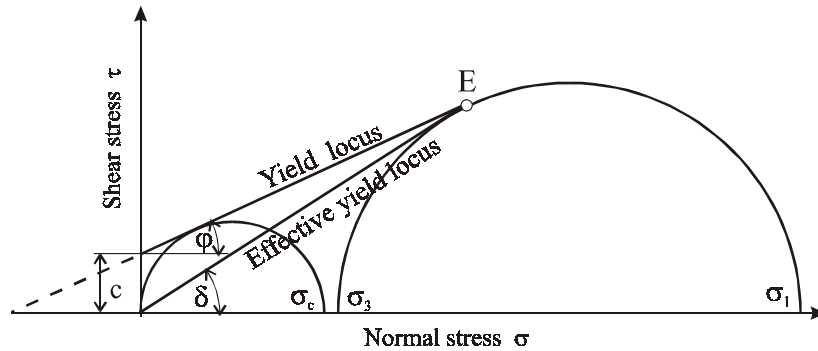


Fig. 8.2. Yield locus and effective yield locus

The parameter of the yield locus is the bulk density ρ_b at preconsolidation. With higher preconsolidation loads, bulk density and material strength increases, and the yield loci move upwards. Each yield locus terminates at a point E in direction of increasing normal stress σ . Point E characterizes steady flow, that is flow with no changes in stresses and bulk density. Two Mohr circles are drawn determined by two normal stresses σ_1 – the major principal stress at steady state flow called major consolidation stress, and σ_c – unconfined yield strength of the sample. Each yield locus gives one pair of values of σ_1 and σ_c . Conducting the test for several values of consolidation pressure gives a set of pairs of the parameters. With these values a plot of σ_c against σ_1 is obtained that is used to characterize flowability of granular material. To characterize flowability, Jenike [74] proposed to use the ratio of the major principal stress at steady state flow σ_1 to the unconfined yield strength σ_c . The classification of materials originally introduced by Jenike was modified by various authors as eg. by Chattopadhyay et al. [34] (see Chapter 4), or by Tomas to the following form (as cited by Schwedes [152]):

$ff < 1$	hardened
$2 < ff < 1$	very cohesive
$2 < ff < 4$	cohesive
$4 < ff < 10$	easy flowing
$10 < ff$	free flowing

The flow function gives the value of stress that lets an arch collapse or lets the material flow through an orifice. The inverse of the slope of flow function is termed the flow index i :

$$i = \sigma_c / \sigma_1 \quad (8.2)$$

which is used as an index of flowability following Jenike classification.

J.R. Johanson, who has been working with Jenike since 1958, summarized the deficiencies of shear cell technique in the article of 1992 [77]. One of the major problems with using the shear cell is that during shear, shear force concentrates at the front of the shear cell. Both shear force and vertical force are applied non-uniformly to the sample. According to Johanson, at best the results represent average stress conditions typically varying from a near zero stress up to the maximum applied. One of early innovations was applying the shear stress through both the top cover and the upper ring. This helps distribute the shear stress but applies a torque to the top disc. This results in concentration of vertical force at the front of the test cell. The non-uniform stresses in the shear cell also cause the major principal stress to be undefined. This undefined direction of principal stresses results in variable “steady state” consolidation and the frequent scatter in the measured failure values of shear stresses. The Jenike method indirectly measures the material unconfined yield strength and as such, requires several test points to establish the yield locus and its accompanying Mohr circle representing the unconfined yield strength. The variations in consolidation stress state as well as physical differences from sample to sample cause scatter in the data points. Objections as cited after Johanson and alike stimulated numerous researchers to look for more simple methods of examination of flowability. These methods will be treated in a wider extent in chapter 12.

9. COEFFICIENT OF FRICTION

9.1. Theories of dry friction

Friction is a set of phenomena taking place in the contact area between two bodies in relative displacement that cause resistance to motion. The measure of friction is the resultant tangential force acting during relative displacement of the two bodies. The earliest researchers of friction explained this effect by the necessity of rising of one of the bodies on the asperities of the other body (Perent, 1704; Euler, 1748 following Hebda and Wachal [62]). In this approach, the coefficient of friction was equal to the angle of inclination of individual asperity. The first wider examinations of friction were performed by Guillaume Amontons. In the publication of 1699 this author formulated two laws of friction that had been forgotten after being formulated by da Vinci in 15th century. The relationship $T = \mu N$, where N is normal force, T is tangential force, μ is coefficient of friction, is known as the Amontons low of friction and in some applications is used up till now [25].

A different point of view was presented by Desaguliers in 1724 [62]. This author indicated that smooth surfaces of metals or other substances may be polished

in such a way that friction would increase, and attributed the behaviour to adhesion acting in true contact areas. This statement initiated long lasting contradiction between adherents of mechanical and molecular theories of friction. In 1781 Coulomb published his “Theory of simple machines” where he acknowledged the influence of adhesion on friction. However he pointed out to the work that had to be done during relative sliding of rough surfaces as the main source of friction. Coulomb expressed the law of friction as follows:

$$T = \mu N + C, \quad (9.1)$$

where C was a constant dependent on the molecular interaction of surfaces in friction (cohesion).

Coulomb postulated that the value of C is constant for flat surfaces, and independent of the normal load. Leslie criticized Coulomb’s theory in 1804 and indicated that it should contain the incorporate deformation of surface asperities as the necessary condition for energy losses to take place. This remark was supported by work of Bowden [21] who claimed that the character of interaction between bodies depended on the relation between their hardness, as well as on temperatures of melting of the substances and the temperature of the contact area. According to Bowden, friction force is composed of the force necessary to shear bonds between asperities and the force necessary to draw a groove in the weaker material. This author did not consider molecular interaction of surfaces nor the influence of surface roughness, and assumed purely mechanical interaction of bodies in friction. Progress in technologies of surface treatment did not result in the elimination of friction, a fact that supported the point of view of followers of molecular theories of friction. In 1929 Tomlison (following Hebda and Wachal, [62]) proposed that friction was a result of adhesion of sliding surfaces. Dispersion of energy was a result of continual changes of pairs of interacting molecules and of the creation of new molecular bonds. Based on laboratory testing, Tomlison formulated an empirical relationship for coefficient of friction in the form of:

$$\mu = 0.18 \cdot 10^8 (A_k + A_p)^{2/3}, \quad (9.2)$$

where A_k and A_p – material parameters.

Another molecular theory of friction was proposed by Deriagin (following Kragelsky *et al.*, [86]). This author proposed that friction depended on molecular roughness of the material that was interrelated with material structure. Deriagin’s concept was valid in the case of ideal sliding, but did not consider frictional wear of sliding materials. In 1939 Kargelsky [86] published the principles of a molecular-

mechanical theory of friction suggesting a “dual nature of friction”. Later investigations by numerous researchers did not lead to any general theory of friction. Currently two types of coefficients of friction are used [19], one that represents friction opposing the onset of relative motion, and one that represents friction opposing the continuance of relative motion once that motion has started. The former is called static coefficient of friction, and the latter – kinetic coefficient of friction. It is currently widely accepted that friction is not an intrinsic material property of the two contacting materials. The system approach has become a tool for the interpretation and use of friction data in modelling friction, developing friction mitigating materials, developing friction test methods, and designing machinery.

9.2. Experimental Methods

Testing the friction of granular materials requires an apparatus in which relative motion of the material and a sample of construction material takes place. Relative motion may be rectilinear or rotary. In the case of rectilinear motion the sliding surface has the shape of a flat plate or band, while in the case of rotary motion it has the shape of a disc or cylinder. In figure 9.1 apparatus used by various authors are presented as reported in literature [11, 24, 26, 46, 52, 89, 97, 117, 141, 142, 151, 153, 161, 164]. The choice of a specific shape of sliding surface decides on important features of the measuring system. Apparatuses with the flat plate (see fig 9.1 a, b) assure uniform distribution of sliding velocity, uniform distribution of normal pressure and easy interchange of sliding surface. However, sliding velocity and sliding path are limited. Use of continuous band (see fig. 9.1 e) allows for uniform distribution of velocity and pressure with higher sliding speed and unlimited sliding path. However, frictional element in this shape is susceptible to vibration and may be produced only out of flexible materials. The shape of cylinder (see fig. 9.1 f) assures uniform distribution of sliding speed, but distribution of pressure is uneven, and obtaining interchangeable frictional surface poses a hard task to design and machine. Disc rotating around vertical axis (see fig. 9.1 c, d) allows for easy change of sliding surface, unlimited sliding path, high sliding velocity and uniform distribution of pressure. However, sliding velocity varies along the disc radius.

Values of coefficient of wall friction presented in the Appendix of this study have been determined following Eurocode 1 [50]. The test apparatus is a cylindrical shear cell as shown in figure 9.2. The diameter of the cylindrical shear cell should be at least 20 times of the maximum particle size and not less than 40 times the mean particle size. The compacted height H of the sample should be between $0.15D$ and $0.2D$.

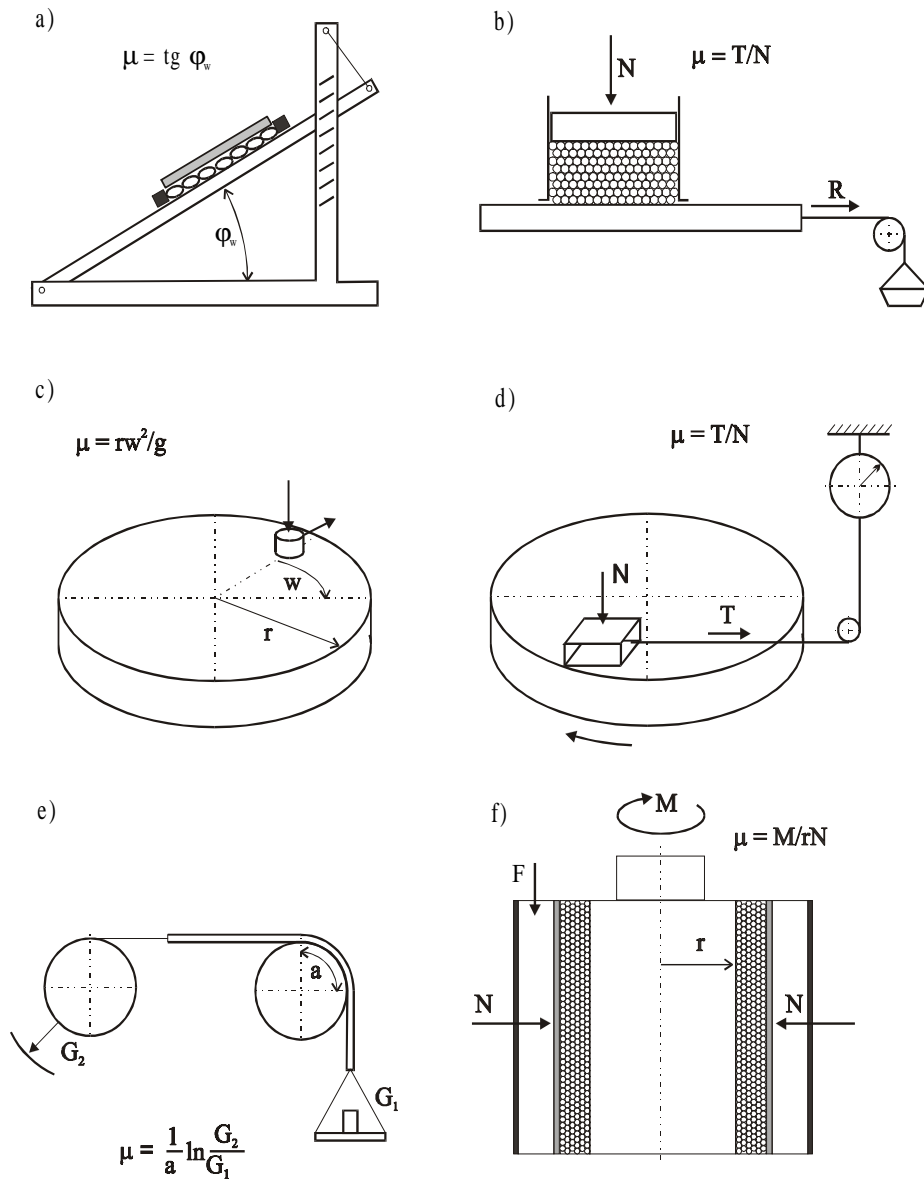


Fig. 9.1. Apparatuses used for determination of coefficient of friction of granular materials against construction material [107]

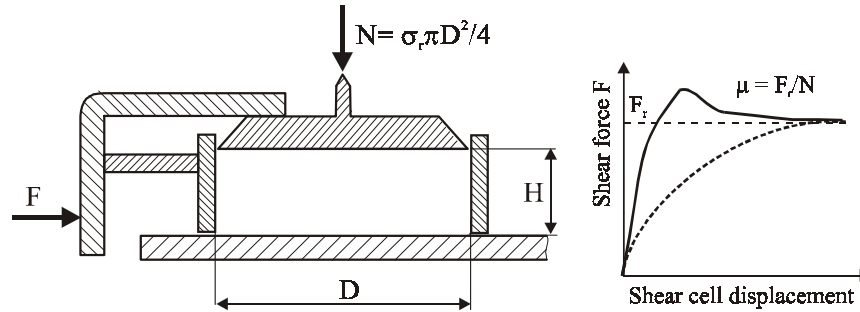


Fig. 9.2. Apparatus for measuring wall friction and typical shear-displacement curves [50]

The procedure is as follows:

1. The reference stress σ_r should be taken as the largest horizontal silo pressure p_h .
2. The sample should be poured into the test cell, without vibration or other compacting forces, and the consolidation stress σ_r applied. A top plate should be rotated clockwise and anticlockwise about the vertical axis several times through an angle of at least 10 degrees to consolidate the sample.
3. After filling the cell and before shearing, the cell should be rotated and lifted slightly of the test surface, so that only friction between the particles and surface is measured.
4. Shearing of the sample should be carried out at a constant rate of approximately 0.04 mm s^{-1} .
5. The residual friction force F_r (see figure 9.2), attained at large deformations, should be used in the calculation of the coefficient of wall friction μ for action calculations.
6. The sample value of the coefficient of wall friction μ for action calculations should be determined as:

$$\mu = \frac{F_r}{N}, \quad (9.3)$$

where:

F_r is the final or residual value of the shear force (figure 9.2)

N is the applied vertical load on the cell.

While testing for this study five levels of normal pressure σ_r were applied of: 20, 30, 40, 50 and 60 kPa, shear velocity was set at 0.35 mm s^{-1} .

The angle of wall friction for the evaluation of flow assessment have been determined following the tilting table method (fig. 9.1 a). The sample of grain confined with the square frame (20x20 cm) was loaded in the range of 0.5-2.5 kPa and tilting angle at initiation of the sample sliding was registered.

9.3. Factors influencing the coefficient of friction

The coefficient of friction of granular materials of plant origin depends on numerous factors, among which the following are regarded as the most important: moisture content, normal pressure, sliding velocity, surface state and ambient conditions. The influence of these factors on the coefficient of friction will be shown below, taking wheat grain as an example.

9.3.1. Moisture content

Already early investigations of grain friction pointed out to moisture content as one of the crucial factors influencing friction. According to Canadian Farm Building Code [29], increase in moisture content of stored grain may result in a six-fold increase in pressure acting on silo wall. Richter [142], based on his investigations on straw, hay and silage, reported an increase in the coefficient of friction with an increase in moisture content. Similar tendency was observed by Brubaker and Pos [24] for friction of wheat against four types of construction materials. These authors suggested that after exceeding 13% of moisture content of grain a particularly fast increase in friction took place. Determination of wheat friction performed by Snyder *et al.* [153] in a climatic chamber showed that increase in grain moisture content as well as increase of air relative humidity resulted in an increase of coefficient of friction. Hanzelik *et al.* [61] did not observe any increase in coefficient of friction with an increase in moisture content. Probable reason for this disagreement with other authors was very low normal load applied in their equipment that was an inclined plate. Stewart *et al.* [157], in their testing on sorgo, confirmed the tendency of faster increase in the coefficient of friction for moisture content above 13%. These authors found also that an increase in moisture content produced a particularly high increase in the coefficient of friction in the case of surfaces of low asperities. Thompson and Ross [161] measured friction of wheat against galvanized steel and found the coefficient of friction versus moisture content characteristic with a maximum for 20% of grain moisture content. These authors suggested that at moisture content from 16% to 20% kernels became soft and deformation around the asperities took place that generated stronger bonds than in the case of hard, dry grains. Further increase in moisture content caused a decrease in the coefficient of friction resulting, according to these authors, from the presence of liquid water in the contact area. Increase of coefficient of friction with an increase in moisture content was confirmed by results of Tsang-Mui-Chung *et al.* [164], Balassy [11], Scherer and Kutzbach [149]. Lawton [93] confirmed the above stated tendency, however for some materials he found a relationship with minimum coefficient of friction for moisture content of 15%.

Molenda *et al.* [107], for wheat sliding against steel surface, also found the relationship between friction force and moisture content with a minimum at approximately 15%, as shown in figure 9.3.

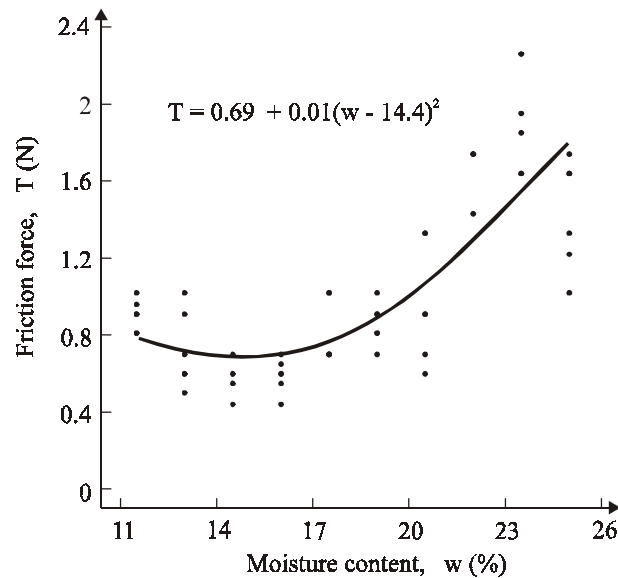


Fig. 9.3. Force of friction versus moisture content for wheat sliding on smooth steel surface. Experimental results and estimated curve [107]

9.3.2. Surface roughness

Researchers were usually interested in friction of grain against materials that were commonly used in the construction of agricultural equipment and storage facilities. In earlier investigations wood, steel and rubber were tested, later investigations on galvanized steel, concrete, aluminium, polyethylene or teflon have been conducted. The state of the surface of investigated material was not precisely defined in a majority of published results because of the complexity of a methods of determination of surface properties. Usually the commercial name of material was given, sometimes with a parameter of surface roughness added. As an example, Cyrus [40] reported an increase in the coefficient of friction of wheat kernel against steel with an increase in parameter R_a in a range from 0.9 to 11 μm . A specific difficulty of investigation of friction is the changing state of surface with prolonging time of measurements. Richter [142] observed that the coefficient of friction decreased with increasing number of performed tests. He suggested polishing sliding surface till the moment of stabilization of frictional force. Thompson and Ross [161] observed considerable variations of coefficient of friction between samples of

galvanized steel received from different sources. These authors reported that coefficient of friction and standard deviation decreased in subsequent measurements. Snyder *et al.* [153], on the contrary, observed a decrease in the coefficient of friction with prolonged frictional contact. Washing the frictional surfaces with carbon tetrachloride reduced the coefficient to its original value. The substance found after evaporation of the solvent was determined to be cutin, a wax-like substance found on the surface of grain kernels. The effect of cutin on the friction coefficient was more noticeable after the metal surface was allowed to age for one or more days. Molenda *et al.* [107] determined the friction coefficient of pairs of wheat grains on steel plates of different roughness. Results of these tests are presented in figure 9.4. In the case of smooth surface, a minimum of μ of 0.06 was found at moisture content of 15.2%. For the plate of surface roughness R_t of 1 μm , the values of coefficient of friction consistently increased with increasing moisture content. For the remaining plates the coefficient of friction increased with increasing surface roughness, but no clear tendency with an increase in moisture content was observed. The apparent inconsistency of observed frictional behaviour is probably a result of varied degree of contribution of basic phenomena in the resultant coefficient of friction. In the case of smooth surface the effect of adhesion prevailed. With increasing surface roughness the first deformation of surface asperities became relevant, while cutting of grain surface took place by asperities of plates of the highest levels of surface roughness.

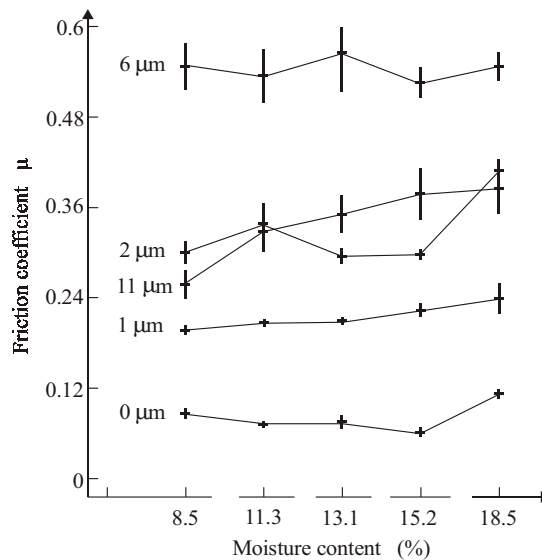


Fig. 9.4. Coefficient of friction versus grain moisture content for wheat grains sliding on steel plate of five levels of surface roughness [107]

9.3.3. Normal pressure

Normal pressure was shown to be another important factor influencing friction. Thompson and Ross [161] applied normal pressure in a range from 7 to 172 kPa and observed a decrease in the coefficient of friction of wheat against steel with an increase in pressure. The authors suggest that with an increase in normal pressure contact stress increased less than proportionally. Hertz's theory [104] postulated that with an increase in normal force N normal contact stress increases as $N^{1/3}$. This way, according to Thompson and Ross [161], frictional forces in the contact area that are proportional to normal loads are weaker than proportional to normal stress. In such a way Hertz's theory would explain the decrease in the coefficient of friction with an increase in normal pressure. A similar tendency was reported by Fiala [52] for different agricultural materials, Lobotka [97] in the case of corn, and Zhang *et al.* [174] for wheat. Moore *et al.* [113] stated an opposite tendency, one of increase in the coefficient of friction with an increase in normal wall load in a silo made of corrugated steel. Typical results of friction of wheat against smooth and corrugated galvanized steel are shown in figure 9.5 after Molenda *et al.* [111]. The tests were performed using the tilting table method and soft red winter wheat of 11.5% moisture content.

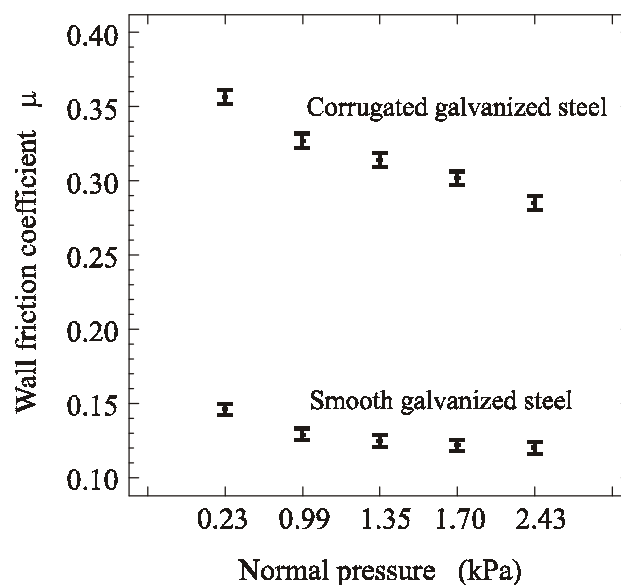


Fig. 9.5. Coefficient of friction of wheat on smooth and corrugated galvanized steel determined using tilting table method. Mean values and 95% confidence intervals for five levels of normal pressure [111]

9.3.4. Velocity of sliding

Because friction on the contact area is a visco-elastic phenomenon, researchers were aware of the influence of velocity on grain to construction material friction. Usually sliding velocity was a parameter under control during testing. However, no in-depth interpretation of the influence of velocity on the coefficient of friction of granular materials of plant origin has been given. Generalizing the findings of numerous authors it may be stated that, in the range of low velocities, the coefficient of friction increases with an increase in sliding velocity. In a range of velocity around 1 m s^{-1} it reaches its maximum, and decreases after surpassing this value [47, 52, 89].

9.3.5. Wear in

Above mentioned changes in the coefficient of friction with prolonged frictional contact cause variations of frictional loads with the time of operation of equipment. Molenda *et al* [108] determined wall and floor loads in a smooth wall model silo as a function of fill and unload cycles. The authors found that repeated loading cycles resulted in a decrease of the coefficient of wall friction. During the first three discharges vibrations of wall load were observed, resulting from the stick-slip friction. Decrease of the coefficient of friction resulted in a decrease in vertical wall loads and an increase in floor loads. The vertical wall load-to-total grain load ratios decreased rapidly for the first several loading cycles. It was approximately 54% for the first loading cycle, 29% for the 9th, and 25% for 23rd LC.

9.3.6. Frictional vibrations, slip-stick effect

Several investigators studying grain friction have observed the slip-stick behaviour. Bucklin *et al.* [27] studied frictional behaviour of wheat by pulling test blades of galvanized steel through pressurized grain. The velocity at which the slip-stick behaviour ended and smooth behaviour begun was defined as the critical velocity. Pressure had no statistically significant influence on the critical velocity. However, a statistically significant relationship was found between the coefficient of friction and the logarithm of the critical velocity. Critical velocity was higher for surfaces which had a high coefficient of friction. In experiments of Molenda *et al.* [111] at lower sliding speeds, longer periods of motionless contact (sticking) were observed for all levels of normal pressure tested. Frictional forces of greater magnitude were also observed at these lower sliding speeds. Probably, longer “stick” time allowed for higher deformation of the system, and more elastic energy could be stored in grain. When the material slips, the energy is released. As the sliding speeds are increased, slippage occurs more often along with the release of the elastic energy. Therefore, the maximum force values and the coefficient of friction decrease.

10. PRESSURE RATIO

The pressure ratio is one of the three most important physical properties of bulk solids, commonly used for calculation of pressure in a silo. Almost all design codes use a Janssen-type [73] pressure distribution to predict silo pressures [170]. The well known Janssen formula uses the equilibrium of a horizontal slice of the granular material to estimate pressures in deep silos. The fundamental assumption of Janssen's method involves a relationship between the average stresses acting on the finite dimension of a slice, and stresses that act at the walls of a silo. Janssen assumed that the ratio between the average vertical stress σ_z and the stress normal to the wall, σ_x is a constant for a given bulk material stored in a silo:

$$\frac{\sigma_x}{\sigma_z} = k = \text{const.} \quad (10.1)$$

and k is to be determined from measurements. Other Janssen's assumptions are: fully mobilized friction at the interface of the bulk material and the walls of the silo, and constant bulk density [45].

Since the work of Janssen, several attempts aiming at an expression for k , based on postulating a mechanical model for bulk solids, have been proposed [38, 45, 115]. A majority of the estimations are based on the assumption that the bulk material stored in or discharged from a silo is at a limiting state of stress. Another important assumption concerning the location of a region inside the slice of material where the yielding conditions occur involves relations between local stresses and the stresses averaged over the area or the perimeter of a slice [45].

In the case of a deep silo the following two stress cases are commonly considered: active for filling and storage mode, and passive for discharging mode. In the active case the vertical stress is higher than the lateral stress, while in the passive case the lateral stress is higher than the vertical one.

10.1. Yielding at the silo centre

Considering yielding at the silo centre, the stress ratio k can be easily obtained from Mohr's circle construction [82, 115] for the active case (fig. 10.1a):

$$k = \frac{1 - \sin \varphi}{1 + \sin \varphi}, \quad (10.2)$$

and for the passive case (fig. 10.1b):

$$k = \frac{1 + \sin \varphi}{1 - \sin \varphi}. \quad (10.3)$$

where φ is the angle of internal friction.

The commonly used assumption that the lateral stress is constant along the slice results in location of Mohr's circle for stresses at the wall outside the yield locus [45]. This assumption does not adequately represent pressure distribution in granular material in a silo.

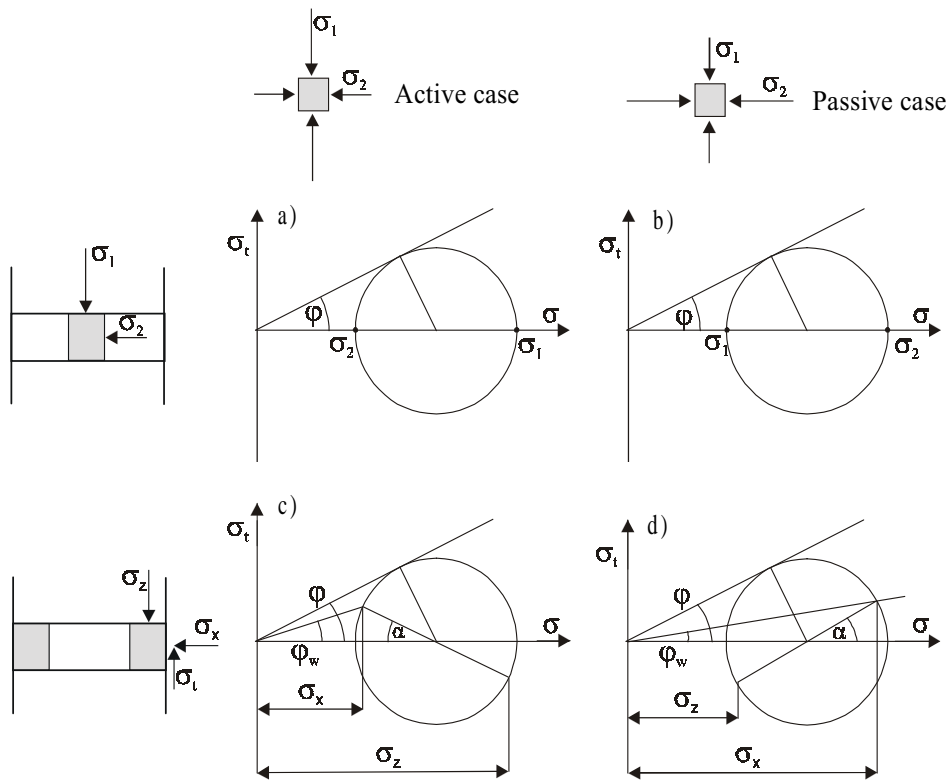


Fig. 10.1. Mohr's circles for active (a), (c) and passive (b), (d) stress cases, (a), (b) – yielding at the centre, (c), (d) – yielding at the wall [67]

10.2. Yielding at the silo wall

Considering the assumption that yielding occurs at the silo wall, the stress ratio k can be determined from the Mohr's circle construction as the function of the angle of internal friction and the angle of wall friction φ_w :

- for the active case (fig. 10.1c):

$$k = \frac{1 - \sin \varphi \cos \alpha}{1 + \sin \varphi \cos \alpha}, \quad (10.4)$$

where:

$$\alpha = \arcsin \frac{\sin \varphi_w}{\sin \varphi} - \varphi_w, \quad (10.5)$$

- and for the passive case (fig. 10.1d):

$$k = \frac{1 + \sin \varphi \cos \alpha}{1 - \sin \varphi \cos \alpha}, \quad (10.6)$$

where:

$$\alpha = \arcsin \frac{\sin \varphi_w}{\sin \varphi} + \varphi_w. \quad (10.7)$$

A plot of the pressure ratio for yielding at the silo wall and the active and the passive stress cases for typical range of values of the angle of internal friction and the angle of wall friction is shown in figure 10.2. The pressure ratio observed in practice varies in a considerably smaller range [91]. A plot of the stress ratio calculated from the angle of internal friction according to the simplified formula recommended by Eurocode 1 [50]:

$$k_\varphi = 1.1(1 - \sin \varphi), \quad (10.8)$$

is shown in figure 10.2. The angle of internal friction φ used in this formula should be determined experimentally in the direct shear test or in the triaxial compression test. The plot of the pressure ratio obtained from formula (54) is located in the upper limit of theoretical values obtained for the active stress case and yielding at the wall (i.e. for the wall friction angle φ_w close to the internal friction angle φ).

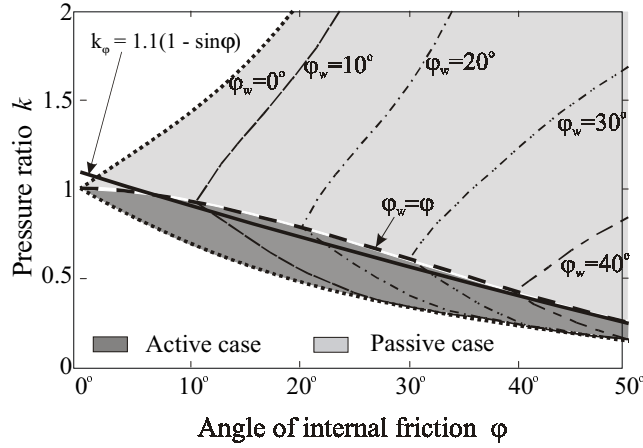


Fig. 10.2. Pressure ratio as a function of the angle of internal friction and the angle of wall friction for yielding at the wall in the active and passive cases [68], — the pressure ratio calculated according to equation 10.8

10.3. Experimental procedures

The most popular method of experimental determination of the lateral to vertical pressure ratio is the uniaxial compression test [90, 110]. An experimental set for the uniaxial compression (fig. 10.3) described in the chapter 6 was built according to the general guideline of the Eurocode 1 standard [50,66]. The sample was poured into the test chamber through centrally located spout, without vibration or other compacting actions. The specimen was loaded to the reference vertical stress of 100 kPa using a universal loading frame at the constant displacement rate of 0.35 mm min^{-1} . The top plate was rotated backwards and forwards three times through an angle of 10 degrees to consolidate the sample. Next, the sample was reloaded to the reference vertical stress, and the slope of the lateral to the vertical pressure increase was determined. The pressure ratio k_s appropriate for filling and storing was determined as [50, 135]:

$$k_s = 1.1 k_{s0}, \quad (10.9)$$

where

$$k_{s0} = \Delta \sigma_x / \Delta \sigma_{zm} \quad (10.10)$$

at the reference vertical stress $\sigma_{zm} = 100 \text{ kPa}$, $\sigma_{zm} = (\sigma_z + \sigma_{z0})/2$.

Experiments were performed for samples of seeds of different size and shape and typical storage moisture content. Extended range of moisture content was applied for tests performed for cereal grain 10-20% (w.b.) and 6-15% (w.b.) for rape seeds. The angle of internal friction of tested seeds was measured using

Jenike shear tester of 210 mm in diameter according to the procedure recommended by Eurocode 1 [50] described in the chapter 7.

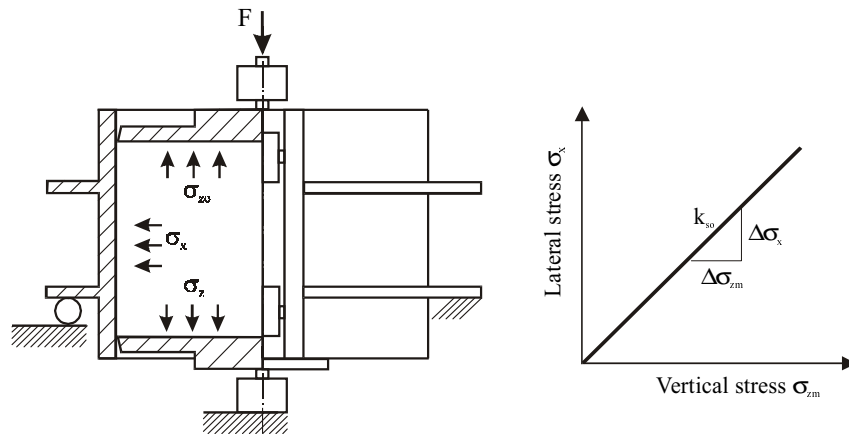


Fig. 10.3. Uniaxial compression tester and graph of the pressure ratio determination

The second series of experiments was performed in the model silo 0.6 m in diameter and 0.6 m high. The experimental set-up allowed for determination of the mean lateral pressure σ_x , tangent wall stress, σ_t , and mean vertical pressure σ_z [110]. The coefficient of wall friction, μ^* , was determined as the ratio of mean tangent wall stress σ_t to mean lateral pressure σ_x . The average value of the stress ratio, k , was calculated utilizing a numerical solution of Janssen's equation for the mean vertical pressure on the bottom of the container. Layer of grain was loaded through flat, rigid top cover and a series of uniaxial compression tests were performed in the same way as in the uniaxial tester. The set-up was used to indicate the influence of filling method resulting in different structure of granular material on the pressure ratio.

10.4. Factors influencing the pressure ratio

The recommended value of the lateral to vertical pressure ratio varies somewhat but the use of a value of approximately 0.4 is common. The pressure ratio depends on the type of grain, moisture content, bulk density and bedding structure of grain formed during the filling process. The angle of internal friction and the angle of friction on the wall material increase with an increase in the moisture content of grain, while the bulk density decreases or increases depending on the pressure level [100, 106, 107, 161]. The angle of friction at the interface of grain and the wall material depends strongly on the roughness of the wall surface. All those three properties of bulk of grain influence the pressure ratio.

10.4.1. Friction force mobilization

During monotonic uniaxial loading the pressure ratio generally increases to an asymptotic value characteristic for the material. For such a loading it can be assumed that the wall friction is fully mobilized but we can not be sure of the same about the internal friction. Therefore the value of the pressure ratio characteristic for yielding at the wall in the active case (equation 10.4) should be treated as the lower boundary of the possible values of the pressure ratio.

Examples of plots of the pressure ratio and the coefficient of friction force mobilization, μ^* ($\mu^* \leq \mu$), versus normal pressure obtained during loading and unloading loops of rape seeds and wheat grain in the model silo are presented in figure 10.4 [68]. During loading the pressure ratio increased to the asymptotic value typical for the given material while the wall friction coefficient decreased to the asymptotic value of the friction coefficient. On the contrary, during unloading the pressure ratio increased and the friction coefficient decreased. On the contrary, during unloading the pressure ratio increased and the friction coefficient decreased.

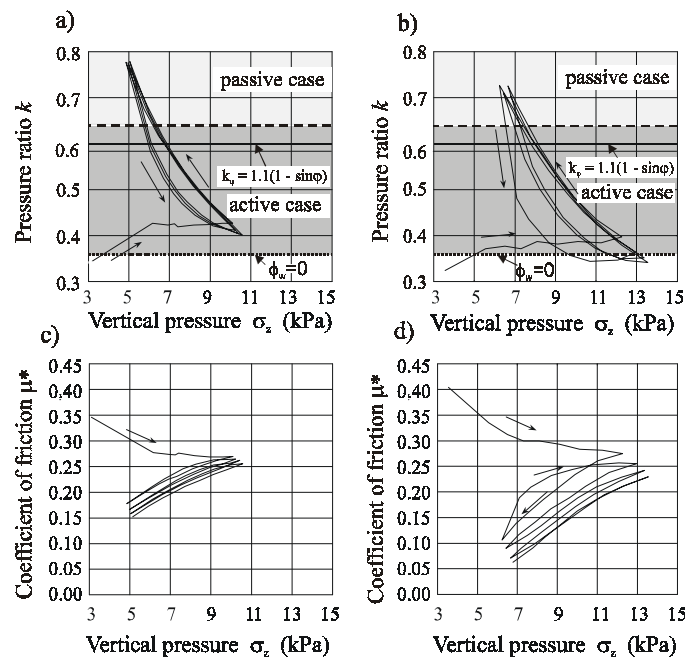


Fig. 10.4. Pressure ratio (a) and wall friction coefficient of rape seeds (c) and wheat grain (b, d) during loading-unloading cycles [68]

During the first cycle of loading the experimental value of the pressure ratio was close to the predicted value for the active case and yielding at the silo centre or yielding in frictionless wall silo (pointed line, $\phi_w = 0^\circ$). It means that the principal stresses were close to the vertical and horizontal directions. The biggest part of the pressure ratio loop was located in the area of values predicted for the case of yielding at the wall in the active case. During unloading the pressure ratio loop went beyond the value calculated according to Eurocode 1 recommendation (solid line) and arrived into the area of values typical for passive case (above dashed line). The pressure ratio loops resulted from superposition of elastic and plastic interactions between grains. Although the limit states of the model comprise only the plastic interactions, the predicted values of the pressure ratio correspond fairly well to the experimental ones.

10.4.2. Packing structure

The pressure ratio is influenced by the procedure of sample preparation [91, 68]. Distributed filling produces higher density as compared to stream filling. This results in a higher angle of internal friction and a lower pressure ratio (fig. 10.5). Filling procedure effects not only the bulk density but also the packing structure of granular material i.e. mutual orientation of particles and distribution of normal direction at contact points. In the case of distributed filling, inter-particle force chains are oriented mainly vertically. Uniaxial compaction strengthens this structure and, as a consequence, the pressure ratio is relatively low. This type of structure results in funnel flow during discharge. On the contrary, concentrated (stream) filling results in looser structure. Particles sliding off along the surface of natural repose cone generate some preferences in particles orientation which additionally influences the stress transition. Finally, the pressure ratio is much higher than in the case of distributed filling and during discharge material tends to mass flow.

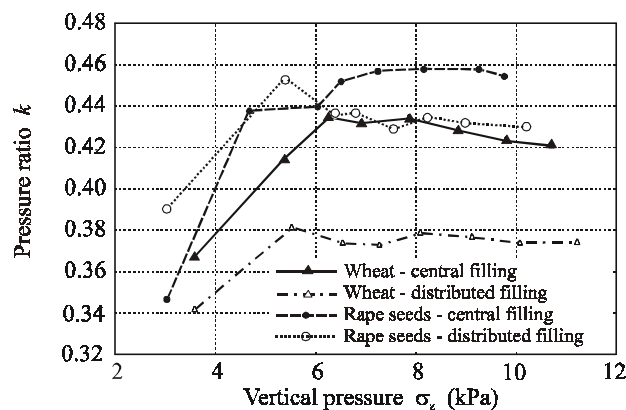


Fig. 10.5. Effect of the filling procedure on the pressure ratio determined on the model silo

10.4.3. Moisture content

With increasing moisture content, the friction force and the cohesion between grains increase. As a result a smaller part of the vertical loading is transmitted into the lateral direction. Consequently, the lateral to vertical pressure ratio should decrease with an increase in moisture content. Tests performed for cereals grain confirm this relationship (fig. 10.6). Nearly a linear decrease of the pressure ratio with an increase in moisture content was obtained for corn, rye and rape seeds. Another course of changes was obtained for barley: the pressure ratio was almost constant in the range of moisture content up to 17.5% and then decreased. This indicates that the influence of some other factors still remains out of control.

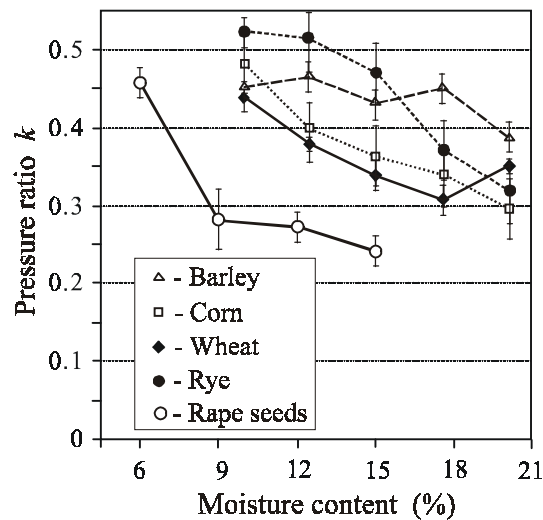


Fig. 10.6. Pressure ratio as influenced by moisture content of grain

10.4.4. Grain shape and surface roughness

The shape, size and roughness of seeds were found to influence the pressure ratio. The influence of surface roughness can be determined in an indirect way by considering its influence on the angle of internal friction. The more rough the surface the higher the angle of internal friction and consequently the lower the pressure ratio. In practice it is difficult to separate the influence of the shape and roughness of grain. It is much easier to observe the combined effect of both factors: the smoother the surface and the closer the shape to a sphere, the higher the pressure ratio. The pressure ratio of the material composed of elongated grains, like cereal grain, is generally lower than the pressure ratio of material composed of spherical grains (Tab. 10.1 and

10.2). The spherical shape of soybeans as compared to the lenticular shape of lentil seeds results in different distribution of contact points in bedding of material. Almost vertical orientation of the shortest axes of lentil seeds obtained during filling the tester results in easier transmission of vertical load into the lateral direction than in the case of spherical (soybean) or irregularly shaped seeds (pea).

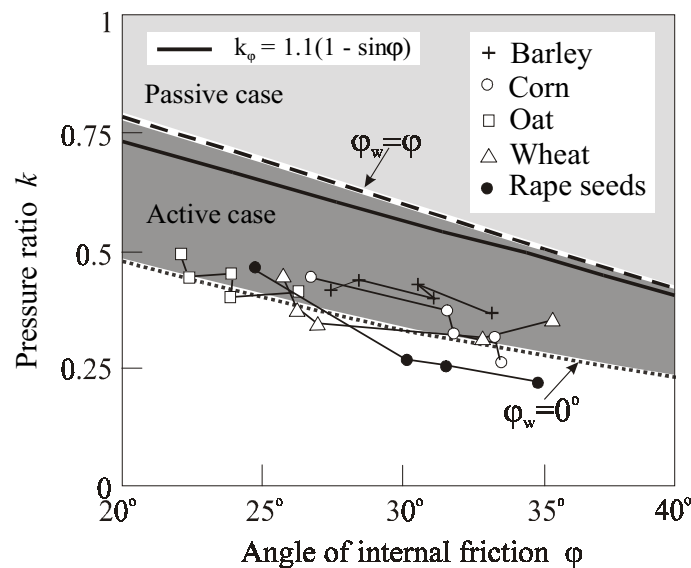


Fig. 10.7. Comparison of the experimental and theoretical values of the pressure ratio [69]

10.5. Concluding remarks

The values of pressure ratio for tested seeds at all levels of moisture content were found to be significantly lower than recommended by Eurocode 1 for filling and storing of cereal grain, and lower than the values obtained from equation 10.8 (table 10.2). Experimental values of the pressure ratio are located near the lower limit of theoretical values obtained for yielding at the wall in the active stress case (i.e. for the wall friction angle φ_w approaching zero, fig. 10.7). Lower limit of the theoretical values of the pressure ratio (dashed line in fig. 10.7 indicated as $\varphi_{w0}=0^\circ$) comprise the case of yielding at the centre of a silo in the active case when directions of the principal stresses are vertical and horizontal. This confirms the opinion that during uniaxial compression test the horizontal and vertical stresses are approximately principal stresses in the test sample, whereas they may not be in the silo [50].

Table 10.1. Measured (k_s) and calculated (k_ϕ) values of the pressure ratio of seeds and corresponding values the angle of internal friction ϕ (mean \pm St.dev)

Seeds	k_s	$k_\phi = 1.1(1 - \sin\phi)$	ϕ (deg)
Amaranthus	0.62 ± 0.02	0.70 ± 0.02	21.3 ± 0.8
Pea	0.53 ± 0.01	0.59 ± 0.01	27.3 ± 0.6
White mustard	0.43 ± 0.01	0.64 ± 0.01	24.7 ± 0.4
Buckwheat	0.59 ± 0.02	0.68 ± 0.02	22.0 ± 0.8
Soybean	0.37 ± 0.02	0.55 ± 0.01	30.1 ± 0.9
Lentil	0.74 ± 0.01	0.80 ± 0.02	15.5 ± 0.6

Table 10.2. Range of variability of the pressure ratio of grain and food powders [145] and values recommended by Eurocode 1 [50]

Material	Experimental		Eurocode 1 [50]
	k_s	$k_\phi = 1.1(1 - \sin\phi)$	K
Barley	0.30-0.47	0.50-0.59	0.59
Corn	0.30-0.67	0.49-0.60	0.53
Oat	0.40-0.49	0.63-0.68	–
Wheat	0.31-0.44	0.46-0.62	0.54
Rye	0.32-0.52	0.58-0.67	–
Rape seeds	0.24-0.46	0.56-0.64	–
Soybens	0.35-0.40	0.54-0.55	0.63
Sugar	0.31-0.47	0.44-0.50	0.50
Wheat flour	0.26-0.37	0.50-0.52	0.36

11. AIRFLOW RESISTANCE

11.1. Effects of density, moisture and packing

The main task of the design of a drying or aeration system is to define the operating airflow that in match with the pressure-drop-air-velocity relationship will assure the desired course of designed process. Apart from air velocity, other factors were found to influence the resistance of the bedding to airflow and, consequently, the pressure drop.

Theoretical modelling of static-bed-drying of grain employs four variables [23]: mass flow rate of air, air humidity ratio, air temperature, and kernel temperature. In developing the mathematical model several simplifying assumptions have to be introduced, one of those being that airflow through the grain is uniform and one dimensional, with no transfer the in transverse direction. However, moisture and temperature distribution in a silo is generally non-uniform in practical storage conditions. Thus for aeration control, location of humidity and temperature probe

is recommended in the area with the least airflow, typically in the centre of the silo, about 30 cm under the grain surface [23]. The goal is to assure safe storage environment everywhere in the silo rather than just average conditions for the silo as a whole. According to Navarro and Noyes [121], the airflow resistance calculated from recommended equations or read from figures is meant for loose-filled, clean, dry grain with airflow in vertical direction and in general gives a conservative estimate. The authors recommend that magnitudes of increase or decrease in such obtained airflow resistance must be determined experimentally. They also point out that the performance efficiency of an aeration system depends primarily on the uniformity of the airflow distribution in different regions of grain bed.

In experimental investigations, density (interrelated with porosity) was recognized first as a factor determining resistance to airflow through a layer of grain. Then the influence of the content of fine material was examined, because it decreased the amount of void space among grains increasing airflow resistance. Calderwood [28] examined resistance to airflow of different types and forms of rice and found that medium-grain rice offered more resistance to airflow than did long-grain rice. This author also stated that the resistance to airflow of brown and milled long-grain rice was nearly the same, but the resistance of brown medium-grain rice was significantly greater than that of medium-grain milled rice. Stephens and Foster [155] in their experiments with corn in commercial silo found increased resistance to airflow of up to 300% when using grain spreaders, as compared to that when no spreader was used. The same authors [156] conducted a similar test program with wheat, corn and sorghum. They observed that spreaders decreased the uniformity of fine material in sorghum, while there was little difference in wheat. Filling the bin with the grain spreader produced airflow resistances 110 % greater in sorghum and 101 % greater in wheat than those produced by filling from the central spout. Probably the crucial factor in these experiments was fine material content which was from 2.6 to 5.5 % in the case of corn, from 1.5 to 2.0 % in the case of sorghum, and 0.2 % in the case of wheat. The authors suggested that a possible reason for the observed increase in bulk density and resistance to airflow could be, in part, compaction due to the action of the spreader, while in grains with higher amounts of fine material, part of the increase arose from fine material occupying spaces between whole kernels.

The direction of airflow also appeared to influence resistance of the bedding to airflow. Kumar and Muir [87] found that at an air velocity of 0.077 m s^{-1} the resistance to vertical airflow compared with horizontal airflow was up to 60% higher for wheat and 115% for barley. Based on air velocity of 0.077 m s^{-1} , airflow resistance for layer filling was higher than for end filling by 25 to 35% for vertical airflow and 50 to 75% for horizontal airflow. Hood and Thorpe [63] found that for the velocity range up to 0.2 m s^{-1} and for ten grains the resistance to airflow in the vertical direction was about double that in the horizontal. These authors indicated that

conventional engineering analyses that consider resistance to be isotropic over-estimate the pressure drop across aerated grain bulks. Experiments and theoretical investigations of Endo *et al.* [48] showed that particle polydispersity and and/or non-spherical particle shape significantly influenced permeation resistance of either gas or liquid through a particle layer.

11.2. Laboratory testing

Typical system used for measuring airflow resistance is shown in 11.1. A cylindrical PVC pipe with a diameter of 0.25 m and a height of 0.49 m was used to hold grain sample during the testing procedures. Air was introduced through a plenum in the bottom of the cylinder. The differential static pressure was measured at depths of 0.05 m and 0.45 m above the bottom of the cylinder. The static pressure was measured using a variable reluctance differential pressure transducer (Validyne DP103, Northridge, CA) with a diaphragm (maximum pressure rating of 1370 Pa (5.5 in H₂O) and an accuracy of $\pm 0.25\%$ full scale. The flow rate was measured using a multiple nozzle outlet chamber according to ANSI/ASHRAE 51-1985 standard and a hot wire anemometer (Alnor Model 2106, Shoreview, MN) [37].

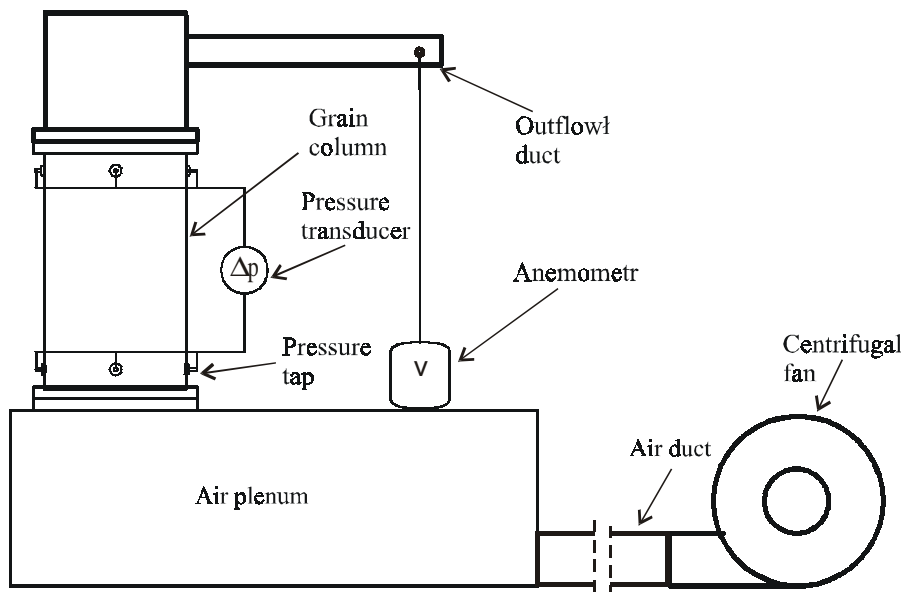


Fig. 11.1. Schematic of apparatus for measuring airflow resistance in grains as a function of bulk density [112]

Experimental airflow resistance as a function of air velocity for three types of seeds and centric filling is shown in figure 11.2. The lowest was airflow resistance of soybeans and the highest – that of wheat. This order does not correspond exactly to the determined porosities that were 0.37, 0.40 and 0.39 for wheat, corn and soybeans, respectively. Higher airflow resistance of corn despite its higher porosity in respect to soybeans may be the result of more complex geometry of pore space due to more irregular shape of corn kernels as compared to the roughly spherical shape of soybeans.

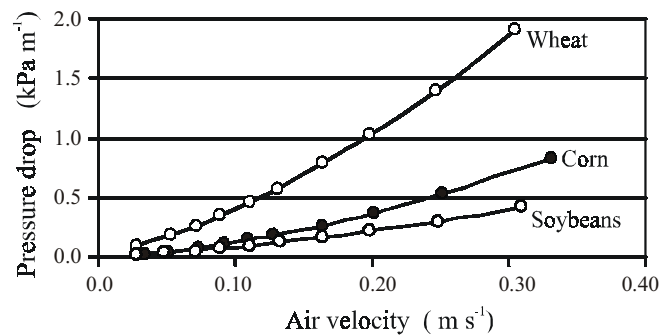


Fig. 11.2. Airflow resistance as a function of airflow velocity for centric filling of grain column with: red soft wheat, corn and soybeans

11.3. Ergun's equation

Pressure drop data for airflow through agricultural products are usually presented as curves or equations [5, 23, 121]. These formulations imply that pressure drop per unit of height is independent of the depth of the grain. This assumption is not correct, because the density and porosity of grain in the silo changes along the height due to compaction from grain load. Fluctuations of filling stream may introduce additional non-homogeneity of the bedding. Li and Sokhansanj [95] concluded that Ergun's equation could be the basis for a generalized model of airflow resistance through agricultural products. Ergun [49] hypothesized that the pressure drop was the summation of viscous and kinetic energy losses. The general equation takes a form as [95]:

$$\frac{\Delta P}{L} = aV_0 + bV_0^2 = 2f_E \frac{1-\psi}{\psi^3} \frac{\rho V_0^2}{D_p} = 2 \left(\frac{k_1}{(Re)_{dp}} + k_2 \right) \frac{1-\psi}{\psi^3} \frac{\rho V_0^2}{d_p}, \quad (11.1)$$

where:

ΔP – pressure drop,

L – length,

a, b – product-dependent coefficients,
 V_0 – superficial air velocity,
 f_E – friction factor,
 ψ – porosity,
 ρ – density of air,
 D_p – specific surface equivalent particle diameter,
 k_1, k_2 – product-dependent coefficients,
 $(Re)_{dp}$ – Reynolds number based on volume equivalent diameter,
 d_p – volume equivalent particle diameter.

Airflow resistance by Ergun's equation was used to predict pressure drop across a column of corn, soft white winter wheat, soft red winter wheat and soybeans at three moisture content levels and two bulk densities [112]. The data collected indicated that Ergun's equation could be successfully applied to grain aeration design and analysis. Previous work indicated that Ergun's equation would not be applicable to grain aeration due to packing effects within the bin. However, previous research indicated also that variations in bulk density and porosity could be estimated using granular mechanics models. The overall error using Ergun's equation was less than 23 Pa m^{-1} , when the pressure drop was less than 500 Pa m^{-1} . When all data were included up to a pressure drop of 1800 Pa m^{-1} , the standard error averaged 76 Pa m^{-1} . The effect of grain orientation that would be typical in storage bins was negligible, less than 10%, increase in airflow resistance. However, the fill method and resulting bulk density increased the airflow resistance by an order of magnitude. Ergun's equation, with an appropriate model of porosity variation during storage, could be utilized for the design and analysis of grain aeration systems.

12. FLOW RATE THROUGH ORIFICES

Numerous cases of design of storage and processing equipment require estimation of flow rate of granular material through orifices. ASAE standard D274.1 [6] gives recommended procedure to estimate the flow rate of specific grains and oilseeds through horizontal and vertical orifices. Recommended graphs and equations can be applied to mass flow from bins and hoppers during emptying. The standard distinguishes between small orifice – that is one whose hydraulic diameter is less than 15 times the minor diameter of the particle, and large orifices with larger hydraulic diameters. The rate of flow of grain or oilseeds through a horizontal or vertical orifice can be predicted by the following equation:

$$Q = C_1 A_0 D^x, \quad (12.1)$$

where:

Q – volume flow rate,
 A_0 – area of the orifice,

D – hydraulic diameter of the orifice,
 C_1 – coefficient from the table, different for horizontal and vertical orifices
 χ – exponent from the table with a value between 0.5 and 1.0.

The equation has been validated for square and circular orifices in both horizontal and vertical directions. The authors propose also a simplified version of the equation with exponent χ set equal to 0.7. With such simplification, the equation is usually accurate with $\pm 6\%$ for large orifices and $\pm 12\%$ for small orifices. Flow rate was found independent of grain depth in the experimental studies cited by the standard. The authors stated that for depths below 1 m flow can be affected by depth. Increased moisture content was found to reduce mass flow rate for corn and wheat, but increased mass flow rate for sorghum.

An orifice in the floor of the silo adjacent to the smooth wall discharged approximately 15% more grain than an orifice in the center of the silo floor.

13. INDICES OF STRENGTH AND FLOWABILITY USED BY PROCESS TECHNOLOGY

Some specialists (see [16]) consider the Jenike method of testing flowability to be much more complex and time consuming than less sophisticated measures. These authors state that the Jenike process takes at least 4 to 6 hours per sample, and the specific ramifications of the resulting flow function are understandable for only very few engineers practicing in the USA. Testing a bulk material with a Jenike cell takes more time and skill than the average producer or consumer of powders is willing to invest, unless there is a major financial stake such as the design of a new silo.

Current state of theory and technology of granular materials does not allow for wider standardization of material parameters and methods of their determination. However, industrial practice needs material parameters for design of processes, as well as measures of quality of products. Increasing number of consulting firms appear on the market and offer help in solutions of technological difficulties or determination of material parameters. High credibility is gained by firms led by specialists of respect established earlier in academia. Probably a good illustration of the demand from practice and proposed solutions are the offers of consulting groups founded by A. Jenike or by J.R. Johanson. These two specialists were earlier employees of academia. The establishment of Jenike addresses its offer to the following industries: chemical, environment protection, food, glass, metallurgy, mineral solids, paper, pharmaceuticals, mining, plastics and metal powders. Jenike and Johanson [75] propose standard tests for determination of cohesion, coefficient of wall friction, angle of internal friction, compressibility, permeability and angle of chute inclination to allow for stable flow. Determination of material parameters may

also be performed as a function of: consolidation time, normal pressure, ambient temperature and humidity. The apparatus applied is a direct shear box (Jenike method) equipped with consolidation bench. Ring shear apparatus is also available that apart of typical application of Jenike tester enables the estimation of wear of material due to attrition. For cases where determination of parameters does not give satisfying description of the process, consultants propose model investigations.

13.1. Quality determination

Quality control is an important task in the production and processing of granular materials because it allows for undisturbed flow of material and keeping constant composition of processed powder. Therefore, several new solutions of material testers have been proposed in recent decades that are currently verified [53]. Quality control has to be carried out in such points along the production line where product properties may change and result in damage of equipment or deterioration of product quality. Determination of quality of raw material is performed for protection against introducing portions of material of low value or undesired flowability. Variations in flowability may be the result of action of numerous factors. For complex processes many ingredients are used that are delivered from different producers. Constancy of properties of raw material depends on the method of production. Confirmation of the consistence of nominal properties of the material and its actual properties requires regular examination.

In numerous processes equipment is tuned during start up procedure when sometimes a large amount of by-product is produced. Examination of this start up product allows to decide if it may be reintroduced in the line. In typical process conditions maximum cohesion is determined to avoid flow problems in the system. In some cases, however, the value of end product is determined by minimum cohesive strength. For certain group of materials the best product is the most difficult to produce, and increase in quality above an acceptable level is very costly. In such cases quality control is particularly important.

Ploof and Carson [134] summarized the quality requirements posted by the market for a powder quality tester. First of all the tester has to be easy to use, with minimum requirement for skills and training. Time needed for performing measurement and analysis of results should be possibly short. Moreover, results of measurements should be precise, repeatable and should deliver significant information about the material. And finally, the construction of the tester should be simple and compact, allowing for mobility. Such a kind of equipment may be easily placed in proper location on the production line instead of delivering material samples to the laboratory.

13.1.1. Peschl rotational split level shear tester

Peschl [131] presented a promising proposal of a rotational shear apparatus with associated method of determination of mechanical properties of powders [132], and a method of quality control of powders for industrial application [133]. The author analysed existing equipment and found that some apparatuses overestimate the values of parameters as compared to values in a full-scale installation, while others underestimate those values. Peschl, based on his examinations of industrial powders, stated that rotational split level (RSL) shear testers give values similar to those encountered in practice. In the RSL apparatus, shearing of the samples takes place through the rotational movement of the lower part of the sample against the upper part of the sample. The horizontal cross-section area of the sample equals 30 cm^2 while its volume is 45 cm^3 . With rotational movement, no limit on shear displacement exists, and the shear plane forms in the middle of sample height where the disturbances from horizontal borders of the sample are the least. The author recommends choosing such experimental procedure that would most closely reflect the conditions of real process for which the material parameters are determined. Peschl preferred not to suggest any standard procedure, but offered the possibility of programming of shear conditions with automatic control of the apparatus. Procedure of data analysis allows for linear or exponential approximation of yield condition. For majority of easy flowing or low-cohesion materials, linear approximation is a sufficient solution. In such a case material parameters have a clear interpretation.

Some materials are characterized by strongly non-linear yield condition in a range of low normal pressures. For this group Peschl [132] suggested linear approximation in two intervals. Out of straight line estimated for the range of higher pressure the higher principal stress σ_1 should be determined, while cohesion c and unconfined yield stress σ_c should be determined out of the course of a straight line estimated for the lower range of normal pressure. If the mentioned above do not give satisfactory accuracy of description of the yield condition, a non-linear approximation using exponential function is necessary. The method of approximation cannot be settled at advance, but must be an outcome of consideration of particular case. Peschl claimed that his method gave the possibility of simulation of all conditions existing in practice, proper determination of parameters and, consequently, reliable operation of industrial installations. The author concluded that powder technology gained the level of engineering science and allowed for design of industrial installations without beforehand experimenting on equipment and installation.

Flowability is a material property of increasing importance. With passage of time, this property is more extensively used as a measure of material quality. Consumers expect constant flowability of washing powder, milk powder or sugar. For mixing, dosing and packing, stable flowability is a crucial parameter for

reliable processing and stable values of end-product. Peschl verified his method testing products of pharmaceutical and coal industry [133] and recommended its use for quality determination. The obtained parameters are: consolidation pressure (σ_1), angle of internal friction (φ) and unconfined compressive strength (σ_c). The only parameter of free flowing material is the angle of internal friction. To characterize a cohesive material two parameters are necessary – the angle of internal friction and cohesion. Consolidation pressure should be set close to the pressure that acts on the material under the conditions of technological process considered. The angle of internal friction is a function of stresses σ_1 and σ_c . As the non-dimensional parameter the author proposed “absolute flowability – *FLA*”:

$$FLA = \frac{(\sigma_1 - \sigma_2) \cdot \rho}{\sigma_c \rho_w} \quad (13.1)$$

where:

- ρ_w – density of water,
- ρ – density of bulk material.

Bell *et al.* [16] examined a number of methods of quality determination of powders regarding their usefulness in industry including the method of Peschl. Two directions in simplification of powder quality assessment were explored: automation of the Jenike approach and elaboration of a new method. The Peschl method is an example of the first approach. Bell *et al.* admitted that the method gave repeatable results in the range of intermediate and low normal pressures. The possibility of performing several measurements on one sample of powder is an advantage of this method, however special care should be taken in the case of materials susceptible to damage in shearing. Automation applied in the tester results in its relatively high price that limits the number of units that can be placed along production lines. Moreover, the advantage of automation became dubious when determination of flowability with time consolidation is required. Such examination requires separate samples consolidated under different pressures and in controlled ambient conditions, thus the same sample cannot be examined without conditioning for every single test.

13.1.2. Johanson’s apparatus and indices

J.R. Johanson separated from Jenike & Johanson in 1985 and before long proposed his own method of determination of mechanical properties of powders [77]. The basic unit of this equipment is an indicizer test cell shown in figure 13.1. The sample is consolidated in a cylindrical mould using a two-piece piston that measures the consolidation pressure directly on the inner piston while the inner and outer

pistons move together. The outer piston receives all the drag effects on the cylinder wall and this way eliminates any drag effects that act on the inner piston when the compaction pressure is measured. The sample is consolidated up to a prescribed level of major principal stress. Once the consolidation is complete, the vertical load is removed. The lower piston drops to allow the sample to be unconfined. The outer, upper piston is then raised relative to the inner piston and the shear failure induced by the downward movement of the inner piston. This way the unconfined yield strength σ_c is directly measured. The author claims that his method gives more accurate results than the Jenike method while the procedure of determination requires less time, and states that it allows the researcher, expert, designer, engineer, purchasing agent or equipment vendor “to access solids flow properties with ease and confidence”.

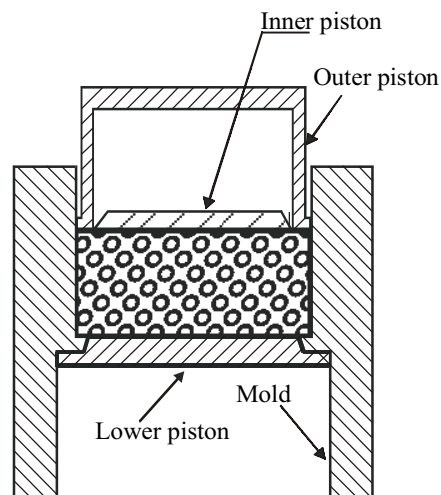


Fig. 13.1. Johanson indicizer test cell [77]

The Johanson indicizer was tested by specialists of DuPont [16]. The authors point out to the importance of flowability determination and inform that in industrial practice the aim of 95% of examinations of powders is performed in regard to product design and quality, not for silo design. The authors state that they were very interested in Johanson’s tester because it was the first unit to be fast in use, relatively simple and available at a moderate price. Examination of several common powders was performed and compared with results of the Jenike method. It was found that the equipment gave highly repeatable results for a relatively large group of materials. Performing measurement does not require long time or special skills of the technician. Calculation of unconfined yield strength σ_c using Johanson’s test parameters showed that the indicizer gave lower values than the direct shear test. When the ratio of

unconfined yield strength to powder density σ_c/γ was used as a measure of flowability, a low degree of consistence with the direct shear test was observed, particularly at low range of normal pressure. At higher levels of normal pressure, both the methods gave fairly close results. The authors [16] performed a ranking of a number of materials based on the Jenike and Johanson methods and found that the two methods gave results in a fairly good agreement. In summary, Johanson's indcizer was found to be a convenient and repeatable tool to use, but its predicted σ_c values and arching and rathole diameters did not correlate well with the results of the Jenike cell. For some materials good agreement of flowability ranking was obtained under certain circumstances, but the basis for these limiting circumstances could not be quantified.

JR Johanson Inc. proposed investigations of materials in a wide range of temperature and moisture content. Standard testing has been offered for determination of density, permeability, strength and angles of friction and adhesion. Testing of flowability using Johanson's indices is also offered. Values of parameters for determination of the indices are measured under pressures and for scale factors corresponding to the dimensions of equipment applied in the process under consideration. Some indices have physical dimensions expressed in US units, as for that market the equipment was meant.

The Arching Index (AI), with a typical range of 0-4 ft (1.22 m), is the conical hopper outlet required for unaided gravity flow after dropping the solids into an empty hopper and ensuring arch collapse in a conical bin. The *AI* is related with material properties as follows: $AI = 2.2\sigma_c/\gamma$, where σ_c i γ are measured under normal consolidation pressure of: $3\gamma d/2$.

The Ratholing Index (RI) – typical range, 0-30 ft (0 to 9.15 m) – is the flow channel size in a hopper required for a solid to collapse into the hole above the outlet, if arching did not occur. *RI* also provides a good indication of lumping tendency. If, after a time at rest, the solids *RI* exceeds 10 ft (3.05 m) a lump breaker may be needed in the system. The *RI* is related with material properties as follows: $RI = 2.5\sigma_c/\gamma$ where σ_c and γ are measured at consolidation pressure of γd .

The Hopper Index (HI) is the minimum half-angle of a conical hopper, required to ensure flow along the hopper walls. Its value is $HI = 42 - \varphi'$, where φ' is the angle of kinetic friction measured at normal consolidation stress of γd , or if φ' increases with an increase in stress value of φ' determined at the stress level of γD .

The Flow Rate Index (FRI) – typical range 1-12000 lb min^{-1} (0.5 to 5400 kg min^{-1}) is the rate at which the solid will flow through a hopper outlet of diameter d when totally deaerated. Low value of *FRI* usually points out to fine, highly compressible powder. Particles of sizes in excess of 400 μm are usually incompressible, very permeable, and have a high *FRI*. Variation in the value of the index may be a signal of segregation or change in composition of powder mixture during processing.

The *Feed Density Index (FDI)* and *Bin Density Index (BDI)* are values of bulk specific weight expected at a conical hopper's discharge outlet or bulk specific weight expected in a container full of solids or in a mixer after agitation stops. The *FDI* is measured at a pressure of γd , while *BDI* is determined at a pressure level of γD .

The set of indices with their physical interpretation is shown in figure 13.2 following Johanson [78]. Basic properties of materials are measured at specific consolidation pressures or a scale factor relative to the process equipment size. Indices cited below are given in U.S. units as a basis of the bin diameter $D = 10$ ft (3.05 m) and a hopper diameter $D = 1$ ft (0.305 m).

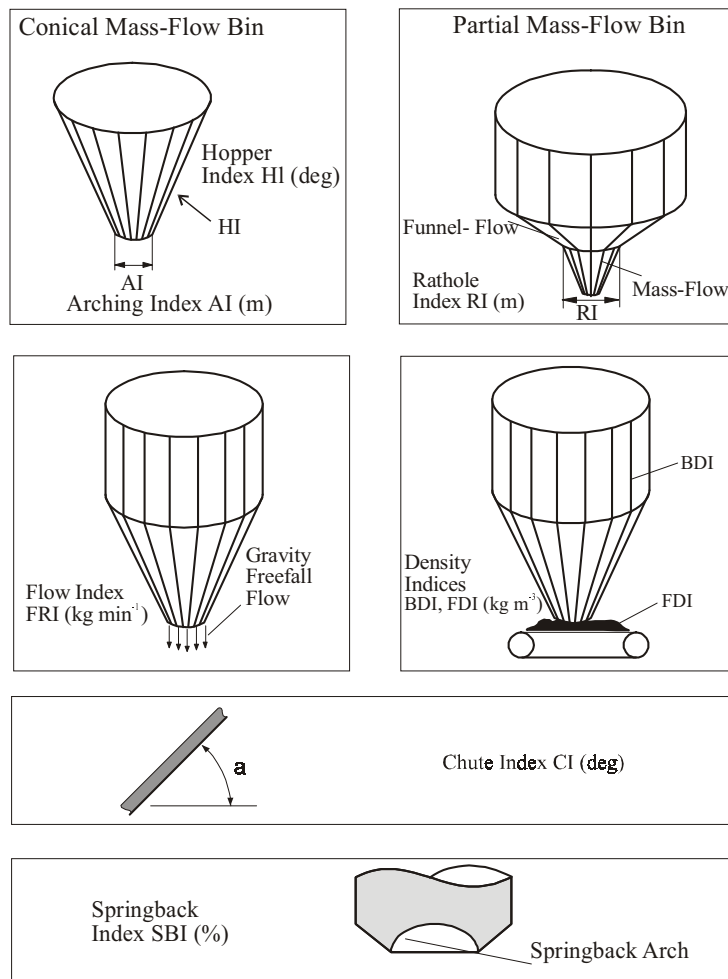


Fig. 13.2. Johanson indices [78]

The *Chute Index (CI)* is recommended chute angle to eliminate solids build up on a chute at impact points. The index takes value of $CI = ASC + 10^\circ$, where *ASC* is an angle of slipping friction along the flat surface of the bulk solid sample compressed with the pressure of 4700 N m^{-2} and unloaded prior to determination of *ASC*.

The *Springback Index (SBI)* is the percentage of elastic springback after consolidation, and indicates when springy solids (as straw, wood, polymer foam) may arch. *SBI* is measured by compressing the solid to a pressure of $D \times BDI$, and then noting the percentage change in the sample height when the load is released.

Knowledge of material characteristics expressed as values of indices allows for design of technological process as anticipated. Johanson [78] presented an example of use of the indices in design of the process of blending without segregation of components.

3.1.3. Jenike & Johanson powder quality tester

Tester of Jenike & Johanson [134] consists of two units: the body containing the sample holder, and the control unit (fig. 13.3). Sample holder of the volume of one US gallon (3.785 dm^3), has a cylindrical upper part while its lower part is conical. The upper lip of the holder may be closed with a tight cover housing a connector for supply of compressed air and fixing of the manometer. Outlet of the conical part of the sample holder can be closed with a sliding perforated plate with aperture diameter lower than the dimension of finest particles of tested material. The procedure requires a period of shaking to aerate the sample.

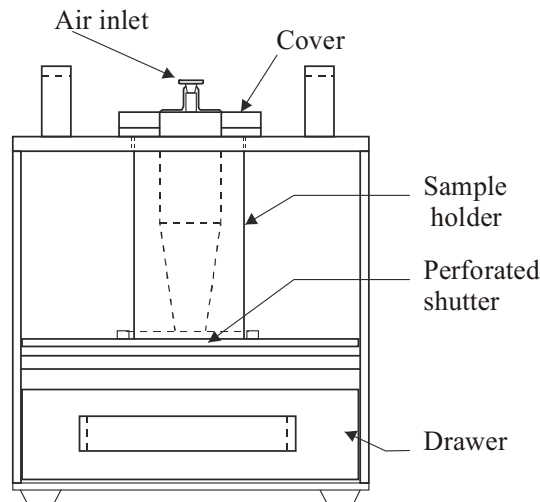


Fig. 13.3. Jenike & Johanson quality control tester [134]

The sample holder proper for particular tested material is placed in the body of the apparatus and thoroughly filled. The holder is closed with the cover and prescribed air pressure is applied that is adjusted with the valve and kept constant for 30 seconds. Then the pressure is decreased to zero and the perforated plate removed to open the outlet. The pressure gauge is turned on, and pressure in the sample holder increased till the moment of collapse of an arch when material flow commences. The measurement cycle from consolidation to outflow is repeated four times (at least) for one level of consolidation pressure. Results obtained with the tester were compared with results of the Jenike method for limestone powder and baking soda. Part of the tests showed fairly good agreement of results of the two methods, while another part was in disagreement. The authors concluded that the tester may be successfully applied for comparison of different lots of the same material [134].

3.1.4. Uniaxial tester of POSTEC

Led by premises similar to those reported by other designers of powder testers, researchers of the Norwegian institution POSTEC proposed their own solution. The tester is a type of indirect shear apparatus, namely uniaxial, and its description here is quoted after Maltby and Enstad [102]. In uniaxial compression test a compressive failure strength similar to the unconfined yield strength σ_c may be determined directly as a function of the consolidation stress σ_l . The measurement is taken in a fraction of time required by other testers. Due to the consolidation procedure used, the tester does not measure the flow function, and therefore should not be used for silo design unless a correction factor is introduced. The procedure used assures the scatter of the results is minimal, which together with the rapidity with which such measurements can be made, makes the test perfectly suitable for quality control purposes. In the POSTEC tester (see fig. 13.4) the sample is confined in a slightly conical die and consolidated by the piston moving vertically down. The flexible membrane is stretched between the outer surface of the piston and inner surface of the lower part of the die. A layer of lubricant is spread between the flexible membrane and the die wall. The die is filled upside down and closed with a tight cover, turned upside down again and placed into the guiding device of the tester. The sample is consolidated by moving the piston until the predetermined value of σ_l is reached, corresponding to a strain ε_l . After a predetermined time of sample stabilization the die is raised up and compressive failure strength is measured with the piston moving down. The maximum value σ_c is reached before the sample falls apart.

The apparatus allows for direct observation of the forming of failure surface that theoretically forms an angle of $\alpha = 45^\circ + \varphi/2$ with the horizontal plane. More complicated shape of failure surface points indicates that the sample was not tall enough. Using precise procedure for examination of BCR-limestone, Maltby and Enstad

obtained the maximum deviation of the strength σ_c not higher than $\pm 0,13$ kPa, not dependent on the level of consolidation pressure. These authors have reported good repeatability of results with deviation not higher than 5%. According to the authors, the reproducibility of the tester, together with operator independence and fairly rapid test procedure make the equipment a suitable tool for quality control of powders. Accuracy of the method allows for flow property deviations from batch to batch in batch production operations. The equipment may be also used for investigations of the compaction properties of slightly compacted samples, determination of the modulus of elasticity, or examinations of stress relaxation and creep phenomena of powders.

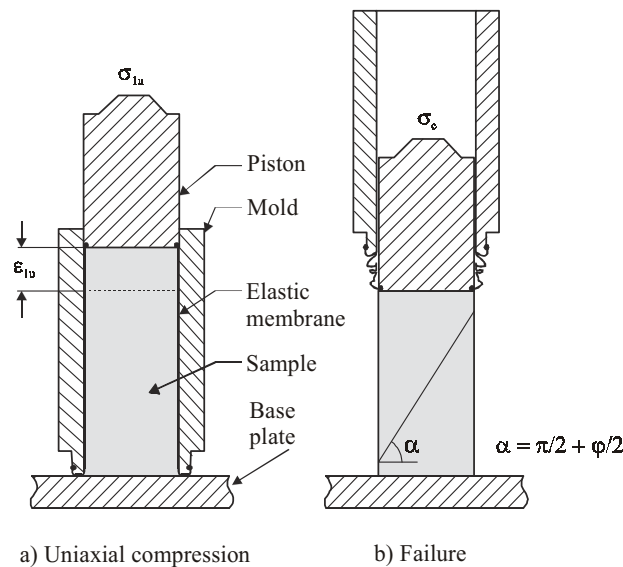


Fig. 13.4. POSTEC uniaxial tester [102]

13.2. Carr Indices

Chemical industry and, particularly, pharmaceutical industry need characterization of fine powders. Flowability determines operations of transport, mixing, dosing, storage granulation or forming tablets. Carr Indices are willingly used by practitioners of those industries, and were standardized by the American Society for Testing Materials [7]. The method can be applied to free flowing and moderately cohesive powders and granular materials up to 2 mm in size. Materials must be able to pour through a 7.0 ± 1.0 mm diameter funnel outlet when in aerated state. The method consists of eight measurements and two calculations to provide ten tests for Carr Indices. These ten tests are as follows:

- A. Measurement of Carr Angle of Repose
- B. Measurement of Carr Angle of Fall
- C. Calculation of Carr Angle of Difference
- D. Measurement of Carr Loose Bulk Density
- E. Measurement of Carr Packed Bulk Density
- F. Calculation of Carr Compressibility
- G. Measurement of Carr Cohesion
- H. Measurement of Carr Uniformity
- I. Measurement of Carr Angle of Spatula
- J. Measurement of Carr Dispersibility.

In practice the Carr Index CI is also popular, that is defined [8] as:

$$CI(\%) = \frac{100 \times (\rho_t - \rho_l)}{\rho_t}, \quad (13.2)$$

where:

ρ_t – tapped bulk density,

ρ_b – loose bulk density.

This parameter is determined, after compaction of material by tapping, in a cylindrical container of a volume from 10 to 1000 ml, with user-defined number of taps (from 10 to 500). Out of the same measurement another popular parameter, the Hausner Ratio, may be calculated as:

$$R_h = \frac{\rho_t}{\rho_l}. \quad (13.3)$$

In industrial practice it is assumed that the powder is easy flowing having CI in range from 5 to 15%, while durable tablets may produced of powder having R_h not higher than 1.6.

13.3. In-line control of structure of granular products

For contemporary highly automated mass production in-line methods of characterization of materials are in the highest demand. In the first approach in-line methods of measurement of particle size distribution were elaborated. Knowledge of particle size distribution allows for efficient process control and control of product quality. Process output continuously increases and delay between laboratory measurement and process correction may be unacceptable. Currently pneumatic conveying is extensively used in industry because it enables

efficient flow control using optical methods. Harvill *et al.* [60] described one of such devices, based on laser diffraction of light and used in a large range of laboratory and industrial applications. Measuring unit consists of an optical head, interface, pc and software. Stream of particles flows through the cylindrical channel across the laser light beam. Velocity of the stream does not influence the result of the measurement. Scattered light passes through the receiver lens and is focused on the log-scaled annular ring detector. The detector is scanned by the interface with high speed and levels of signal on the separate rings are recorded. Each ring of the detector measures the total signal intensity. Each particle scatters light on all rings of the detector, therefore the measured signal is the summation of all the light scattered from all particles. After acquiring a significant number of scans, relative particle concentration is calculated by the software. The instrument allows for efficient determination of both particle size distribution and particle concentration directly and in real time. It has been successfully used in production of pharmaceuticals for optimization of the mill. The instrument provides continuous feedback control to compensate for mill-setting drift, wear, operator errors, variations in raw material etc.

Like in pharmaceutical industry, in-line process control may increase efficiency of food industry. The basic factor in food product quality is its structure. Bijnen *et al.* [18] analysed current trends in development of process sensors in food industry. Market requirements enforce precise process control. The development of these new process regimes requires better understanding of the structure-process-equipment relationships. Precise in-line measurements become necessary. Basic attributes of product microstructure are: overall product composition, properties and state of all phases, distribution properties of dispersed phases and spatial organization of dispersed entities. The authors reviewed methods that might be applied for in-line measurements and pointed out their limitations.

- Sensors for the determination of product composition (the content of: water, fat/oil, carbohydrates, and proteins) currently achieve a relative accuracy of 0.1 to 1%. These are often sufficient, but the calibration procedures (if any) in a rapid changing product portfolio should be minimal.
- Sensors for monitoring the state of phase will be mainly applied for understanding the basic phenomena underlying the process, for development of new processes and process control. The use of laser-based acoustic pulse sensors and detectors seems promising for monitoring the properties of phase state because of the flexibility due to remote sensing. In-line quality assessment will remain often difficult because in many food products the final state of phase (rate of crystallization or gelation) is formed after the filling operation and during storage.

- Current solutions of in-line particle size detection allow mainly for quantification in relation to droplet size empirically calibrated. For a rapid changing product portfolio and variable ingredients, these abilities may prove insufficient.
- Some options for absolute in-line particle size quantifications are present, but current solutions are able only to determine qualitative relation to droplet size calibrated empirically. For a rapid changing product portfolio and variable ingredients, these abilities may prove insufficient. In-line imaging and image analysis may deliver quantitative information necessary for process control in flexible factory conditions. Close monitoring of this information may allow for process control and quality assessment at the same time.
- The area of characterization of particles arrangement inside a product matrix remains still in too early a stage of exploration for having significant implications on the process measurement instrumentation.

13.4. Tendencies in development of applications

Last two decades of 20th century observed an increase in interest in particulate materials. Industry has been using more and more raw products, and produced increasing amounts of products in granular form. Global competition enforced increase in the scale of production that required automatic process control. Market demands stable quality of products delivered under the same trade mark. Material in granular form is much easier for storage, processing, mixing dosing, packing and distribution. Requirements of practice stimulated development of knowledge about granular materials, particularly in three areas:

- theoretical investigations seeking constitutive model of material,
- methods of determination of material characteristics for use in design of processes and equipment, and
- elaboration of methods of quality assessment and indices to measure quality.

Beginning in the 80-ties of the previous century, an unprecedented increase in calculation power of computers commonly accessible took place that enabled new possibilities of theoretical investigations. New theoretical approaches appeared, two of them gained matured form: numerical modelling including interactions in contact areas between individual particles, and the application of earlier known theories that required extensive calculations.

Regarding modelling behaviour of the bedding of material based on interactions in contact points between particles, the DEM method that originates from work of Cundall and Strack [39] remains promising. Good examples of a new approach to known methods are the applications of the theory of non-symmetric elasticity of Cosserats by Mühlhaus and co-authors [119] or by Chang and co-authors [33].

In the field of experimental investigations, new measurement methods have been elaborated and known methods have been improved to interpret unclear phenomena or to facilitate strenuous and time consuming measurement procedures. Regarding determination of strength parameters of granular materials, Jenike method [74] has been widely accepted and standardized in many national design codes as well as in international Eurocode 1 [50]. From among numerous earlier elaborated instruments, the ring shear tester will probably gain the position of recognized measurement technique. It is particularly useful in investigations of food products and granular plant materials. Because of high deformability of particles these materials require long shearing path to reach steady flow, and deformation in the ring shear apparatus is unlimited. The second significant advantage of the ring shear apparatus is the possibility of examinations under low level of normal load. Vertical loading force related to the relatively large surface of lateral section of the channel of the apparatus gives low values of normal pressure. Description of mechanical behaviour of granular materials under low normal load (in thin layer) is currently in particular interest of industrial practice. The two advantages of the ring shear tester open new fields of its application as well as promise the possibility of interpretation of some phenomena that still remain unclear.

Two other old methods for the measurement of angle of repose and of angle of friction with inclined table will probably remain as standards for the determination of mechanical properties of granular material thanks to their simplicity.

Search for methods of examination of product quality and for quality indices has been a symptomatic trend of technology of granular materials in the last several years. Quality assessment in the sense of granular mechanics means the determination of material flowability. Within the approach of Jenike [74] that is recently widely accepted the measure of flowability is the flow function $ff = \sigma_c(\sigma_1)$, i.e. the relationship between unconfined compression strength and major consolidation pressure. The direct shear tester or the Jenike method has, however, some disadvantages pointed out by practitioners. Testing is tedious and time consuming, while elaboration and interpretation of results require significant knowledge. Industrial practitioners demand a quick and simple method with an unmistakable and intelligible quality index. Academic laboratories and consulting firms put their propositions on the market one after the other, but none of them gained wide acceptance till now. Probably, for process engineering the set of Johanson's indices has been accepted, while in the pharmaceutical industry Carr indices are commonly used.

14. REFERENCES

1. ACI 313-91. Standard practice for design and construction of concrete silos and stacking tubes for storing granular materials. American Concrete Institute. Box 19150 Redford Station. Detroit Michigan 48219, 1995.
2. **Allen J.R.L.:** Notes towards a theory of concentration of solids in natural sand. *Geological Magazine*, (106) 4, 309-321, 1969.
3. ASAE Standards, D241.4: Density, specific gravity, and mass-moisture relationships of grain for storage. St. Joseph, MI, ASAE, 1999.
4. ASAE Standards, EP433. Loads exerted by free-flowing grain on bins. St. Joseph, MI, ASAE, 1999.
5. ASAE Standards, D272.3 MAR96. Resistance to airflow of grains, seeds, other agricultural products and perforated metal sheets. *ASAE Standards 1997*, 532-538, 1997.
6. ASAE Standards, D274.1 FEB03. Flow of grain and seeds through orifices. *ASAE Standards 2003*: 576-578, 2003.
7. ASTM – D6393 Standard Test Method for Bulk Solids Characterization by Carr Indices. American Society for Testing and Materials, West Conshohocken, PA, 1999.
8. ASTM – D4781 Standard Test Method for Mechanically Tapped Packing Density of Fine Catalyst Particles and Catalyst Carrier Particles. American Society for Testing and Materials, West Conshohocken, PA, 2000.
9. ASTM – D6128 Standard Test Method for Shear Testing of Bulk Solids Using the Jenike Shear Cell. American Society for Testing and Materials, West Conshohocken, PA, 2000.
10. AS 3774-1996. Loads on bulk solids containers. Standards Australia. 1 The Crescent, Home bush, NSW 2140, 1996.
11. **Balassy Z., Horabik J., Molenda M.:** On friction properties of wheat grain. *Zesz. Probl. Post. Nauk Roln.*, 378, 11-19, 1989.
12. **Bardet J.P., Proubet J.:** Adaptive dynamic relaxation for statics of granular materials. *Computers and Structures*, 39(3/4), 221-229, 1991.
13. **Bardet J.P., Proubet J.:** Shear-band analysis in idealized granular material. *J. Enene Mechanics*, 118(2), 397-415, 1992.
14. **Bathurst R.J., Rothenberg L.:** Micromechanical aspects of isotropic granular assemblies with linear contact interactions. *Journal of Applied Mechanics*, 55(1), 17-23, 1988.
15. **Bednarski T.:** Mechanics of plastic flow (in Polish). PWN, Warszawa, 1995.
16. **Bell T.A., Ennis B.J., Grygo R.J., Scholten W.J.F., Schenkel M.M.:** Practical Evaluation of the Johanson hang-up indicizer. *Bulk Solids Handling*, 14(1), 117-125, 1994.
17. **Bickert W.G., Buelow F.W.:** Kinetic friction of grains on surfaces. *Trans. of the ASAE*, 9(1), 124-129, 1966.
18. **Bijnen F.G.C., H. van Aalst, Baillif P.Y., Blonk J.C.G., Kersten D., Kleinherenbrink F., Lenke R., van der Stappen M.L.M.:** In-line structure measurement of food products. *Powder Technology*, 124, 188-194, 2002.
19. **Blau P.:** The significance and use of the friction coefficient. *Tribology International*, 34, 585-591, 2001.
20. **Blair D.L., Mueggenburg N.W., Marshal A.H., Jaeger H.M., Nagel S.R.:** Force distributions in three-dimensional granular assemblies: Effects of packing order and interparticle friction. *Physical review E*, 63, 041304, 1-8, 2001.
21. **Bowden F.P., Tabor D.:** Introduction to tribology (in Polish). Warszawa, WNT 1980.

22. **Britton M.G., Moyses E.B.:** Grain properties in the proposed new engineering practice on bin loads. ASAE Paper No. 86-4502, St. Joseph, MI, 1986.
23. **Brooker D.B., Baaker-Arkema F.W., Hall C.W.:** Drying and storage of grains and oilseeds. Van Nostrand Reinhold, New York, 1992.
24. **Brubaker J.E., Pos J.:** Determining static coefficients of friction of grains on structural surfaces. Transactions of the ASAE, 1, 53-55, 1965.
25. **Buckley D.H.:** Surface effects in adhesion, friction, wear and lubrication. Elsevier, Amsterdam – Oxford – New York, 1981.
26. **Bucklin R.A., Thompson S.A., Ross I.J., Biggs R.H.:** Apparent coefficient of friction of wheat on bin wall material. Transactions of the ASAE, 5, 1769-1773, 1989.
27. **Bucklin R.A., Molenda M., Bridges T.C., Ross I.J.:** Slip – stick frictional behavior of wheat on galvanized steel. Transactions of the ASAE, 39(2), 649-653, 1996.
28. **Calderwood D.L.:** Resistance to airflow of rough brown and milled rice. Transactions of the ASAE, 16(3), 525-527, 532, 1973.
29. Canadian Farm Building Code. National Research Council of Canada. Ottawa 1977.
30. **Cassagrande A.:** Characteristics of cohesionless soils affecting the slopes of slopes and earth fills. J. of Boston Society of Civil Engrs, 23, 13-32, 1936.
31. **Chang C.S., Converse H.H., Martin C.R.:** Bulk properties of grain as affected by self-propelled rotational type grain spreaders. Transactions of the ASAE, 26(5), 1543-1550, 1983.
32. **Chang C.S., Liao C.L.:** Constitutive relation for a particulate medium with the effect of particle rotation. Int. J. Solid Structure, 26(4), 437-453, 1990.
33. **Chang C.S., Ma L.:** Modelling of discrete granulates as micropolar continua. Journal of Engineering Mechanics, 116(12), 2703-2721, 1990.
34. **Chattopadhyay A., Rao K.R., Parameswaran M.A.:** On the classification of bulk solids. Bulk Solids Handling, 14(2), 339-344, 1994.
35. **Christoffersen J., Mehrabadi M.M., Nemat-Nasser S.:** A micromechanical description of granular material behaviour. J. Of Applied Mechanics, 48, 339-344, 1981.
36. **Clover R.E., Ross I.J., White G.M.:** Properties of compressible granular materials as related to forces in bulk storage structures, Transactions of the ASAE, 478-481, 1973.
37. **Colliver, D.G., Murphy, W.E., Sun W.:** Evaluation of the techniques for the measurement of air leakage of building components. ASHRAE Research Project 438-RP. ASHRAE, Atlanta, GA, 1992.
38. **Cowin S.C.:** The theory of static loads in bins. Journal of Applied Mechanics, 44(3), 409-412, 1977.
39. **Cundall P.A., Strack O.D.L.:** Discrete numerical model for granular assemblies. Geotechnique, 29 (1), 47-65, 1979.
40. **Cyrus P.:** Tribometer for measuring the friction coefficient of grain during the shearing on sliding support plate. Sbornik '85 mechanizacni fakulty VSZ v Praze, 17-23, 1985.
41. **Delwiche S.R.:** Wheat endosperm strength properties as affected by moisture. Transactions of the ASAE, 43(2), 365-373, 2000.
42. DIN 66145: Darstellung von Korn-(Teilchen-) grössenverteilungen. 1976.
43. **Dobrzański B.:** Methodical aspects of estimation of mechanical properties of pea seeds (in Polish). PhD thesis. Instytut Agrofizyki PAN, Lublin 1990.
44. **Drescher A., De Josselin de Jong G.:** Photoelastic Verification of a Mechanical model for the Flow of a Granular Material. J. Mech. Phys. Solids, 20(4), 337-351, 1972.
45. **Drescher A.:** Analytical methods in bin-load analysis. Elsevier, Amsterdam-Oxford-New York-Tokyo 1991.

46. **Drozdow J.N., Pawlow W.G., Puczkow W.N.:** Friction and wear in extremal conditions (in Czech). Moskwa: Maszynostrojnie 1986.
47. **Ducho P., Lobotka J., Zahorsky J.:** Friction coefficient in lucerne and maize at way – milky maturity in motion. *Acta technologica agriculturae*, Nitra, 93-105, 1967.
48. **Endo Y., Chen Da-Ren, Puio D.Y.H.:** Theoretical consideration of permeation resistance of fluid through a particle packed layer. *Powder Technology* 124, 119-126, 2002.
49. **Ergun S.:** Fluid flow through granular beds. *Chem. Eng Progress*. 48(2), 89-94, 1952.
50. Eurocode 1. Basis of design and actions on structures – Part 4: Actions in silos and tanks. European Committee for Standardization. Central Secretariat: rue de Stassart 36, B-1050 Brussels, 2003.
51. **Feda J.:** Mechanics of particulate solids (in Czech). Academia. Praha, 1977.
52. **Fiala J.:** Friction of agricultural materials (in Czech). *Zemedska technika*, 4, 205-220, 1965.
53. **Frączek J., Kaczorowski J., Ślipek Z., Horabik J., Molenda M.:** Standardization of methods of determination of physico-mechanical properties of plant granular solids (in Polish). *Acta Agrophysica*, 92, 2003.
54. **Frontczak J., Metzger T.:** The studies on the slip angle geometrical features of corn grain in the moisture function. *Sbornik '85 mechanizacni fakulty VSZ v Praze*, 225-238, 1985.
55. **Glenn G.M., Younce F.L., Pitts M.J.:** Fundamental physical properties characterizing the hardness of wheat endosperm. *Journal of Cereal Science*, 13, 179-194, 1991.
56. **Gózdź A., Pietrow M.:** Quantum mechanical approach to randomly-packed beds of spheres in the container. *Int. Agrophysics*, 13, 185-189, 1999.
57. **Gózdź A.:** Mechanics of cell and granular media. Description based on quantum mechanics formalism (in Polish). *Acta Agrophysica*, 24, 57-65, 1999.
58. **Grundas S., Hnilica P.:** Types of wheat endosperm and its mechanical properties (in Polish). *Zesz. Probl. Post. Nauk Roln.*, z. 320, 127-133, 1987.
59. **Gu Z.H., Arnold P.C., McLean A.G.:** Consolidation- related density and permeability models for bulk solids. *Powder Technology*, 72, 39-44, 1992.
60. **Harvill T.L., Hoog J.H., Holve D.J.:** In-process particle size distribution measurement for pharmaceutical applications. *Powder Handling and Processing*, 7(2), 139-141, 1995.
61. **Hanzelik F., Keleman P., Tomoveik J.:** Deformation and friction of wheat grains. *Acta Technologica Agriculturae*, Nitra, 30-42, 1968.
62. **Hebda M., Wachal A.:** Trybologia. WNT, Warszawa 1980.
63. **Hood T.J.A., Thorpe G.R.:** The effects of the anisotropic resistance to airflow on the design of aeration systems for bulk stored grains. *Agricultural Engineering Australia*, 21 (1 and 2), 18-23, 1992.
64. **Horabik J., Łukaszuk J., Grochowicz M.:** Formation of shear band in a granular material during triaxial compression test. *International Agrophysics*, 14, 273-278, 2000.
65. **Horabik J., Molenda M.:** True contact area between wheat grain and a flat surface. *Zesz. Probl. Post. Nauk Roln.*, 378, 63-68, 1989.
66. **Horabik J., Molenda M.:** Device for determination of pressure ratio of granular materials (in Polish). Patent Application No. P-340014, Bulletin of Patent Office No. 22(700), A1(21) 340017, 2000.
67. **Horabik J., M. Molenda.:** Physical properties of granular food materials (in Polish). *Acta Agrophysica*, 74, 2002.
68. **Horabik H., Rusinek R.:** Determination of the pressure ratio of plant granular solids. Part I. Theoretical considerations. Part II. Experimental investigations (in Polish). *Acta Agrophysica*, 37, 61-81, 2000.

69. **Horabik J., Rusinek R.:** Pressure ratio of cereal grains determined in uniaxial compression test. *International Agrophysics*, 16(1), 23-28, 2002.
70. **Hueckel T., Drescher A.:** Nonlinear description of deformation of elastoplastic particulated materials (in Polish). *Prace IPPT PAN*, 65, 1972.
71. ISO 3535: Continuous mechanical handling equipment – Classification and symbolisation of bulk materials. International Standard. ISO, Geneva, 1977.
72. **Iwashita K., Oda M.:** Micro-deformation mechanism of shear banding process based on modified distinct element method. *Powder Technology*, 109, 192-205, 2000.
73. **Janssen, H. A.:** Investigations of pressure of grain in silo (in German). *Verein Deutscher Ingenieure, Zeitschrift (Dusseldorf)*, 39, 1045-1049, 1895.
74. **Jenike A.W.:** Gravity Flow of Bulk Solids. *Bulletin of the University of Utah (52)29*, Salt Lake City, Utah, 1961.
75. Jenike & Johanson, Inc. Bulk Solids: Science/Engineering/Design; <http://www.jenike.com/>, 2005.
76. **Jenike A.W.:** Storage and flow of solids. *Bull. 123, Eng. Expt. Sta. Utah State Univ.*, 1964.
77. **Johanson J.R.:** The Johanson indicizer system vs. the Jenike shear tester. *Bulk Solids Handling*, 12(2), 237-240, 1992.
78. **Johanson J.R.:** Smooth out solids blending problems. *Chemical Engineering Progress*, (96) 4, 21-37, 2000.
79. **Kanatani K.:** A micropolar continuum theory for the flow of granular materials. *Int. J. Engng. Sci.*, 17(4), 419-432, 1979.
80. **Kanatani K.:** A theory of contact force distribution in granular materials. *Powder Technology*, 28(2), 167-172, 1981.
81. **Kanatani K.:** Distribution of directional data and fabric tensors. *International Journal of Engineering Science*, 22(2), 149-164, 1984.
82. **Kezdi A.:** Handbook of soil mechanics. *Akademiai Kiado. Budapest*, 1974.
83. **Konishi J., Oda M., Nemat-Nasser S.:** Inherent anisotropy and shear strength of assembly of oval cross-sectional rods. *Deformation and failure of granular materials. A.A. BALKEMA/Rotterdam*, 1982.
84. **Koper R., Grundas S.:** Young modulus and strain absorption in wheat grain of differentiated moisture content (in Polish). *Zesz. Probl. Post. Nauk Roln., z. 320*, 151-157, 1987.
85. **Kou H.P., Knight P.C., Parker D.J., Tsuji Y., Adams M.J., Seville J.P.K.:** The influence of DEM simulation parameters on the particle behaviour in a V-mixer. *Chemical Engineering Science*, 57, 3621-3638, 2002.
86. **Kragelsky I.V., Dobytychin M.N., Kombalov V.S.:** Principles of calculation of friction and wear (in Russian). *Moskva, Maschinostroenie*, 1977.
87. **Kumar A. Muir W.E.:** Airflow resistance of wheat and barley affected by airflow direction, filling method and dockage. *Transactions of the ASAE*, 29(5), 1423-1426, 1986.
88. **Kustermann M.F., Kutzbach H.D.:** Young's modulus dependent on deformation velocity. *ASAE Paper No. 82-3055. St. Joseph, MI*, 1982.
89. **Kutzbach H.D., Scherer R.:** Internal friction of cereal grain- review (in German). *Landtechnik* 6, 213-219, 1977.
90. **Kwade A., Schulze D., Schwedes J.:** Determination of the stress ratio in uniaxial compression tests- Part 1. *Powder Handling and Processing*, 6(1), 61-65, 1994.
91. **Kwade A., Schulze, D. Schwedes J.:** Determination of the stress ratio in uniaxial compression tests- Part 2. *Powder Handling and Processing*, 6(2), 199-203, 1994.

92. **Lade P.V., Nelson B.R., Marvin Ito Y.:** Nonassociated flow and stability of granular materials. *J. Engrg. Mech.*, 113(9), 1302-1318, 1987.
93. **Lawton P.J.:** Coefficients of friction between cereal grain and various silo wall materials. *J. agric. Engrg Res.*, 25, 75-86, 1980.
94. **Li Y., Zang Q., Puri V.M., Manbeck H.B.:** Physical properties effect on stress-strain behavior of wheat en masse – part 1, load response dependence on initial bulk density and moisture content. *Transactions of ASAE*, 32(1),194-202, 1989.
95. **Li W., Sokhansanj S.:** Generalized equation for airflow resistance of bulk grains with variable density, moisture content, and fines. *Drying Tech.*, 12(3), 649-667, 1994.
96. **Loewer Jr.O.J., Ross L.J., Kratzer D.D., Walker .N.:** Properties of ground shelled corn as related to forces in bulk storage structures. *Transactions of the ASAE*, 20(1), 155-156, 1977.
97. **Lobotka J.:** Coefficient of friction of chopped feed (in Czech). *Zemedelska Technika*, 13, 81-93, 1967.
98. **Lapko A.:** Effects of interaction of granular material on reinforced concrete walls in grain silos. *Zeszyty Naukowe Politechniki Białostockiej*, 71, Białystok 1989.
99. **Lapko A., Prusiel J.A.:** Investigation on thermal effects in reinforced concrete cylindrical silo structures. *Proc. of the 3rd Israeli Conference for Conveying and Handling of Particulate Solids 1*, 4.25-4.30, 2000.
100. **Lukaszuk J., Stasiak M., Rusinek R., Horabik J.:** Effect of moisture content on the angle of internal friction of cereal grain (in Polish). *Acta Agrophysica*, 46, 105-113, 2001.
101. **Lukaszuk J., Horabik J.:** Determination of angle of internal friction of plant granular solids (in Polish). *Acta Agrophysica*, 64, 1-94, 2002.
102. **Maltby L.P., Enstad G.G.:** Uniaxial tester for quality control and flow property characterization of powders. *Bulk Solids Handling*, 13(1), 135-139, 1993.
103. **Masson S., Martinez J.:** Effect of particle mechanical properties on silo flow and stresses from distinct element simulations. *Powder Technology*, 109, 164-178, 2000.
104. **Mindlin R.D.:** Compliance of elastic bodies in contact. *J. Appl. Mechanics*, 16, 259-268, 1949.
105. **Mohsenin N.N.:** Physical properties of plant and animal materials. New York-London-Paris: Gordon and Breach Science Publishers 1978.
106. **Molenda M., Horabik J.:** Normal and tangential stresses in the frictional contact area between wheat grain and flat surface. *International Agrophysics*, 8, 277-282, 1994.
107. **Molenda M., Horabik J., Grochowicz J., Szot B.:** Friction of wheat grain (in Polish). *Acta Agrophysica*, 4, 1995.
108. **Molenda M., Horabik J., Ross L.J.:** Wear-in effect of loads and flow in a smooth-well bin, *Transactions of the ASAE*, 39(1), 225-231, 1996.
109. **Molenda M., Horabik J., Ross L.J.:** Stress and deformation of wheat in direct shear test. *International Agrophysics*, 12(2), 115-118, 1998.
110. **Molenda M., Horabik J.:** Lateral to vertical pressure ratio in a model grain silo. *Proceedings of the Seminar "Operations on granular materials"*, Lublin, 31-39, 1998.
111. **Molenda M., Thompson S.A., Ross L.J.:** Friction of wheat on corrugated and smooth galvanized steel surfaces. *Jornal of Agricultural Engineering Research*, 77(2), 209-219, 2000.
112. **Molenda M., Montross M.D., McNeill S.G., Horabik J.:** Airflow resistance of seeds at different bulk densities using Ergun's equation. *Transactions of the ASAE*, 48(3), 1137-1145, 2005.
113. **Moore D.W., White G.M., Ross L.J.:** Friction of wheat on corrugated metal surfaces. *Transactions of the ASAE*, 6, 1842-1847, 1984.

114. **Morland L.W., Sawicki A., Milne P.C.:** Uni-axial compaction of a granular material. *J. Mech. Phys. Solids*, 41(11), 1755-1779, 1993.
115. **Moysey E.B.:** Active and passive pressures in deep grain bin. *Transactions of the ASAE*, 77, 1409-1413, 1979.
116. **Moysey E.B.:** The effect of grain spreaders on grain friction and bin wall pressures. *J. Agric. Engng. Res.*, 30, 149-156, 1984.
117. **Moysey E.B., Hiltz S.:** Friction properties of fertilizers. *Canadian Agricultural Engineering* 2, 79-83, 1985.
118. **Mróz Z., Drescher A., Hueckel T.:** Improvement of methods of investigations of flow parameters of granular materials (in Polish). *Prace IPPT PAN*, 54/73, 1973.
119. **Mühlhaus H.-B., Vardoulakis I.:** The thickness of shear bands in granular material. *Geotechnique*, 37(3), 271-283, 1987.
120. **Münch-Andersen J.:** The boundary layer in rough silos. *Transactions of the Inst. of Engineers, Australia*, ME 12(3), 167-170, 1987.
121. **Navarro S., Noyes R.:** The mechanics and physics of modern grain aeration management. CRC Press, 2002.
122. **Nedderman R.M., Laohakul C.:** The thickness of the shear zone of flowing granular materials. *Powder Technology*, 25, 91-100, 1980.
123. **Niedostatkiewicz M., Tejchman J.:** Experimental and Theoretical studies on Resonance Dynamic Effects During Silo Flow. *Powder Handling and Processing*, (1) 15, 36-42, 2003.
124. **Nielsen J.:** Load distribution in silos influenced by anisotropic grain behaviour. *International Conference on Bulk Materials Storage, Handling and Transportation*, New Castle, NSW, Australia, August, 1983.
125. **Nielsen J., Askegaard V.:** Scale errors in model tests on granular media with special reference to silo models. *Powder technology*, 16, 123-130, 1977.
126. **Oda M.:** Deformation mechanism of sand in triaxial compression tests. *Soil and Foundations*, 12(4), 45-63, 1972.
127. **Oda M.:** Fabrics and their effects on the deformation behaviours of sand. *Dept. Found. Engng. Fac. Engng. Saitama University, Special Issue*, 1976.
128. **Oda M.:** Coordination Number and its Relation to Shear Strength of granular material. *Soil and Foundations*, 17(2), 29-42, 1977.
129. **Oda M.:** Significance of fabric in granular mechanics. *Proc. US-Japan Seminar*, Sendai, Japan, 7-26, 1978.
130. **Oda M., Konishi J., Nemat-Nasser S.:** Some experimentally based fundamental results on the mechanical behaviour of granular materials. *Geotechnique*, 30, 479-495, 1980.
131. **Peschl I.A.S.Z.:** Equipment for the measurement of mechanical properties of bulk materials. *Powder Handling and Processing*, (1) 1, 73-81, 1989.
132. **Peschl I.A.S.Z.:** Measurement and evaluation of mechanical properties of powders. *Powder Handling and Processing*, (1) 2, 135-141, 1989.
133. **Peschl I.A.S.Z.:** Quality control of powders for industrial application. *Powder Handling and Processing*, (1) 4, 357-363, 1989.
134. **Ploof D.A., Carson J.W.:** Quality control tester to measure relative flowability of powders. *Bulk Solids Handling*, 14(1), 127-132, 1994.
135. **PN-B-03254-2002:** Concrete bins for granular materials. Calculation, design, performance and operation (in Polish).

136. PN-70/R-74010. Polish Standard. Cereal grains and edible legume seeds. Sampling. Wydawnictwa Normalizacyjne "ALFA" (in Polish).
137. PN-73/R-74007. Polish Standard. Cereal grains. Determination of density. Wydawnictwa Normalizacyjne "ALFA" (in Polish).
138. PN-74/Z-04002.07. Polish Standard. Air purity protection. Tests of dust physical properties. Determination of angle of repose dust. Polski Komitet Normalizacji i Miar (in Polish).
139. **Prusiel J.A., Nikitin W.:** Analyses of thermal effects in cylindrical concrete silos for bulk solids (in Polish). XI Konferencja „Żelbetowe i sprężone zbiorniki na materiały sypkie i ciecze”, 161-168, Świeradów Zdrój, 2000.
140. **Pukos A.:** Deformations of soil as influenced by distribution of pore size and solid phase particles (in Polish). Problemy Agrofizyki, Ossolineum, Wrocław, 61, 1990.
141. **Raltchev A., Barov W.:** New apparatus for determination of coefficient of internal friction (in Czech). Problemy obrabotki poczwy, Sofia, 169-177, 1970.
142. **Richter D.W.:** Friction coefficients of some agricultural materials. Agricultural Engineering, June, 411-413, 1954.
143. **Roscoe K.H.:** The influence of strains in soil mechanics. 10th Rankine Lecture. Géotechnique, 20(2), 127-170, 1970.
144. **Rowe P.W.:** The relation between the shear strength of sands in triaxial compression, plane strain and direct shear. Geotechnique, 19(1), 75-86, 1969
145. **Rusinek R.:** Pressure ratio of plant glant granular solids. PhD Dissertation, Institute of Agrophysics, Lublin, Poland 2005.
146. **Sakaguchi E., Kawasaki S., Tobita F.:** Simulation of flowing phenomena of grains by Distinct Element Method. AGENG, Milano'94, Report N.94-G-025, 1994.
147. **Sakaguchi E., Kawasaki S., Suzuki M., Urakawa T., Favier J.F.:** Effective use of DEM Simulations for Development of Grain Processing Technology. AngEng Oslo 98, 98-F-021, 1998.
148. **Sawicki A., Świdziński W.:** Cyclic compaction of soils, grains and powders. Powder Technology, 85, 97-104, 1995.
149. **Scherer R., Kutzbach H.D.:** Mechanische Eigenschaften von Kernerfruchten. Grundlagen Landtechnik, 1, 6-12, 1978.
150. **Schott R.W., Britton M.B.:** Plane strain behaviour of bulk grain. Paper No. NCR84-503, ASAE St. Joseph, MI 1984.
151. **Schwedes J.:** Shearing behaviour of slightly compressed cohesive granular materials. Powder Technol., 11, 59-67, 1975.
152. **Schwedes J.:** Review on testers for measuring flow properties. Granular Matter, 5, 1-43, 2003.
153. **Snyder L.H., Roller W.L., Hall G.E.:** Coefficients of kinetic friction of wheat on various metal surfaces. Transactions of the ASAE, 3, 411-419, 1967.
154. **Stasiak M., Molenda M.:** Influence of moisture content on stress-strain relationship of wheat bed (in Polish). VI Konferencja Międzynarodowa "Inżynieria mechaniczna żywności", Inżynieria Maszyn, 75-80, Bydgoszcz, 2001.
155. **Stephens L.E., Foster G.H.:** Grain bulk properties as affected by mechanical grain spreaders. Transactions of the ASAE, 19(2), 354-358, 1976.
156. **Stephens L.E., Foster G.H.:** Bulk properties of wheat and grain sorghum as affected by a mechanical grain spreaders. Transactions of the ASAE, 21(2), 1217-1221, 1978.
157. **Stewart B.R., Hossain Q.A., Kunze O.R.:** Friction coefficients of sorghum grain on steel, teflon and concrete surfaces. Transactions of the ASAE, 4, 415-418, 1969.

158. **Stępniewski A.:** Influence of moisture content and temperature on variability of mechanical properties of rapeseeds (in Polish). PhD thesis, Instytut Agrofizyki PAN, Lublin 1997.
159. **Ślaska – Grzywna B.:** Method of determination of limit values of compaction of granular materials (in Polish). PhD thesis. Akademia Rolnicza w Lublinie. Wydział Techniki Rolniczej, 1995.
160. **Tejchman J., Wu W.:** Experimental and numerical study of sand-steel interfaces. *Int. J. Numer. Anal. Methods Geomech.*, 19, 513-536, 1995.
161. **Thompson S.A., Ross L.J.:** Compressibility and frictional coefficient of wheat. *Transactions of the ASAE*, 26(4), 1171-1176, 1983.
162. **Timoshenko S., Goodier J.N.:** Theory of elasticity. 3rd Ed. New York, Hill, 1970.
163. **Tomas J.:** Particle adhesion fundamentals and bulk powder consolidation. *Powder, Handling and Processing*, 12(2), 131-138, 2000.
164. **Tsang-Mui-Chung M., Verma L. Lalit, Wright M.E.:** A device for friction measurement of grains. *Transactions of the ASAE*, 4, 1938-1944, 1984.
165. **Tripodi M.A., Puri V.M., Manbeck H.B., Messing G.L.:** Constitutive models for cohesive particulate materials. *J. Agric. Engng Res.*, 52, 1-21, 1992.
166. **Versavel P.A., Britton M.G.:** In-bin bulk density of grain. Paper No. 84-4004, ASAE, St. Joseph, MI, 1984.
167. **Voyiadjis G.Z., Thiagarajan G., Petrakis E.:** Constitutive modelling for granular media using an anisotropic distortional yield model. *Acta Mechanica*, 110, 151-171, 1995.
168. **Walton K.:** The effective elastic moduli of a random packing of spheres. *J. of Mech. Phys. of Solids*, 35(2), 213-226, 1987.
169. **Weiner W.:** Displacement of wheat grain in string conveyor. *Rozprawy 96*, University of Technology and Agriculture in Bydgoszcz, 1999.
170. **Wilms H.:** Criteria for evaluation of silo design codes. *Bulk Solids Handling*, 11 (1), 55-61, 1991.
171. **Woźniak W.:** Mechanical properties of wheat grain in internal cracks. *Int. Agrophysics*, 15, 59-64, 2001
172. **Yang S.H., Hsiao S.S.:** The simulation and experimental study of granular materials discharged from a silo with the placement of inserts. *Powder Technology*, 120, 244-255, 2001.
173. **Zhang Q., Puri V.M., Manbeck H.B.:** Determination of elastoplastic constitutive parameters for wheat en masse. *Transactions of the ASAE*, 29(6), 1739-1746, 1986.
174. **Zhang Q., Puri V.M., Manbeck H.B., Wang M.C.:** Elastoplastic constitutive parameters for wheat en masse for a cyclic load model. *Transactions of the ASAE*, 31(3), 910-916, 1988.
175. **Zhang Q., Puri V.M., Manbeck H.B.:** Model for frictional behaviour of wheat on structural materials. *Transactions of the ASAE*, 3, 898-903, 1988.
176. **Zhang Y.H., Jofriet J.C.:** Equivalent stress-strain relationship for soybean and corn. ASAE Paper No. 934506. ASAE, St. Joseph, MI 49085, 1993.
177. **Zhang Q., Britton M.G., Kieper R.J.:** Interactions between wheat and a corrugated steel surface. *Transactions of the ASAE*, 37(3), 951-956, 1994.

15. SUMMARY

The purpose of the authors of this book was to focus attention of the reader on what we believe is important for understanding of the mechanical behaviour of granular materials of biological origin. The main features of agro and food materials that make them different from mineral materials are strong influence of moisture content on mechanical behaviour and high deformability of granules. These differences bring about certain peculiar behaviours and necessity of adjustments of models of material, experimental techniques and technological solutions.

The material of “Mechanical Properties of Granular Agro-Materials and Food Powders for Industrial Practice” has been presented in two volumes. Part I “Characterization of mechanical properties of particulate solids for storage and handling” concerns mainly issues relevant for these operations, but contains also considerable amount of related matters. The main theoretical approaches – from the origins of soil mechanics to micropolar theory and DEM modelling have been addressed. A review of commonly applied experimental methods and material parameters has been presented. Finally, a catalogue of material parameters drawn from laboratory testing of the authors was attached for reference as well as for comparison with results of other laboratories. The final chapter: “Physical properties of granular food materials” presents a set of the physical properties of food powders and granular materials of a wide range of grain size: from cereal grains to flour and sugar. The catalogue contains following properties of granular solids: geometrical parameters, the porosity, the bulk density, the coefficient and the angle of wall friction, the angle of natural repose, the angle of internal friction, the cohesion, the flow index, the lateral to vertical pressure ratio, the modulus of elasticity and the Poisson’s ratio. In the case of cereal grains the influence of the moisture content was considered and in the case of food powders the influence of the consolidation pressure.

Keywords: granular materials, bulk solids, particulate media grain, seeds, food powders

16. APPENDIX – Physical Properties of Grain and Food Powders

16.1. Basic characteristics**Table 16.1.** Mean values of grain dimensions, the mass of 1000 grains and the specific gravity

Material	Moisture content (%)	Length (mm)	Width (mm)	Thickness (mm)	Mass of 1000 seeds (g)	Specific gravity (kN m^{-3})
Wheat Begra	10	6.7	3.2	2.9	40.5	13.8
Rye Amilo	10	7.3	2.3	2.2	20.5	12.3
Barley Rudnik	10	8.4	3.6	2.8	45.2	13.2
Corn Mieszko	10	9.4	8.2	5.1	295	13.7
Oats Borowiak	10	11.5	3.1	2.6	35.6	13.7
Triticale Fidelio	10	7.2	2.9	2.6	29.4	13.5

Table 16.2. Mean values of seeds dimensions, the mass of 1000 seeds and the specific gravity

Material	Moisture content (%)	Length (mm)	Width (mm)	Thickness (mm)	Mass of 1000 seeds (g)	Specific gravity (kN m^{-3})
Rape seeds Licosmos	6	1.8	1.7	1.7	3.5	11.1
Amaranth Rawa	8	0.85	0.85	0.85	0.76	14.8
White mustard Borowska	9	2.5	2.3	2.3	8.6	12.3
Pea Piast	10	7.9	7.2	6.7	300	14.3
Buckwheat Kora	10	6.1	3.6	3.5	29.3	14.5
Lentils Tina	8	5.6	2.3	2.3	49.8	14.8
Soybean Aldana	8	8.2	6.6	5.6	185	13.0

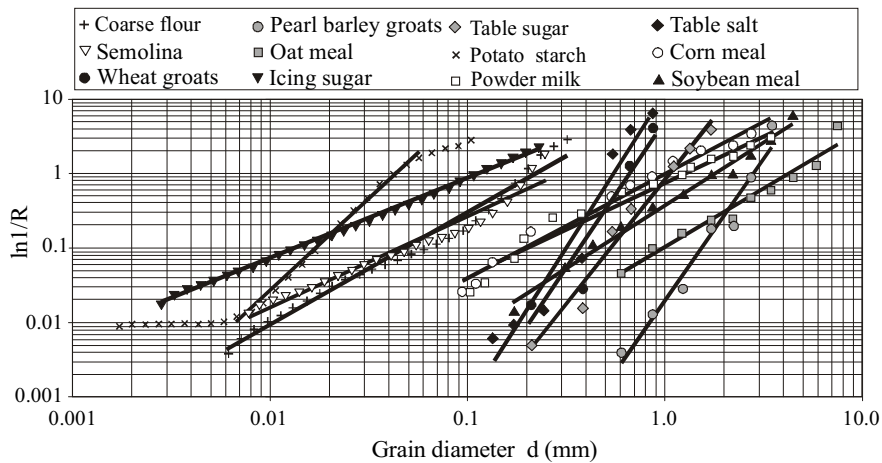


Fig. 16.1. Size distributions of food powders [67]

The Rosin-Ramler-Sperling-Bennet (DIN 66145 [42]) equation was used to describe the particle size distribution:

$$R = \exp(-(d/d^*)^n), \quad (16.1)$$

where: R – distribution function, d – particle diameter, d^* – mean particle diameter, n – coefficient of nonuniformity.

Table 16.3. Parameters of the RRSB equation (16.1) describing size distribution of food powders

Material	Moisture content (%)	Mean particle diameter d^* (mm)	Coefficient of uniformity n	Pearson's coefficient of correlation (%)
Coarse flour	13.4	0.147	1.673	98.8
Semolina	12.7	0.176	1.332	98.0
Wheat groats	13.6	0.683	0.480	94.0
Pearl barley groats	13.2	2.849	3.807	98.0
Oat meal	11.0	4.499	1.577	99.7
Icing sugar	0.4	0.061	1.171	99.9
Table sugar	0.4	1.070	3.348	98.7
Potato starch	18.2	0.033	2.737	99.8
Powder milk	4.4	1.252	1.276	98.1
Table salt	0.2	0.553	4.132	96.9
Corn meal	11.7	1.050	1.391	99.1
Soybean meal	8.5	1.827	1.688	99.3

16.2. Density and porosity

Table 16.4. Mean values (\pm St. Dev.) of bulk density, bulk density of material compacted according to Eurocode 1 [50], tapped density and porosity of cereal grain at the moisture content of 10-20%

Material	Moisture content (%)	Bulk density (kg m ⁻³)	Bulk density of compacted material (kg m ⁻³)	Tapped density (kg m ⁻³)	Porosity (%)
Wheat Begra	10	773 \pm 3	779 \pm 2	871 \pm 4	49.8
	12.5	765 \pm 3	799 \pm 9	861 \pm 7	48.8
	15	694 \pm 4	784 \pm 2	860 \pm 10	50.9
	17.5	705 \pm 4	778 \pm 5	868 \pm 9	52.8
	20	713 \pm 5	790 \pm 5	823 \pm 11	54.3
Rye Amilo	10	698 \pm 5	754 \pm 9	793 \pm 6	51.4
	12.5	688 \pm 5	772 \pm 8	805 \pm 7	49.8
	15	677 \pm 4	786 \pm 1	787 \pm 8	50.7
	17.5	682 \pm 5	785 \pm 4	801 \pm 3	48.6
	20	684 \pm 4	803 \pm 1	808 \pm 10	49.2
Barley Rudnik	10	686 \pm 3	787 \pm 3	780 \pm 3	50.9
	12.5	689 \pm 2	785 \pm 2	806 \pm 2	49.6
	15	680 \pm 5	781 \pm 2	801 \pm 3	50.1
	17.5	675 \pm 4	771 \pm 2	794 \pm 3	50.5
	20	667 \pm 3	780 \pm 7	783 \pm 9	52.8
Corn Mieszko	10	742 \pm 3	826 \pm 10	873 \pm 6	45.0
	12.5	728 \pm 3	847 \pm 3	878 \pm 4	45.0
	15	698 \pm 3	844 \pm 9	829 \pm 2	45.6
	17.5	672 \pm 2	825 \pm 15	845 \pm 4	47.5
	20	663 \pm 2	834 \pm 10	800 \pm 1	48.6
Oat Borowiak	10	557 \pm 2	646 \pm 9	632 \pm 12	60.8
	12.5	574 \pm 2	647 \pm 3	650 \pm 8	59.5
	15	547 \pm 2	656 \pm 8	624 \pm 12	61.0
	17.5	528 \pm 2	704 \pm 10	632 \pm 4	62.4
	20	527 \pm 3	698 \pm 7	639 \pm 10	62.5
Triticale Fidelio	10	615 \pm 5	711 \pm 2	684 \pm 3	55.5
	12.5	618 \pm 7	744 \pm 11	698 \pm 12	53.0
	15	605 \pm 6	739 \pm 11	689 \pm 5	54.2
	17.5	591 \pm 4	774 \pm 10	691 \pm 7	55.6
	20	571 \pm 4	781 \pm 3	665 \pm 12	57.0

Table 16.5. Mean values (\pm St. Dev.) of bulk density, bulk density of material compacted according to Eurocode 1 [50], tapped density and porosity of rape seeds variety Licosmos at the moisture content of 6-16%

Material	Moisture content (%)	Bulk density (kg m^{-3})	Bulk density of compacted material (kg m^{-3})	Tapped density (kg m^{-3})	Porosity (%)
Rape seeds	6	645 ± 5	712 ± 5	756 ± 4	41.8
	9	661 ± 2	740 ± 4	761 ± 6	41.5
	12	655 ± 3	788 ± 5	760 ± 6	40.2
	16	644 ± 2	800 ± 5	760 ± 5	41.9

Table 16.6. Mean values (\pm St. Dev.) of bulk density, bulk density of material compacted according to Eurocode 1 [50], tapped density and porosity of selected seeds

Material	Moisture content (%)	Bulk density (kg m^{-3})	Bulk density of compacted material (kg m^{-3})	Tapped density (kg m^{-3})	Porosity (%)
Amaranth. Rawa	8	823 ± 3	883 ± 3	934 ± 4	45.1
White mustard	9	707 ± 2	799 ± 2	824 ± 2	42.3
Pea. Piast	10	810 ± 3	869 ± 5	929 ± 7	43.2
Buckwheat. Kora	10	654 ± 2	686 ± 2	773 ± 2	55.2
Lentils.Tina	8	783 ± 2	840 ± 3	931 ± 9	47.1
Soybeans. Aldana	8	739 ± 3	795 ± 5	869 ± 4	45.2

Table 16.7. Mean values (\pm St. Dev.) of bulk density, bulk density of material compacted according to Eurocode 1 [50], tapped density and porosity of selected food powders

Material	Moisture content (%)	Bulk density (kg m^{-3})	Bulk density of compacted material (kg m^{-3})	Tapped density (kg m^{-3})	Porosity (%)
Flour	12.7	612 ± 2	717 ± 4	767 ± 7	67.6
Coarse flour	13.4	647 ± 1	758 ± 3	790 ± 7	61.7
Semolina	12.7	652 ± 2	705 ± 7	785 ± 7	57.7
Coarse flour	13.6	738 ± 2	767 ± 3	866 ± 10	51.0
Semolina	13.2	702 ± 2	802 ± 3	874 ± 9	52.7
Wheat groats	11.0	444 ± 1	490 ± 14	557 ± 4	71.5
Pearl barley groats	0.4	726 ± 2	757 ± 4	957 ± 9	64.5
Oat meal	0.4	858 ± 2	895 ± 7	1070 ± 7	49.2
Icing sugar	18.2	685 ± 1	725 ± 7	762 ± 7	66.0
Table sugar	4.4	577 ± 2	604 ± 1	701 ± 4	67.9
Potato starch	7.9	378 ± 2	419 ± 1	413 ± 7	83.4
Granulated milk	0.2	1087 ± 3	1326 ± 1	1531 ± 11	41.7
Table salt	11.7	614 ± 2	769 ± 1	755 ± 7	60.4
Corn meal	8.5	656 ± 4	816 ± 1	848 ± 6	63.1

16.3. Coefficient of friction

Table 16.8. Mean values (\pm St. Dev.) of the friction coefficient μ of wheat grain variety Begra at the moisture content of 10-20% against stainless steel, galvanized steel and concrete B30 determined at the normal pressure of 20-60 kPa

Moisture content (%)	Normal stress (kPa)	Coefficient of wall friction μ		
		Stainless steel	Galvanized steel	Concrete B30
10	20	0.189 \pm 0.003	0.174 \pm 0.010	0.541 \pm 0.014
	30	0.160 \pm 0.002	0.183 \pm 0.004	0.497 \pm 0.020
	40	0.152 \pm 0.004	0.170 \pm 0.003	0.496 \pm 0.007
	50	0.159 \pm 0.006	0.169 \pm 0.002	0.476 \pm 0.010
	60	0.160 \pm 0.004	0.165 \pm 0.003	0.468 \pm 0.005
12.5	20	0.186 \pm 0.001	0.178 \pm 0.004	0.502 \pm 0.009
	30	0.163 \pm 0.006	0.186 \pm 0.003	0.524 \pm 0.007
	40	0.156 \pm 0.004	0.173 \pm 0.003	0.510 \pm 0.018
	50	0.170 \pm 0.005	0.173 \pm 0.005	0.480 \pm 0.009
	60	0.163 \pm 0.002	0.171 \pm 0.001	0.489 \pm 0.006
15	20	0.191 \pm 0.007	0.209 \pm 0.001	0.540 \pm 0.030
	30	0.189 \pm 0.008	0.201 \pm 0.001	0.605 \pm 0.018
	40	0.174 \pm 0.012	0.184 \pm 0.002	0.546 \pm 0.023
	50	0.212 \pm 0.002	0.139 \pm 0.001	0.529 \pm 0.009
	60	0.182 \pm 0.003	0.165 \pm 0.004	0.519 \pm 0.007
17.5	20	0.249 \pm 0.011	0.204 \pm 0.005	0.571 \pm 0.035
	30	0.217 \pm 0.004	0.180 \pm 0.001	0.574 \pm 0.014
	40	0.220 \pm 0.009	0.169 \pm 0.003	0.593 \pm 0.003
	50	0.252 \pm 0.009	0.161 \pm 0.002	0.605 \pm 0.008
	60	0.287 \pm 0.020	0.143 \pm 0.004	0.602 \pm 0.004
20	20	0.340 \pm 0.028	0.245 \pm 0.014	0.562 \pm 0.009
	30	0.321 \pm 0.023	0.274 \pm 0.028	0.587 \pm 0.021
	40	0.277 \pm 0.022	0.224 \pm 0.020	0.598 \pm 0.009
	50	0.277 \pm 0.012	0.201 \pm 0.018	0.580 \pm 0.006
	60	0.279 \pm 0.016	0.191 \pm 0.008	0.595 \pm 0.010

Table 16.9. Mean values (\pm St. Dev.) of the friction coefficient μ of rye grain variety Amilo at the moisture content of 10-20% against stainless steel, galvanized steel and concrete B30 determined at the normal pressure of 20-60 kPa

Moisture content (%)	Normal stress (kPa)	Coefficient of wall friction μ		
		Stainless steel	Galvanized steel	Concrete B30
10	20	0.205 \pm 0.004	0.155 \pm 0.005	0.349 \pm 0.002
	30	0.195 \pm 0.009	0.169 \pm 0.001	0.354 \pm 0.007
	40	0.219 \pm 0.013	0.175 \pm 0.014	0.349 \pm 0.006
	50	0.214 \pm 0.013	0.143 \pm 0.001	0.337 \pm 0.007
	60	0.218 \pm 0.011	0.150 \pm 0.003	0.337 \pm 0.004
12.5	20	0.219 \pm 0.026	0.178 \pm 0.002	0.448 \pm 0.012
	30	0.256 \pm 0.010	0.172 \pm 0.013	0.420 \pm 0.016
	40	0.273 \pm 0.004	0.188 \pm 0.009	0.391 \pm 0.005
	50	0.284 \pm 0.001	0.195 \pm 0.006	0.358 \pm 0.019
	60	0.285 \pm 0.001	0.209 \pm 0.003	0.369 \pm 0.002
15	20	0.196 \pm 0.002	0.171 \pm 0.008	0.427 \pm 0.017
	30	0.217 \pm 0.010	0.164 \pm 0.004	0.399 \pm 0.006
	40	0.242 \pm 0.012	0.175 \pm 0.001	0.382 \pm 0.008
	50	0.230 \pm 0.012	0.142 \pm 0.006	0.406 \pm 0.007
	60	0.246 \pm 0.001	0.148 \pm 0.001	0.400 \pm 0.007
17.5	20	0.219 \pm 0.006	0.197 \pm 0.013	0.602 \pm 0.008
	30	0.247 \pm 0.009	0.171 \pm 0.014	0.574 \pm 0.009
	40	0.261 \pm 0.004	0.170 \pm 0.003	0.559 \pm 0.004
	50	0.258 \pm 0.012	0.159 \pm 0.005	0.539 \pm 0.015
	60	0.225 \pm 0.021	0.156 \pm 0.001	0.502 \pm 0.003
20	20	0.277 \pm 0.023	0.235 \pm 0.007	0.453 \pm 0.016
	30	0.286 \pm 0.001	0.234 \pm 0.002	0.451 \pm 0.009
	40	0.293 \pm 0.014	0.213 \pm 0.002	0.442 \pm 0.008
	50	0.290 \pm 0.008	0.211 \pm 0.001	0.487 \pm 0.013
	60	0.255 \pm 0.015	0.211 \pm 0.001	0.514 \pm 0.009

Table 16.10. Mean values (\pm St. Dev.) of the friction coefficient μ of barley grain variety Rudnik at the moisture content of 10-20% against stainless steel, galvanized steel and concrete B30 determined at the normal pressure of 20-60 kPa

Moisture content (%)	Normal stress (kPa)	Coefficient of wall friction μ		
		Stainless steel	Galvanized steel	Concrete B30
10	20	0.176 \pm 0.006	0.217 \pm 0.014	0.487 \pm 0.013
	30	0.163 \pm 0.008	0.193 \pm 0.009	0.468 \pm 0.007
	40	0.157 \pm 0.002	0.173 \pm 0.010	0.451 \pm 0.012
	50	0.160 \pm 0.006	0.171 \pm 0.003	0.444 \pm 0.004
	60	0.150 \pm 0.005	0.171 \pm 0.007	0.426 \pm 0.004
12.5	20	0.152 \pm 0.002	0.153 \pm 0.005	0.478 \pm 0.018
	30	0.148 \pm 0.001	0.145 \pm 0.006	0.483 \pm 0.011
	40	0.149 \pm 0.001	0.146 \pm 0.001	0.483 \pm 0.011
	50	0.157 \pm 0.004	0.139 \pm 0.003	0.496 \pm 0.004
	60	0.163 \pm 0.001	0.144 \pm 0.001	0.480 \pm 0.010
15	20	0.143 \pm 0.005	0.166 \pm 0.020	0.537 \pm 0.022
	30	0.139 \pm 0.009	0.152 \pm 0.009	0.547 \pm 0.012
	40	0.133 \pm 0.003	0.160 \pm 0.009	0.518 \pm 0.011
	50	0.131 \pm 0.003	0.147 \pm 0.009	0.522 \pm 0.002
	60	0.131 \pm 0.001	0.142 \pm 0.003	0.490 \pm 0.014
17.5	20	0.166 \pm 0.015	0.169 \pm 0.001	0.507 \pm 0.021
	30	0.141 \pm 0.006	0.156 \pm 0.004	0.540 \pm 0.012
	40	0.146 \pm 0.016	0.144 \pm 0.005	0.554 \pm 0.012
	50	0.145 \pm 0.005	0.145 \pm 0.005	0.520 \pm 0.009
	60	0.162 \pm 0.006	0.155 \pm 0.010	0.543 \pm 0.007
20	20	0.245 \pm 0.006	0.200 \pm 0.014	0.549 \pm 0.014
	30	0.230 \pm 0.017	0.185 \pm 0.013	0.566 \pm 0.012
	40	0.220 \pm 0.013	0.184 \pm 0.009	0.594 \pm 0.007
	50	0.215 \pm 0.008	0.176 \pm 0.008	0.561 \pm 0.014
	60	0.225 \pm 0.009	0.176 \pm 0.012	0.582 \pm 0.005

Table 16.11. Mean values (\pm St. Dev.) of the friction coefficient μ of corn grain variety Mieszko at the moisture content of 10-20% against stainless steel, galvanized steel and concrete B30 determined at the normal pressure of 20-60 kPa

Moisture content (%)	Normal stress (kPa)	Coefficient of wall friction μ		
		Stainless steel	Galvanized steel	Concrete B30
10	20	0.161 \pm 0.006	0.157 \pm 0.008	0.352 \pm 0.007
	30	0.157 \pm 0.008	0.140 \pm 0.008	0.349 \pm 0.004
	40	0.170 \pm 0.008	0.145 \pm 0.007	0.352 \pm 0.007
	50	0.155 \pm 0.003	0.146 \pm 0.007	0.352 \pm 0.003
	60	0.172 \pm 0.007	0.136 \pm 0.003	0.346 \pm 0.003
12.5	20	0.144 \pm 0.001	0.128 \pm 0.011	0.528 \pm 0.013
	30	0.136 \pm 0.001	0.125 \pm 0.003	0.519 \pm 0.011
	40	0.134 \pm 0.001	0.124 \pm 0.002	0.511 \pm 0.005
	50	0.138 \pm 0.001	0.137 \pm 0.009	0.549 \pm 0.007
	60	0.143 \pm 0.004	0.136 \pm 0.007	0.580 \pm 0.010
15	20	0.214 \pm 0.011	0.136 \pm 0.007	0.629 \pm 0.007
	30	0.171 \pm 0.009	0.131 \pm 0.003	0.615 \pm 0.015
	40	0.163 \pm 0.008	0.128 \pm 0.004	0.607 \pm 0.013
	50	0.151 \pm 0.001	0.127 \pm 0.001	0.593 \pm 0.005
	60	0.147 \pm 0.004	0.117 \pm 0.005	0.584 \pm 0.010
17.5	20	0.221 \pm 0.003	0.141 \pm 0.002	0.626 \pm 0.019
	30	0.178 \pm 0.005	0.132 \pm 0.002	0.611 \pm 0.006
	40	0.167 \pm 0.002	0.131 \pm 0.001	0.601 \pm 0.011
	50	0.153 \pm 0.002	0.129 \pm 0.002	0.610 \pm 0.006
	60	0.150 \pm 0.004	0.122 \pm 0.003	0.597 \pm 0.008
20	20	0.242 \pm 0.012	0.149 \pm 0.011	0.670 \pm 0.017
	30	0.243 \pm 0.003	0.157 \pm 0.008	0.644 \pm 0.020
	40	0.239 \pm 0.001	0.164 \pm 0.006	0.658 \pm 0.018
	50	0.225 \pm 0.001	0.172 \pm 0.004	0.625 \pm 0.002
	60	0.208 \pm 0.016	0.173 \pm 0.008	0.594 \pm 0.049

Table 16.12. Mean values (\pm St. Dev.) of the friction coefficient μ of oat grain variety Borowiak at the moisture content of 10-20% against stainless steel, galvanized steel and concrete B30 determined at the normal pressure of 20-60 kPa

Moisture content (%)	Normal stress (kPa)	Coefficient of wall friction μ		
		Stainless steel	Galvanized steel	Concrete B30
10	20	0.158 \pm 0.004	0.195 \pm 0.014	0.345 \pm 0.005
	30	0.150 \pm 0.001	0.200 \pm 0.008	0.328 \pm 0.001
	40	0.147 \pm 0.004	0.180 \pm 0.004	0.324 \pm 0.002
	50	0.148 \pm 0.003	0.180 \pm 0.002	0.327 \pm 0.001
	60	0.149 \pm 0.004	0.176 \pm 0.003	0.343 \pm 0.009
12.5	20	0.160 \pm 0.007	0.199 \pm 0.018	0.304 \pm 0.006
	30	0.152 \pm 0.002	0.203 \pm 0.012	0.294 \pm 0.004
	40	0.151 \pm 0.007	0.182 \pm 0.007	0.310 \pm 0.011
	50	0.150 \pm 0.002	0.182 \pm 0.003	0.342 \pm 0.008
	60	0.153 \pm 0.006	0.179 \pm 0.006	0.360 \pm 0.009
15	20	0.181 \pm 0.009	0.167 \pm 0.008	0.363 \pm 0.019
	30	0.180 \pm 0.003	0.161 \pm 0.009	0.389 \pm 0.012
	40	0.168 \pm 0.005	0.163 \pm 0.005	0.415 \pm 0.002
	50	0.161 \pm 0.004	0.162 \pm 0.009	0.409 \pm 0.023
	60	0.159 \pm 0.003	0.158 \pm 0.004	0.427 \pm 0.016
17.5	20	0.181 \pm 0.007	0.160 \pm 0.008	0.483 \pm 0.016
	30	0.179 \pm 0.012	0.172 \pm 0.005	0.514 \pm 0.008
	40	0.187 \pm 0.004	0.161 \pm 0.002	0.526 \pm 0.010
	50	0.170 \pm 0.006	0.157 \pm 0.001	0.512 \pm 0.012
	60	0.161 \pm 0.011	0.161 \pm 0.002	0.476 \pm 0.001
20	20	0.151 \pm 0.021	0.160 \pm 0.004	0.479 \pm 0.016
	30	0.137 \pm 0.007	0.157 \pm 0.016	0.508 \pm 0.002
	40	0.155 \pm 0.009	0.146 \pm 0.004	0.518 \pm 0.008
	50	0.141 \pm 0.008	0.147 \pm 0.005	0.498 \pm 0.007
	60	0.151 \pm 0.002	0.136 \pm 0.006	0.511 \pm 0.007

Table 16.13. Mean values (\pm St. Dev.) of the friction coefficient μ of triticale grain variety Fidelio at the moisture content of 10-20% against stainless steel, galvanized steel and concrete B30 determined at the normal pressure of 20-60 kPa

Moisture content (%)	Normal stress (kPa)	Coefficient of wall friction μ		
		Stainless steel	Galvanized steel	Concrete B30
10	20	0.181 \pm 0.018	0.249 \pm 0.009	0.473 \pm 0.031
	30	0.180 \pm 0.002	0.237 \pm 0.017	0.448 \pm 0.007
	40	0.189 \pm 0.005	0.236 \pm 0.004	0.439 \pm 0.006
	50	0.173 \pm 0.007	0.215 \pm 0.005	0.439 \pm 0.010
	60	0.176 \pm 0.013	0.198 \pm 0.001	0.427 \pm 0.008
12.5	20	0.223 \pm 0.019	0.167 \pm 0.014	0.344 \pm 0.005
	30	0.244 \pm 0.016	0.189 \pm 0.005	0.401 \pm 0.020
	40	0.245 \pm 0.026	0.190 \pm 0.009	0.416 \pm 0.014
	50	0.247 \pm 0.030	0.184 \pm 0.007	0.413 \pm 0.016
	60	0.281 \pm 0.013	0.200 \pm 0.007	0.407 \pm 0.010
15	20	0.296 \pm 0.015	0.214 \pm 0.018	0.522 \pm 0.014
	30	0.322 \pm 0.005	0.214 \pm 0.003	0.547 \pm 0.022
	40	0.300 \pm 0.021	0.240 \pm 0.023	0.559 \pm 0.009
	50	0.306 \pm 0.010	0.225 \pm 0.002	0.561 \pm 0.008
	60	0.281 \pm 0.004	0.265 \pm 0.026	0.521 \pm 0.018
17.5	20	0.297 \pm 0.015	0.240 \pm 0.002	0.587 \pm 0.021
	30	0.318 \pm 0.005	0.240 \pm 0.001	0.592 \pm 0.016
	40	0.305 \pm 0.008	0.270 \pm 0.003	0.572 \pm 0.011
	50	0.304 \pm 0.005	0.290 \pm 0.003	0.584 \pm 0.008
	60	0.297 \pm 0.007	0.250 \pm 0.001	0.579 \pm 0.004
20	20	0.358 \pm 0.023	0.281 \pm 0.006	0.623 \pm 0.010
	30	0.366 \pm 0.017	0.306 \pm 0.022	0.605 \pm 0.015
	40	0.333 \pm 0.013	0.308 \pm 0.021	0.592 \pm 0.015
	50	0.350 \pm 0.004	0.350 \pm 0.006	0.605 \pm 0.023
	60	0.237 \pm 0.013	0.323 \pm 0.015	0.619 \pm 0.030

Table 16.14. Mean values (\pm St. Dev.) of the friction coefficient μ of rape seeds variety Licosmos at the moisture content of 6-15% against stainless steel, galvanized steel and concrete B30 determined at the normal pressure of 20-60 kPa

Moisture content (%)	Normal stress (kPa)	Coefficient of wall friction μ		
		Stainless steel	Galvanized steel	Concrete B30
6	20	0.173 \pm 0.009	0.191 \pm 0.011	0.353 \pm 0.004
	30	0.157 \pm 0.006	0.185 \pm 0.004	0.355 \pm 0.008
	40	0.148 \pm 0.005	0.171 \pm 0.009	0.351 \pm 0.004
	50	0.148 \pm 0.004	0.161 \pm 0.003	0.359 \pm 0.004
	60	0.142 \pm 0.005	0.163 \pm 0.006	0.352 \pm 0.005
9	20	0.165 \pm 0.007	0.173 \pm 0.014	0.357 \pm 0.008
	30	0.151 \pm 0.004	0.164 \pm 0.001	0.346 \pm 0.012
	40	0.153 \pm 0.005	0.150 \pm 0.009	0.342 \pm 0.016
	50	0.163 \pm 0.004	0.148 \pm 0.004	0.349 \pm 0.023
	60	0.157 \pm 0.006	0.152 \pm 0.006	0.363 \pm 0.005
12	20	0.106 \pm 0.002	0.133 \pm 0.026	0.366 \pm 0.002
	30	0.106 \pm 0.001	0.121 \pm 0.003	0.383 \pm 0.008
	40	0.106 \pm 0.004	0.102 \pm 0.002	0.404 \pm 0.010
	50	0.114 \pm 0.002	0.096 \pm 0.002	0.405 \pm 0.009
	60	0.123 \pm 0.009	0.087 \pm 0.003	0.416 \pm 0.003
15	20	0.219 \pm 0.022	0.120 \pm 0.006	0.400 \pm 0.002
	30	0.174 \pm 0.003	0.113 \pm 0.001	0.425 \pm 0.006
	40	0.170 \pm 0.005	0.111 \pm 0.001	0.448 \pm 0.005
	50	0.174 \pm 0.002	0.113 \pm 0.005	0.459 \pm 0.006
	60	0.173 \pm 0.003	0.125 \pm 0.013	0.463 \pm 0.009

Table 16.15. Mean values (\pm St. Dev.) of the friction coefficient μ of selected seeds against stainless steel, galvanized steel and concrete B30 determined at the normal pressure of 20-60 kPa

Material, moisture content (%)	Normal stress (kPa)	Coefficient of wall friction μ		
		Stainless steel	Galvanized steel	Concrete B30
Amaranth Rawa 8	20	0.119 \pm 0.004	0.136 \pm 0.007	0.378 \pm 0.001
	30	0.115 \pm 0.001	0.125 \pm 0.007	0.370 \pm 0.006
	40	0.111 \pm 0.001	0.128 \pm 0.010	0.378 \pm 0.009
	50	0.107 \pm 0.001	0.120 \pm 0.005	0.371 \pm 0.008
	60	0.108 \pm 0.003	0.109 \pm 0.002	0.372 \pm 0.003
White mustard Borowska 9	20	0.134 \pm 0.003	0.108 \pm 0.004	0.352 \pm 0.008
	30	0.128 \pm 0.009	0.100 \pm 0.002	0.353 \pm 0.007
	40	0.132 \pm 0.008	0.098 \pm 0.006	0.354 \pm 0.012
	50	0.125 \pm 0.008	0.097 \pm 0.002	0.340 \pm 0.007
	60	0.123 \pm 0.009	0.097 \pm 0.003	0.315 \pm 0.012
Pea Piast 10	20	0.146 \pm 0.013	0.138 \pm 0.023	0.292 \pm 0.006
	30	0.135 \pm 0.007	0.121 \pm 0.003	0.318 \pm 0.001
	40	0.147 \pm 0.016	0.120 \pm 0.006	0.323 \pm 0.005
	50	0.153 \pm 0.015	0.123 \pm 0.013	0.331 \pm 0.006
	60	0.136 \pm 0.009	0.123 \pm 0.006	0.337 \pm 0.002
Buckwheat Kora 10	20	0.156 \pm 0.009	0.177 \pm 0.002	0.379 \pm 0.011
	30	0.154 \pm 0.002	0.150 \pm 0.004	0.385 \pm 0.011
	40	0.158 \pm 0.003	0.150 \pm 0.003	0.372 \pm 0.006
	50	0.157 \pm 0.001	0.149 \pm 0.004	0.369 \pm 0.006
	60	0.161 \pm 0.005	0.149 \pm 0.002	0.371 \pm 0.008
Lentils Tina 8	20	0.160 \pm 0.015	0.160 \pm 0.007	0.258 \pm 0.014
	30	0.160 \pm 0.013	0.142 \pm 0.012	0.267 \pm 0.012
	40	0.141 \pm 0.012	0.142 \pm 0.010	0.263 \pm 0.005
	50	0.140 \pm 0.005	0.131 \pm 0.003	0.259 \pm 0.002
	60	0.135 \pm 0.005	0.136 \pm 0.007	0.263 \pm 0.006
Soybeans Aldana 8	20	0.147 \pm 0.003	0.165 \pm 0.024	0.405 \pm 0.012
	30	0.169 \pm 0.010	0.202 \pm 0.008	0.413 \pm 0.014
	40	0.175 \pm 0.002	0.178 \pm 0.011	0.412 \pm 0.012
	50	0.170 \pm 0.023	0.162 \pm 0.010	0.424 \pm 0.010
	60	0.169 \pm 0.017	0.198 \pm 0.019	0.434 \pm 0.011

Table 16.16. Mean values (\pm St. Dev.) of the friction coefficient μ of selected food powders against stainless steel and galvanized steel determined at the normal pressure of 20-60 kPa

Material, moisture content (%)	Normal stress (kPa)	Coefficient of wall friction μ	
		Stainless steel	Galvanized steel
1	2	3	4
Flour 12.7	20	0.172 \pm 0.019	0.238 \pm 0.009
	30	0.159 \pm 0.020	0.267 \pm 0.013
	40	0.143 \pm 0.002	0.260 \pm 0.012
	50	0.146 \pm 0.001	0.247 \pm 0.015
	60	0.152 \pm 0.002	0.244 \pm 0.007
Coarse flour 13.4	20	0.167 \pm 0.001	0.203 \pm 0.027
	30	0.161 \pm 0.002	0.204 \pm 0.002
	40	0.162 \pm 0.004	0.215 \pm 0.007
	50	0.160 \pm 0.004	0.231 \pm 0.008
	60	0.159 \pm 0.002	0.231 \pm 0.006
Semolina 12.7	20	0.102 \pm 0.003	0.088 \pm 0.001
	30	0.099 \pm 0.001	0.082 \pm 0.003
	40	0.107 \pm 0.008	0.085 \pm 0.002
	50	0.123 \pm 0.005	0.087 \pm 0.003
	60	0.100 \pm 0.005	0.098 \pm 0.007
Wheat groats 13.6	20	0.180 \pm 0.007	0.219 \pm 0.040
	30	0.188 \pm 0.008	0.169 \pm 0.011
	40	0.170 \pm 0.013	0.150 \pm 0.010
	50	0.182 \pm 0.005	0.155 \pm 0.013
	60	0.172 \pm 0.006	0.154 \pm 0.003
Pearl barley groats 13.2	20	0.324 \pm 0.020	0.276 \pm 0.032
	30	0.284 \pm 0.011	0.220 \pm 0.019
	40	0.240 \pm 0.011	0.180 \pm 0.010
	50	0.211 \pm 0.008	0.164 \pm 0.001
	60	0.192 \pm 0.004	0.139 \pm 0.003
Oat meal 11.0	20	0.119 \pm 0.006	0.132 \pm 0.012
	30	0.123 \pm 0.007	0.131 \pm 0.004
	40	0.124 \pm 0.005	0.121 \pm 0.001
	50	0.111 \pm 0.009	0.117 \pm 0.008
	60	0.112 \pm 0.002	0.121 \pm 0.001

Table 16.16. Cont.

1	2	3	4
Icing sugar 0.4	20	0.174 ± 0.032	0.201 ± 0.013
	30	0.233 ± 0.018	0.260 ± 0.008
	40	0.257 ± 0.010	0.284 ± 0.013
	50	0.269 ± 0.005	0.294 ± 0.014
	60	0.298 ± 0.011	0.292 ± 0.008
Table sugar 0.4	20	0.180 ± 0.013	0.157 ± 0.014
	30	0.236 ± 0.025	0.188 ± 0.018
	40	0.277 ± 0.012	0.213 ± 0.005
	50	0.274 ± 0.022	0.224 ± 0.033
	60	0.314 ± 0.016	0.270 ± 0.035
Potato starch 18.2	20	0.205 ± 0.016	0.324 ± 0.029
	30	0.252 ± 0.009	0.365 ± 0.009
	40	0.277 ± 0.004	0.399 ± 0.012
	50	0.287 ± 0.007	0.385 ± 0.004
	60	0.304 ± 0.016	0.374 ± 0.017
Powder milk 4.4	20	0.174 ± 0.008	0.173 ± 0.009
	30	0.188 ± 0.003	0.181 ± 0.002
	40	0.197 ± 0.006	0.180 ± 0.002
	50	0.185 ± 0.003	0.183 ± 0.002
	60	0.189 ± 0.003	0.187 ± 0.007
Granulated milk 7.9	20	0.147 ± 0.003	0.151 ± 0.001
	30	0.156 ± 0.002	0.151 ± 0.001
	40	0.163 ± 0.003	0.161 ± 0.005
	50	0.168 ± 0.002	0.168 ± 0.002
	60	0.175 ± 0.004	0.175 ± 0.004
Table salt 0.2	20	0.257 ± 0.009	0.341 ± 0.013
	30	0.246 ± 0.007	0.345 ± 0.012
	40	0.234 ± 0.005	0.345 ± 0.008
	50	0.226 ± 0.001	0.318 ± 0.011
	60	0.228 ± 0.009	0.335 ± 0.016
Corn meal 11.7	20	0.176 ± 0.003	0.116 ± 0.009
	30	0.159 ± 0.002	0.110 ± 0.002
	40	0.135 ± 0.007	0.116 ± 0.004
	50	0.134 ± 0.009	0.118 ± 0.002
	60	0.140 ± 0.013	0.122 ± 0.001
Soybean meal 8.5	20	0.152 ± 0.007	0.108 ± 0.005
	30	0.141 ± 0.003	0.107 ± 0.005
	40	0.139 ± 0.007	0.091 ± 0.002
	50	0.128 ± 0.010	0.093 ± 0.001
	60	0.117 ± 0.006	0.092 ± 0.002

16.4. Angle of wall friction

Tables below contain values of coefficient of friction of granular material, $\mu = \text{tg } \varphi_w$, against stainless steel, galvanized steel and concrete of B30 class calculated from of the angle of wall friction, φ_w , for the evaluation of flow assessment determined according to the tilting table method for the normal pressure ranging from 0.5 to 2.5 kPa.

Table 16.17. Mean values (\pm St. Dev.) of the friction coefficient μ of wheat grain variety Begra at the moisture content of 10-20% against stainless steel, galvanized steel and concrete B30 determined at the normal pressure of 0.5-2.5 kPa

Moisture content (%)	Normal stress (kPa)	Coefficient of friction μ		
		Stainless steel	Galvanized steel	Concrete B30
10	0.5	0.282 \pm 0.005	0.32 \pm 0.005	0.422 \pm 0.010
	1.0	0.275 \pm 0.007	0.30 \pm 0.008	0.388 \pm 0.012
	1.5	0.249 \pm 0.002	0.27 \pm 0.004	0.425 \pm 0.015
	2.1	0.260 \pm 0.004	0.26 \pm 0.003	0.399 \pm 0.013
	2.5	0.257 \pm 0.003	0.23 \pm 0.011	0.409 \pm 0.022
12.5	0.5	0.265 \pm 0.010	0.34 \pm 0.007	0.379 \pm 0.006
	1.0	0.248 \pm 0.009	0.31 \pm 0.011	0.438 \pm 0.012
	1.5	0.269 \pm 0.008	0.28 \pm 0.008	0.408 \pm 0.015
	2.1	0.259 \pm 0.010	0.27 \pm 0.004	0.458 \pm 0.016
	2.5	0.262 \pm 0.009	0.26 \pm 0.006	0.434 \pm 0.010
15	0.5	0.335 \pm 0.003	0.34 \pm 0.013	0.476 \pm 0.011
	1.0	0.310 \pm 0.003	0.33 \pm 0.003	0.458 \pm 0.006
	1.5	0.280 \pm 0.003	0.31 \pm 0.013	0.441 \pm 0.026
	2.1	0.287 \pm 0.004	0.29 \pm 0.003	0.476 \pm 0.011
	2.5	0.292 \pm 0.008	0.26 \pm 0.021	0.462 \pm 0.013
17.5	0.5	0.383 \pm 0.003	0.42 \pm 0.016	0.479 \pm 0.012
	1.0	0.344 \pm 0.004	0.41 \pm 0.019	0.494 \pm 0.013
	1.5	0.323 \pm 0.005	0.42 \pm 0.022	0.472 \pm 0.006
	2.1	0.326 \pm 0.001	0.37 \pm 0.016	0.527 \pm 0.006
	2.5	0.313 \pm 0.007	0.35 \pm 0.017	0.494 \pm 0.013
20	0.5	0.414 \pm 0.003	0.44 \pm 0.007	0.536 \pm 0.050
	1.0	0.375 \pm 0.009	0.42 \pm 0.003	0.546 \pm 0.007
	1.5	0.346 \pm 0.004	0.41 \pm 0.007	0.483 \pm 0.006
	2.1	0.341 \pm 0.009	0.40 \pm 0.009	0.527 \pm 0.006
	2.5	0.335 \pm 0.012	0.34 \pm 0.026	0.508 \pm 0.011

Table 16.18. Mean values (\pm St. Dev.) of the friction coefficient μ of rye grain variety Amilo at the moisture content of 10-20% against stainless steel, galvanized steel and concrete B30 determined at the normal pressure of 0.5-2.5 kPa

Moisture content (%)	Normal stress (kPa)	Coefficient of friction μ		
		Stainless steel	Galvanized steel	Concrete B30
10	0.5	0.230 \pm 0.004	0.196 \pm 0.005	0.369 \pm 0.020
	1.0	0.227 \pm 0.010	0.196 \pm 0.005	0.366 \pm 0.019
	1.5	0.235 \pm 0.005	0.196 \pm 0.005	0.363 \pm 0.014
	2.1	0.213 \pm 0.005	0.194 \pm 0.005	0.329 \pm 0.018
	2.5	0.224 \pm 0.001	0.199 \pm 0.008	0.338 \pm 0.009
12.5	0.5	0.244 \pm 0.005	0.255 \pm 0.005	0.360 \pm 0.014
	1.0	0.255 \pm 0.005	0.241 \pm 0.001	0.332 \pm 0.019
	1.5	0.264 \pm 0.005	0.241 \pm 0.001	0.341 \pm 0.019
	2.1	0.270 \pm 0.005	0.235 \pm 0.005	0.360 \pm 0.039
	2.5	0.284 \pm 0.001	0.221 \pm 0.005	0.388 \pm 0.006
15	0.5	0.258 \pm 0.009	0.221 \pm 0.005	0.411 \pm 0.006
	1.0	0.273 \pm 0.005	0.216 \pm 0.008	0.350 \pm 0.011
	1.5	0.287 \pm 0.010	0.219 \pm 0.005	0.379 \pm 0.006
	2.1	0.287 \pm 0.010	0.224 \pm 0.001	0.287 \pm 0.020
	2.5	0.287 \pm 0.005	0.213 \pm 0.005	0.252 \pm 0.010
17.5	0.5	0.276 \pm 0.009	0.255 \pm 0.005	0.428 \pm 0.012
	1.0	0.278 \pm 0.005	0.255 \pm 0.005	0.428 \pm 0.015
	1.5	0.278 \pm 0.010	0.250 \pm 0.001	0.434 \pm 0.000
	2.1	0.290 \pm 0.005	0.241 \pm 0.001	0.376 \pm 0.010
	2.5	0.290 \pm 0.005	0.235 \pm 0.005	0.360 \pm 0.011
20	0.5	0.341 \pm 0.011	0.273 \pm 0.005	0.372 \pm 0.005
	1.0	0.363 \pm 0.005	0.287 \pm 0.005	0.401 \pm 0.015
	1.5	0.379 \pm 0.006	0.284 \pm 0.001	0.354 \pm 0.011
	2.1	0.388 \pm 0.006	0.281 \pm 0.013	0.345 \pm 0.030
	2.5	0.374 \pm 0.003	0.287 \pm 0.010	0.357 \pm 0.009

Table 16.19. Mean values (\pm St. Dev.) of the friction coefficient μ of barley grain variety Rudnik at the moisture content of 10-20% against stainless steel, galvanized steel and concrete B30 determined at the normal pressure of 0.5-2.5 kPa

Moisture content (%)	Normal stress (kPa)	Coefficient of friction μ		
		Stainless steel	Galvanized steel	Concrete B30
10	0.5	0.257 \pm 0.002	0.252 \pm 0.003	0.428 \pm 0.015
	1.0	0.242 \pm 0.009	0.244 \pm 0.006	0.402 \pm 0.008
	1.5	0.241 \pm 0.012	0.237 \pm 0.010	0.405 \pm 0.018
	2.1	0.234 \pm 0.009	0.225 \pm 0.004	0.383 \pm 0.007
	2.5	0.226 \pm 0.005	0.228 \pm 0.007	0.408 \pm 0.006
12.5	0.5	0.280 \pm 0.008	0.269 \pm 0.003	0.347 \pm 0.019
	1.0	0.245 \pm 0.010	0.266 \pm 0.002	0.335 \pm 0.014
	1.5	0.239 \pm 0.010	0.259 \pm 0.005	0.351 \pm 0.019
	2.1	0.239 \pm 0.008	0.248 \pm 0.007	0.258 \pm 0.001
	2.5	0.252 \pm 0.005	0.233 \pm 0.021	0.273 \pm 0.022
15	0.5	0.258 \pm 0.006	0.273 \pm 0.005	0.382 \pm 0.015
	1.0	0.256 \pm 0.009	0.264 \pm 0.004	0.401 \pm 0.009
	1.5	0.241 \pm 0.007	0.250 \pm 0.003	0.323 \pm 0.014
	2.1	0.234 \pm 0.014	0.247 \pm 0.012	0.293 \pm 0.024
	2.5	0.232 \pm 0.004	0.246 \pm 0.012	0.317 \pm 0.032
17.5	0.5	0.278 \pm 0.010	0.325 \pm 0.012	0.368 \pm 0.020
	1.0	0.267 \pm 0.002	0.267 \pm 0.007	0.338 \pm 0.001
	1.5	0.256 \pm 0.007	0.247 \pm 0.010	0.320 \pm 0.009
	2.1	0.240 \pm 0.005	0.256 \pm 0.018	0.332 \pm 0.005
	2.5	0.238 \pm 0.004	0.240 \pm 0.008	0.302 \pm 0.015
20	0.5	0.279 \pm 0.012	0.352 \pm 0.004	0.414 \pm 0.010
	1.0	0.266 \pm 0.006	0.298 \pm 0.009	0.438 \pm 0.006
	1.5	0.252 \pm 0.012	0.281 \pm 0.019	0.428 \pm 0.006
	2.1	0.251 \pm 0.015	0.273 \pm 0.013	0.386 \pm 0.035
	2.5	0.245 \pm 0.011	0.283 \pm 0.008	0.369 \pm 0.024

Table 16.20. Mean values (\pm St. Dev.) of the friction coefficient μ of corn grain variety Mieszko at the moisture content of 10-20% against stainless steel, galvanized steel and concrete B30 determined at the normal pressure of 0.5-2.5 kPa

Moisture content (%)	Normal stress (kPa)	Coefficient of friction μ		
		Stainless steel	Galvanized steel	Concrete B30
10	0.5	0.292 \pm 0.001	0.273 \pm 0.007	0.402 \pm 0.002
	1.0	0.294 \pm 0.003	0.259 \pm 0.008	0.326 \pm 0.022
	1.5	0.289 \pm 0.007	0.258 \pm 0.005	0.376 \pm 0.030
	2.1	0.269 \pm 0.003	0.234 \pm 0.002	0.393 \pm 0.014
	2.5	0.246 \pm 0.006	0.232 \pm 0.007	0.382 \pm 0.020
12.5	0.5	0.262 \pm 0.014	0.290 \pm 0.005	0.369 \pm 0.005
	1.0	0.261 \pm 0.016	0.249 \pm 0.007	0.369 \pm 0.027
	1.5	0.259 \pm 0.015	0.265 \pm 0.007	0.441 \pm 0.021
	2.1	0.253 \pm 0.013	0.251 \pm 0.006	0.398 \pm 0.011
	2.5	0.249 \pm 0.010	0.260 \pm 0.005	0.385 \pm 0.010
15	0.5	0.267 \pm 0.015	0.248 \pm 0.011	0.408 \pm 0.006
	1.0	0.259 \pm 0.006	0.245 \pm 0.009	0.418 \pm 0.011
	1.5	0.252 \pm 0.006	0.245 \pm 0.009	0.431 \pm 0.023
	2.1	0.245 \pm 0.010	0.244 \pm 0.013	0.405 \pm 0.020
	2.5	0.242 \pm 0.014	0.238 \pm 0.006	0.332 \pm 0.005
17.5	0.5	0.253 \pm 0.011	0.263 \pm 0.016	0.476 \pm 0.028
	1.0	0.268 \pm 0.005	0.266 \pm 0.007	0.501 \pm 0.025
	1.5	0.255 \pm 0.019	0.252 \pm 0.005	0.469 \pm 0.016
	2.1	0.255 \pm 0.012	0.252 \pm 0.006	0.509 \pm 0.039
	2.5	0.235 \pm 0.007	0.251 \pm 0.013	0.497 \pm 0.011
20	0.5	0.303 \pm 0.010	0.284 \pm 0.008	0.501 \pm 0.013
	1.0	0.268 \pm 0.012	0.269 \pm 0.012	0.479 \pm 0.012
	1.5	0.265 \pm 0.018	0.260 \pm 0.010	0.494 \pm 0.013
	2.1	0.254 \pm 0.023	0.254 \pm 0.009	0.577 \pm 0.001
	2.5	0.253 \pm 0.009	0.256 \pm 0.019	0.554 \pm 0.023

Table 16.21. Mean values (\pm St. Dev.) of the friction coefficient μ of oat grain variety Borowiak at the moisture content of 10-20% against stainless steel, galvanized steel and concrete B30 determined at the normal pressure of 0.5-2.5 kPa

Moisture content (%)	Normal stress (kPa)	Coefficient of friction μ		
		Stainless steel	Galvanized steel	Concrete B30
10	0.5	0.268 \pm 0.004	0.271 \pm 0.010	0.359 \pm 0.015
	1.0	0.260 \pm 0.006	0.253 \pm 0.001	0.359 \pm 0.003
	1.5	0.246 \pm 0.006	0.255 \pm 0.007	0.356 \pm 0.002
	2.1	0.237 \pm 0.004	0.246 \pm 0.007	0.380 \pm 0.021
	2.5	0.237 \pm 0.006	0.237 \pm 0.006	0.353 \pm 0.039
12.5	0.5	0.257 \pm 0.001	0.262 \pm 0.003	0.404 \pm 0.001
	1.0	0.251 \pm 0.001	0.260 \pm 0.002	0.404 \pm 0.001
	1.5	0.247 \pm 0.011	0.247 \pm 0.001	0.369 \pm 0.001
	2.1	0.252 \pm 0.008	0.241 \pm 0.001	0.347 \pm 0.001
	2.5	0.245 \pm 0.005	0.236 \pm 0.006	0.372 \pm 0.006
15	0.5	0.264 \pm 0.009	0.260 \pm 0.005	0.335 \pm 0.005
	1.0	0.259 \pm 0.005	0.253 \pm 0.004	0.335 \pm 0.011
	1.5	0.250 \pm 0.006	0.241 \pm 0.007	0.344 \pm 0.005
	2.1	0.250 \pm 0.009	0.235 \pm 0.002	0.314 \pm 0.005
	2.5	0.235 \pm 0.003	0.231 \pm 0.006	0.296 \pm 0.005
17.5	0.5	0.267 \pm 0.002	0.265 \pm 0.004	0.357 \pm 0.009
	1.0	0.262 \pm 0.004	0.262 \pm 0.006	0.369 \pm 0.005
	1.5	0.243 \pm 0.010	0.246 \pm 0.004	0.372 \pm 0.005
	2.1	0.240 \pm 0.009	0.239 \pm 0.005	0.350 \pm 0.005
	2.5	0.235 \pm 0.014	0.230 \pm 0.010	0.357 \pm 0.016
20	0.5	0.276 \pm 0.004	0.269 \pm 0.002	0.388 \pm 0.011
	1.0	0.251 \pm 0.006	0.247 \pm 0.008	0.376 \pm 0.010
	1.5	0.235 \pm 0.004	0.242 \pm 0.004	0.392 \pm 0.015
	2.1	0.244 \pm 0.005	0.234 \pm 0.005	0.428 \pm 0.006
	2.5	0.233 \pm 0.005	0.229 \pm 0.006	0.434 \pm 0.001

Table 16.22. Mean values (\pm St. Dev.) of the friction coefficient μ of triticale grain variety Fidelio at the moisture content of 10-20% against stainless steel, galvanized steel and concrete B30 determined at the normal pressure of 0.5-2.5 kPa

Moisture content (%)	Normal stress (kPa)	Coefficient of friction μ		
		Stainless steel	Galvanized steel	Concrete B30
10	0.5	0.252 \pm 0.005	0.216 \pm 0.008	0.354 \pm 0.005
	1.0	0.261 \pm 0.005	0.224 \pm 0.001	0.317 \pm 0.010
	1.5	0.273 \pm 0.005	0.219 \pm 0.005	0.369 \pm 0.020
	2.1	0.281 \pm 0.005	0.210 \pm 0.005	0.366 \pm 0.025
	2.5	0.278 \pm 0.005	0.213 \pm 0.005	0.325 \pm 0.029
12.5	0.5	0.255 \pm 0.005	0.227 \pm 0.005	0.387 \pm 0.003
	1.0	0.258 \pm 0.009	0.230 \pm 0.005	0.385 \pm 0.026
	1.5	0.252 \pm 0.005	0.213 \pm 0.005	0.388 \pm 0.011
	2.1	0.252 \pm 0.005	0.221 \pm 0.005	0.373 \pm 0.028
	2.5	0.238 \pm 0.005	0.219 \pm 0.010	0.382 \pm 0.006
15	0.5	0.293 \pm 0.009	0.243 \pm 0.004	0.428 \pm 0.015
	1.0	0.311 \pm 0.001	0.230 \pm 0.005	0.385 \pm 0.019
	1.5	0.314 \pm 0.005	0.238 \pm 0.005	0.428 \pm 0.015
	2.1	0.308 \pm 0.005	0.238 \pm 0.005	0.434 \pm 0.010
	2.5	0.293 \pm 0.009	0.247 \pm 0.005	0.408 \pm 0.006
17.5	0.5	0.388 \pm 0.006	0.311 \pm 0.000	0.472 \pm 0.012
	1.0	0.361 \pm 0.012	0.314 \pm 0.005	0.472 \pm 0.012
	1.5	0.344 \pm 0.005	0.320 \pm 0.009	0.435 \pm 0.017
	2.1	0.360 \pm 0.005	0.329 \pm 0.001	0.455 \pm 0.010
	2.5	0.369 \pm 0.005	0.317 \pm 0.010	0.445 \pm 0.010
20	0.5	0.445 \pm 0.020	0.411 \pm 0.006	0.525 \pm 0.006
	1.0	0.458 \pm 0.016	0.392 \pm 0.006	0.527 \pm 0.006
	1.5	0.487 \pm 0.001	0.418 \pm 0.006	0.519 \pm 0.011
	2.1	0.472 \pm 0.012	0.401 \pm 0.006	0.479 \pm 0.006
	2.5	0.451 \pm 0.006	0.395 \pm 0.001	0.472 \pm 0.006

Table 16.23. Mean values (\pm St. Dev.) of the friction coefficient μ of rape seeds variety Licosmos at the moisture content of 6-15% against stainless steel, galvanized steel and concrete B30 determined at the normal pressure of 0.5-2.5 kPa

Moisture content (%)	Normal stress (kPa)	Coefficient of friction μ		
		Stainless steel	Galvanized steel	Concrete B30
6	0.5	0.279 \pm 0.007	0.245 \pm 0.008	0.351 \pm 0.023
	1.0	0.234 \pm 0.006	0.242 \pm 0.006	0.336 \pm 0.018
	1.5	0.237 \pm 0.007	0.231 \pm 0.012	0.294 \pm 0.002
	2.1	0.240 \pm 0.006	0.232 \pm 0.005	0.276 \pm 0.017
	2.5	0.237 \pm 0.008	0.220 \pm 0.007	0.289 \pm 0.004
9	0.5	0.279 \pm 0.007	0.245 \pm 0.010	0.357 \pm 0.040
	1.0	0.275 \pm 0.007	0.237 \pm 0.011	0.314 \pm 0.014
	1.5	0.270 \pm 0.002	0.227 \pm 0.004	0.335 \pm 0.028
	2.1	0.267 \pm 0.012	0.223 \pm 0.005	0.302 \pm 0.009
	2.5	0.254 \pm 0.002	0.211 \pm 0.021	0.302 \pm 0.009
12	0.5	0.300 \pm 0.018	0.240 \pm 0.007	0.308 \pm 0.005
	1.0	0.301 \pm 0.019	0.243 \pm 0.004	0.332 \pm 0.005
	1.5	0.289 \pm 0.021	0.239 \pm 0.009	0.335 \pm 0.005
	2.1	0.287 \pm 0.015	0.228 \pm 0.005	0.308 \pm 0.005
	2.5	0.298 \pm 0.004	0.217 \pm 0.002	0.335 \pm 0.005
15	0.5	0.292 \pm 0.010	0.240 \pm 0.006	0.332 \pm 0.005
	1.0	0.278 \pm 0.012	0.235 \pm 0.014	0.314 \pm 0.005
	1.5	0.271 \pm 0.017	0.237 \pm 0.008	0.317 \pm 0.005
	2.1	0.264 \pm 0.008	0.228 \pm 0.008	0.317 \pm 0.005
	2.5	0.274 \pm 0.011	0.215 \pm 0.003	0.335 \pm 0.011

Table 16.24. Mean values (\pm St. Dev.) of the friction coefficient μ of selected seeds at the storage moisture content against stainless steel, galvanized steel and concrete B30 determined at the normal pressure of 0.5-2.5 kPa

Material, moisture content (%)	Normal stress (kPa)	Coefficient of friction μ		
		Stainless steel	Galvanized steel	Concrete B30
Amaranth Rawa	0.5	0.271 \pm 0.006	0.271 \pm 0.005	0.411 \pm 0.006
	1.0	0.262 \pm 0.002	0.243 \pm 0.005	0.350 \pm 0.011
	1.5	0.242 \pm 0.003	0.224 \pm 0.006	0.379 \pm 0.006
	2.1	0.237 \pm 0.013	0.224 \pm 0.005	0.287 \pm 0.020
	2.5	0.224 \pm 0.004	0.226 \pm 0.003	0.252 \pm 0.010
White mustard Borowska	0.5	0.252 \pm 0.003	0.257 \pm 0.004	0.372 \pm 0.005
	1.0	0.244 \pm 0.006	0.241 \pm 0.003	0.401 \pm 0.015
	1.5	0.237 \pm 0.010	0.239 \pm 0.005	0.354 \pm 0.011
	2.1	0.225 \pm 0.010	0.230 \pm 0.006	0.345 \pm 0.030
	2.5	0.228 \pm 0.007	0.225 \pm 0.003	0.357 \pm 0.009
Pea Piast	0.5	0.257 \pm 0.007	0.258 \pm 0.007	0.428 \pm 0.012
	1.0	0.251 \pm 0.003	0.246 \pm 0.006	0.428 \pm 0.015
	1.5	0.236 \pm 0.001	0.240 \pm 0.004	0.434 \pm 0.001
	2.1	0.232 \pm 0.003	0.236 \pm 0.005	0.376 \pm 0.010
	2.5	0.229 \pm 0.006	0.236 \pm 0.007	0.360 \pm 0.011
Buckwheat Kora	0.5	0.231 \pm 0.005	0.245 \pm 0.006	0.369 \pm 0.020
	1.0	0.225 \pm 0.005	0.232 \pm 0.002	0.366 \pm 0.019
	1.5	0.217 \pm 0.003	0.228 \pm 0.005	0.363 \pm 0.014
	2.1	0.226 \pm 0.002	0.222 \pm 0.005	0.329 \pm 0.018
	2.5	0.220 \pm 0.004	0.227 \pm 0.006	0.338 \pm 0.009
Lentils Tina	0.5	0.252 \pm 0.005	0.278 \pm 0.005	0.273 \pm 0.005
	1.0	0.241 \pm 0.001	0.267 \pm 0.001	0.299 \pm 0.005
	1.5	0.247 \pm 0.005	0.281 \pm 0.005	0.302 \pm 0.001
	2.1	0.250 \pm 0.001	0.276 \pm 0.001	0.338 \pm 0.009
	2.5	0.250 \pm 0.001	0.276 \pm 0.001	0.344 \pm 0.005
Soybeans Aldana	0.5	0.223 \pm 0.007	0.270 \pm 0.013	0.354 \pm 0.005
	1.0	0.233 \pm 0.008	0.252 \pm 0.010	0.347 \pm 0.016
	1.5	0.230 \pm 0.005	0.241 \pm 0.001	0.354 \pm 0.005
	2.1	0.235 \pm 0.005	0.230 \pm 0.005	0.366 \pm 0.001
	2.5	0.247 \pm 0.005	0.230 \pm 0.005	0.369 \pm 0.005

Table 16.25. Mean values (\pm St. Dev.) of the friction coefficient μ of selected food powders against stainless steel and galvanized steel determined at the normal pressure of 0.5-2.5 kPa

Material, moisture content (%)	Normal stress (kPa)	Coefficient of friction μ	
		Stainless steel	Galvanized steel
1	2	3	4
Flour 12.7	0.5	0.268 \pm 0.009	0.252 \pm 0.005
	1.0	0.237 \pm 0.005	0.222 \pm 0.009
	1.5	0.222 \pm 0.000	0.216 \pm 0.005
	2.1	0.206 \pm 0.005	0.222 \pm 0.000
	2.5	0.197 \pm 0.005	0.206 \pm 0.005
Coarse flour 13.4	0.5	0.194 \pm 0.000	0.197 \pm 0.005
	1.0	0.197 \pm 0.005	0.194 \pm 0.009
	1.5	0.188 \pm 0.005	0.176 \pm 0.000
	2.1	0.185 \pm 0.000	0.179 \pm 0.005
	2.5	0.194 \pm 0.000	0.170 \pm 0.005
Semolina 12.7	0.5	0.259 \pm 0.009	0.293 \pm 0.005
	1.0	0.234 \pm 0.005	0.271 \pm 0.005
	1.5	0.225 \pm 0.005	0.240 \pm 0.009
	2.1	0.222 \pm 0.000	0.219 \pm 0.005
	2.5	0.213 \pm 0.000	0.231 \pm 0.000
Wheat groats 13.6	0.5	0.222 \pm 0.000	0.265 \pm 0.005
	1.0	0.213 \pm 0.009	0.240 \pm 0.000
	1.5	0.222 \pm 0.000	0.237 \pm 0.005
	2.1	0.222 \pm 0.000	0.210 \pm 0.005
	2.5	0.210 \pm 0.005	0.210 \pm 0.005
Pearl barley groats 13.2	0.5	0.222 \pm 0.009	0.284 \pm 0.005
	1.0	0.216 \pm 0.005	0.252 \pm 0.005
	1.5	0.234 \pm 0.005	0.284 \pm 0.011
	2.1	0.213 \pm 0.000	0.262 \pm 0.005
	2.5	0.210 \pm 0.005	0.243 \pm 0.005
Oat meal 11.0	0.5	0.237 \pm 0.005	0.252 \pm 0.005
	1.0	0.203 \pm 0.009	0.234 \pm 0.005
	1.5	0.206 \pm 0.005	0.219 \pm 0.005
	2.1	0.194 \pm 0.000	0.206 \pm 0.005
	2.5	0.197 \pm 0.005	0.200 \pm 0.005

Table 16.25. Cont.

1	2	3	4
	0.5	0.303 ± 0.005	0.364 ± 0.000
Icing sugar	1.0	0.287 ± 0.009	0.322 ± 0.005
	1.5	0.277 ± 0.000	0.325 ± 0.000
0.4	2.1	0.252 ± 0.005	0.338 ± 0.005
	2.5	0.252 ± 0.005	0.348 ± 0.005
	0.5	0.249 ± 0.000	0.284 ± 0.005
Table sugar	1.0	0.252 ± 0.005	0.265 ± 0.005
	1.5	0.249 ± 0.000	0.293 ± 0.005
0.4	2.1	0.240 ± 0.000	0.280 ± 0.011
	2.5	0.225 ± 0.005	0.293 ± 0.005
	0.5	0.284 ± 0.005	0.381 ± 0.005
Potato starch	1.0	0.287 ± 0.016	0.384 ± 0.017
	1.5	0.265 ± 0.005	0.411 ± 0.012
18.2	2.1	0.252 ± 0.005	0.407 ± 0.005
	2.5	0.246 ± 0.005	0.449 ± 0.006
	0.5	0.249 ± 0.009	0.335 ± 0.009
Powder milk	1.0	0.222 ± 0.009	0.303 ± 0.014
	1.5	0.206 ± 0.005	0.296 ± 0.009
4.4	2.1	0.188 ± 0.005	0.287 ± 0.000
	2.5	0.188 ± 0.005	0.290 ± 0.005
	0.5	0.210 ± 0.005	0.265 ± 0.019
Granulated milk	1.0	0.194 ± 0.000	0.228 ± 0.005
	1.5	0.185 ± 0.000	0.216 ± 0.053
7.9	2.1	0.167 ± 0.000	0.200 ± 0.005
	2.5	0.158 ± 0.000	0.185 ± 0.000
	0.5	0.246 ± 0.005	0.280 ± 0.005
Table salt	1.0	0.234 ± 0.005	0.274 ± 0.014
	1.5	0.231 ± 0.000	0.280 ± 0.011
0.2	2.1	0.231 ± 0.000	0.287 ± 0.000
	2.5	0.234 ± 0.005	0.293 ± 0.005
	0.5	0.188 ± 0.005	0.222 ± 0.009
Corn meal	1.0	0.200 ± 0.005	0.222 v0.009
	1.5	0.194 ± 0.009	0.240 ± 0.000
11.7	2.1	0.194 ± 0.000	0.213 ± 0.000
	2.5	0.191 ± 0.005	0.216 ± 0.005
	0.5	0.213 ± 0.000	0.213 ± 0.000
Soybean meal	1.0	0.194 ± 0.000	0.194 ± 0.000
	1.5	0.182 ± 0.005	0.182 ± 0.005
8.5	2.1	0.158 ± 0.000	0.158 ± 0.000
	2.5	0.161 ± 0.005	0.161 ± 0.005

16.5. Angle of internal friction, cohesion, flow index, and angle of repose

Table 16.26. Mean values (\pm St. Dev.) of the angle of internal friction φ , the cohesion c and the angle of natural repose Φ of cereal grain at the moisture content of 10-20%

Material	Moisture content (%)	Angle of internal friction φ (deg)	Cohesion c (kPa)	Angle of natural repose Φ (deg)
Wheat Begra	10	25.7 \pm 0.3	0.9 \pm 0.5	24.3 \pm 0.5
	12.5	26.2 \pm 0.4	2.8 \pm 0.5	29.0 \pm 0.7
	15	27.0 \pm 0.5	2.1 \pm 0.7	33.3 \pm 0.6
	17.5	33.0 \pm 1.0	5.1 \pm 0.5	37.6 \pm 0.5
	20	35.5 \pm 0.5	2.3 \pm 0.9	35.4 \pm 0.4
Rye Amilo	10	23.0 \pm 1.0	6.2 \pm 1.4	29.0 \pm 0.6
	12.5	24.4 \pm 1.1	6.6 \pm 1.5	27.1 \pm 0.5
	15	25.1 \pm 0.5	4.7 \pm 0.7	31.4 \pm 0.2
	17.5	28.4 \pm 1.2	3.2 \pm 1.4	29.9 \pm 0.3
	20	28.0 \pm 1.0	7.7 \pm 1.4	30.3 \pm 0.2
Barley Rudnik	10	27.8 \pm 0.4	3.6 \pm 0.6	26.8 \pm 0.7
	12.5	28.5 \pm 0.5	4.7 \pm 0.8	28.9 \pm 0.7
	15	31.2 \pm 0.3	3.9 \pm 0.4	29.5 \pm 0.7
	17.5	30.6 \pm 1.0	2.9 \pm 0.5	30.5 \pm 0.8
	20	33.2 \pm 0.5	5.5 \pm 0.7	32.1 \pm 0.8
Corn Mieszko	10	26.7 \pm 0.6	3.4 \pm 0.9	23.5 \pm 0.4
	12.5	31.7 \pm 0.5	6.1 \pm 0.9	33.8 \pm 0.2
	15	32.0 \pm 1.4	5.6 \pm 1.8	30.6 \pm 0.3
	17.5	33.4 \pm 0.8	5.9 \pm 1.1	34.2 \pm 0.5
	20	33.6 \pm 1.5	8.8 \pm 1.6	31.9 \pm 0.6
Oats Borowiak	10	22.1 \pm 1.1	0.4 \pm 1.4	28.4 \pm 0.4
	12.5	22.4 \pm 0.9	1.1 \pm 1.3	28.7 \pm 1.0
	15	24.0 \pm 0.5	2.2 \pm 0.6	31.3 \pm 0.5
	17.5	23.9 \pm 1.0	4.0 \pm 1.1	32.8 \pm 0.5
	20	26.4 \pm 1.7	6.5 \pm 2.0	34.7 \pm 0.4
Triticale Fidelio	10	23.6 \pm 0.7	5.7 \pm 1.0	29.9 \pm 0.4
	12.5	23.0 \pm 1.2	9.4 \pm 1.6	28.4 \pm 0.2
	15	25.3 \pm 1.1	12.1 \pm 1.3	30.5 \pm 0.1
	17.5	28.8 \pm 1.2	10.7 \pm 1.5	35.4 \pm 0.2
	20	28.4 \pm 1.2	11.1 \pm 1.8	38.3 \pm 0.2

Table 16.27. Mean values (\pm St. Dev.) of the angle of internal friction φ , the cohesion c and the angle of natural repose Φ of rape seeds variety Licosmos at the moisture content of 6-16%

Material	Moisture content (%)	Angle of internal friction φ (deg)	Cohesion c (kPa)	Angle of natural repose Φ (deg)
Rape seeds Licosmos	6	24.7 \pm 0.5	1.3 \pm 0.7	25.3 \pm 0.8
	9	30.6 \pm 0.4	2.1 \pm 0.5	23.2 \pm 0.9
	12	31.7 \pm 0.7	7.5 \pm 0.9	25.5 \pm 0.9
	14	34.8 \pm 0.7	7.7 \pm 0.9	24.5 \pm 0.9
	16	33.2 \pm 0.9	12.5 \pm 1.2	29.1 \pm 0.7

Table 16.28. Mean values (\pm St. Dev.) of the angle of internal friction φ , the cohesion c and the angle of natural repose Φ of selected seeds

Material	Moisture content (%)	Angle of internal friction φ (deg)	Cohesion c (kPa)	Angle of natural repose Φ (deg)
Amaranth. Rawa	8	21.3 \pm 0.8	2.0 \pm 0.5	26.2 \pm 0.5
White mustard . Borowska	9	24.7 \pm 0.4	2.2 \pm 0.9	25.6 \pm 0.5
Pea. Piast	10	27.3 \pm 0.6	1.6 \pm 0.4	21.5 \pm 0.6
Buckwheat. Kora	10	22.0 \pm 0.8	1.6 \pm 0.7	28.2 \pm 0.5
Lentils.Tina	8	14.3 \pm 0.4	2.1 \pm 0.6	24.6 \pm 0.7
Soybeans. Aldana	8	30.1 \pm 0.9	1.8 \pm 1.0	32.5 \pm 0.5

Table 16.29. Mean values (\pm St. Dev.) of the effective angle of internal friction δ , the angle of internal friction φ , the cohesion c , the flow index i and the angle of natural repose Φ of selected food powders determined at the consolidation pressure of 30-100 kPa

Material, moisture content (%)	Consolidation stress (kPa)	Effective angle of internal friction δ (deg)	Angle of internal friction φ (deg)	Cohesion c (kPa)	Flow index i	Angle of natural repose Φ (deg)
1	2	3	4	5	6	7
Flour 450 12.7	30	30.4 \pm 2.7	26.5 \pm 1.0	2.7 \pm 0.4	0.15	44.4 \pm 0.7
	60	30.7 \pm 1.4	29.0 \pm 0.5	2.3 \pm 0.4	0.07	
	80	31.8 \pm 2.8	30.8 \pm 1.0	1.8 \pm 1.1	0.04	
	100	31.0 \pm 5.0	30.4 \pm 1.8	1.3 \pm 2.5	0.02	
Coarse flour 13.4	30	28.3 \pm 2.4	25.9 \pm 0.9	1.5 \pm 0.4	0.09	40.0 \pm 0.7
	60	27.6 \pm 1.8	26.1 \pm 0.7	2.0 \pm 0.6	0.06	
	80	27.9 \pm 1.5	27.1 \pm 0.6	1.5 \pm 0.6	0.03	
	100	26.8 \pm 2.1	25.5 \pm 0.8	2.8 \pm 1.2	0.05	
Semolina 12.7	30	34.1 \pm 4.4	31.3 \pm 1.1	2.0 \pm 1.1	0.10	33.0 \pm 1.6
	60	33.0 \pm 3.0	32.0 \pm 0.7	1.5 \pm 0.9	0.04	
	80	33.9 \pm 1.7	33.7 \pm 0.1	0.6 \pm 0.7	0.01	
	100	33.3 \pm 3.5	32.8 \pm 0.8	1.3 \pm 1.7	0.02	
Wheat groats 13.6	30	28.9 \pm 2.1	25.8 \pm 0.6	1.9 \pm 0.3	0.11	33.4 \pm 1.3
	60	30.9 \pm 3.2	29.9 \pm 1.1	1.3 \pm 0.4	0.04	
	80	29.8 \pm 2.6	27.6 \pm 0.8	3.9 \pm 1.1	0.08	
	100	30.2 \pm 0.7	27.8 \pm 0.2	5.2 \pm 0.4	0.08	
Pearl barley groats 13.2	30	33.3 \pm 3.8	33.0 \pm 1.3	0.2 \pm 0.5	0.01	32.1 \pm 1.4
	60	33.4 \pm 2.2	31.0 \pm 0.7	3.3 \pm 0.6	0.09	
	80	29.7 \pm 3.1	26.6 \pm 1.1	5.9 \pm 1.4	0.11	
	100	31.5 \pm 3.3	29.0 \pm 1.7	10.5 \pm 0.5	0.10	
Oat meal 11.0	30	22.0 \pm 3.5	20.8 \pm 1.0	0.7 \pm 0.6	0.04	35.2 \pm 1.1
	60	19.4 \pm 2.2	18.8 \pm 1.2	0.7 \pm 0.3	0.02	
	80	21.5 \pm 2.3	19.8 \pm 0.9	2.7 \pm 1.1	0.06	
	100	21.4 \pm 2.5	19.2 \pm 0.9	2.8 \pm 1.5	0.05	
Icing sugar 0.4	30	34.2 \pm 3.6	31.0 \pm 0.7	5.4 \pm 0.5	0.12	48.7 \pm 0.7
	60	34.1 \pm 3.2	32.5 \pm 0.8	5.3 \pm 0.9	0.06	
	80	32.5 \pm 3.9	28.7 \pm 2.6	7.0 \pm 3.2	0.14	
	100	36.9 \pm 2.5	34.6 \pm 0.6	6.2 \pm 1.6	0.09	

Table 16.29. Cont.

1	2	3	4	5	6	7
Table sugar 0.4	30	33.1 ± 7.5	27.8 ± 2.1	3.6 ± 1.1	0.09	25.9 ± 0.9
	60	34.0 ± 7.9	31.5 ± 1.9	3.6 ± 2.3	0.09	
	80	34.6 ± 6.9	33.1 ± 1.9	3.2 ± 1.4	0.06	
	100	34.7 ± 3.7	33.2 ± 6.0	3.9 ± 1.2	0.06	
Potato starch 18.2	30	39.8 ± 2	39.3 ± 0.7	0.4 ± 0.3	0.02	49.5 ± 0.8
	60	39.4 ± 4	37.5 ± 1.5	2.3 ± 1.2	0.07	
	80	37.5 ± 3	35.2 ± 1.0	5.5 ± 1.1	0.10	
	100	35.0 ± 2	35.8 ± 0.8	4.9 ± 1.1	0.08	
Powder milk 4.4	30	35.5 ± 3	34.2 ± 1.1	0.7 ± 0.5	0.05	41.1 ± 0.8
	60	35.8 ± 6	34.6 ± 3.4	1.6 ± 0.3	0.06	
	80	35.8 ± 1	32.6 ± 0.2	6.2 ± 0.3	0.12	
	100	37.6 ± 4	35.7 ± 1.4	4.9 ± 1.9	0.11	
Granulated milk 7.9	30	40.8 ± 4.5	37.8 ± 1.5	2.2 ± 0.4	0.11	36.2 ± 1.0
	60	38.0 ± 2.2	32.7 ± 0.6	7.4 ± 0.6	0.20	
	80	37.2 ± 6.7	31.5 ± 2.2	11.9 ± 2.5	0.21	
	100	35.0 ± 3	30.8 ± 0.6	10.0 ± 0.9	0.16	
Table salt 0.2	30	34.4 ± 7.1	33.0 ± 1.7	0.9 ± 0.3	0.05	27.4 ± 0.6
	60	32.9 ± 3.5	31.9 ± 0.9	1.5 ± 1.0	0.04	
	80	35.0 ± 3.5	33.9 ± 0.9	2.2 ± 1.4	0.04	
	100	33.3 ± 3.2	32.6 ± 0.8	1.6 ± 1.5	0.03	
Corn meal 11.7	30	33.6 ± 3.9	27.7 ± 1.9	4.1 ± 1.0	0.10	30.6 ± 1.0
	60	31.8 ± 8.8	29.9 ± 2.3	2.6 ± 2.5	0.07	
	80	33.3 ± 3.2	32.1 ± 0.8	2.3 ± 1.2	0.04	
	100	33.4 ± 0.7	31.2 ± 0.3	5.3 ± 0.7	0.08	
Soybean meal 8.5	30	36.6 ± 2.8	32.4 ± 0.6	2.9 ± 0.4	0.15	41.7 ± 0.7
	60	33.9 ± 4.4	31.6 ± 1.1	3.4 ± 1.2	0.09	
	80	34.8 ± 3.8	33.7 ± 0.9	2.2 ± 1.4	0.04	
	100	33.8 ± 1.4	31.3 ± 0.4	6.2 ± 0.7	0.10	

16.6. Pressure ratio

Table 16.30. Mean values (\pm St. Dev.) of the pressure ratio k_s and k_φ and the angle of internal friction φ of cereal grain at the moisture content of 10-20%

Material	Moisture content (%)	k_s	$k_\varphi = 1.1(1-\sin\varphi)$	Angle of internal friction φ (deg)
Wheat Begra	10	0.44 ± 0.02	0.62 ± 0.01	25.7 ± 0.3
	12.5	0.38 ± 0.01	0.61 ± 0.01	26.2 ± 0.4
	15	0.34 ± 0.02	0.60 ± 0.01	27.0 ± 0.5
	17.5	0.31 ± 0.02	0.50 ± 0.02	33.0 ± 1.0
	20	0.35 ± 0.01	0.46 ± 0.01	35.5 ± 0.5
Rye Amilo	10	0.52 ± 0.01	0.67 ± 0.02	23.0 ± 1.0
	12.5	0.51 ± 0.04	0.64 ± 0.02	24.4 ± 1.1
	15	0.47 ± 0.06	0.63 ± 0.02	25.1 ± 0.5
	17.5	0.37 ± 0.04	0.58 ± 0.02	28.4 ± 1.2
	20	0.32 ± 0.05	0.58 ± 0.02	28.0 ± 1.0
Barley Rudnik	10	0.45 ± 0.02	0.59 ± 0.01	27.8 ± 0.4
	12.5	0.47 ± 0.03	0.57 ± 0.01	28.5 ± 0.5
	15	0.43 ± 0.02	0.53 ± 0.01	31.2 ± 0.3
	17.5	0.45 ± 0.03	0.54 ± 0.02	30.6 ± 1.0
	20	0.39 ± 0.03	0.50 ± 0.01	33.2 ± 0.5
Corn Mieszko	10	0.48 ± 0.04	0.60 ± 0.01	26.7 ± 0.6
	12.5	0.40 ± 0.03	0.52 ± 0.01	31.7 ± 0.5
	15	0.36 ± 0.05	0.51 ± 0.02	32.0 ± 1.4
	17.5	0.34 ± 0.03	0.50 ± 0.02	33.4 ± 0.8
	20	0.30 ± 0.05	0.49 ± 0.03	33.6 ± 1.5
Oats Borowiak	10	0.49 ± 0.03	0.68 ± 0.02	22.1 ± 1.1
	12.5	0.44 ± 0.04	0.68 ± 0.02	22.4 ± 0.9
	15	0.45 ± 0.03	0.65 ± 0.01	24.0 ± 0.5
	17.5	0.40 ± 0.03	0.65 ± 0.02	23.9 ± 1.0
	20	0.41 ± 0.06	0.61 ± 0.03	26.4 ± 1.7
Triticale Fidelio	10	0.49 ± 0.03	0.66 ± 0.02	23.6 ± 0.7
	12.5	0.51 ± 0.03	0.67 ± 0.02	23.0 ± 1.2
	15	0.52 ± 0.04	0.63 ± 0.02	25.3 ± 1.1
	17.5	0.39 ± 0.03	0.57 ± 0.02	28.8 ± 1.2
	20	0.38 ± 0.06	0.58 ± 0.02	28.4 ± 1.2

Table 16.31. Mean values (\pm St. Dev.) of the pressure ratio k_s and k_φ and the angle of internal friction φ of rape seeds variety Licosmos at the moisture content of 6-15%

Material	Moisture content (%)	k_s	$k_\varphi = 1.1(1 - \sin\varphi)$	Angle of int. friction φ (deg)
Rape seeds	6	0.46 ± 0.02	0.64 ± 0.02	24.7 ± 0.5
	9	0.28 ± 0.04	0.54 ± 0.01	30.6 ± 0.4
Licosmos	12	0.27 ± 0.02	0.52 ± 0.01	31.7 ± 0.7
	15	0.24 ± 0.02	0.47 ± 0.01	34.8 ± 0.7

Table 16.32. Mean values (\pm St. Dev.) of the pressure ratio k_s and k_φ and the angle of internal friction φ of selected seeds

Material	Moisture content (%)	k_s	$k_\varphi = 1.1(1 - \sin\varphi)$	Angle of int. friction φ (deg)
Amaranth. Rawa	8	0.62 ± 0.02	0.70 ± 0.02	21.3 ± 0.8
White mustard.				
Borowska	9	0.43 ± 0.01	0.64 ± 0.01	24.7 ± 0.4
Pea. Piast	10	0.53 ± 0.01	0.59 ± 0.01	27.3 ± 0.6
Buckwheat. Kora	10	0.59 ± 0.02	0.68 ± 0.02	22.0 ± 0.8
Lentils. Tina	8	0.56 ± 0.01	0.82 ± 0.02	14.3 ± 0.4
Soybeans. Aldana	8	0.37 ± 0.02	0.55 ± 0.01	30.1 ± 0.9

Table 16.33. Mean values (\pm St. Dev.) of the pressure ratio k_s and k_φ and the angle of internal friction φ of selected food powders

Material	Moisture content (%)	k_s	$k_\varphi = 1.1(1 - \sin\varphi)$	Angle of int. friction φ (deg)
Flour	12.7	0.26 ± 0.01	0.56 ± 0.02	29.2 ± 1.0
Coarse flour	13.4	0.37 ± 0.02	0.62 ± 0.02	26.1 ± 0.8
Semolina	12.7	0.38 ± 0.02	0.51 ± 0.02	32.4 ± 1.0
Wheat groats	13.6	0.37 ± 0.02	0.59 ± 0.02	27.8 ± 1.0
Pearl barley groats	13.2	0.36 ± 0.02	0.55 ± 0.02	30.0 ± 1.0
Oat meal	11.0	0.40 ± 0.01	0.72 ± 0.02	20.0 ± 1.0
Icing sugar	0.4	0.31 ± 0.02	0.52 ± 0.02	31.7 ± 1.0
Table sugar	0.4	0.47 ± 0.02	0.53 ± 0.04	31.4 ± 2.0
Potato starch	18.2	0.47 ± 0.02	0.44 ± 0.02	37.0 ± 1.0
Powder milk	4.4	0.40 ± 0.02	0.48 ± 0.03	34.3 ± 1.5
Granulated milk	7.9	0.34 ± 0.02	0.50 ± 0.03	33.2 ± 1.5
Table salt	0.2	0.31 ± 0.01	0.50 ± 0.03	32.8 ± 1.5
Corn meal	11.7	0.45 ± 0.02	0.55 ± 0.02	30.2 ± 1.1
Soybean meal	8.5	0.53 ± 0.02	0.51 ± 0.03	32.2 ± 1.6

16.7. Modulus of elasticity and Poisson's ratio

Table 16.34. Mean values (\pm St. Dev.) of the elasticity modulus E and the Poisson's ratio ν of cereal grain at the moisture content of 10-20%

Material	Moisture content (%)	Modulus of elasticity E (MPa)	Poisson's ratio ν
Wheat Begra	10	22.4 \pm 4.6	0.22 \pm 0.01
	12.5	22.2 \pm 4.4	0.18 \pm 0.02
	15	19.3 \pm 2.5	0.20 \pm 0.03
	17.5	17.2 \pm 3.6	0.20 \pm 0.01
	20	11.1 \pm 1.1	0.19 \pm 0.01
Rye Amilo	10	23.6 \pm 2.3	0.19 \pm 0.01
	12.5	20.9 \pm 1.2	0.20 \pm 0.01
	15	20.2 \pm 1.9	0.21 \pm 0.01
	17.5	20.0 \pm 1.8	0.21 \pm 0.01
	20	15.1 \pm 1.5	0.21 \pm 0.01
Barley Rudnik	10	14.2 \pm 1.6	0.19 \pm 0.01
	12.5	14.0 \pm 1.8	0.16 \pm 0.01
	15	13.8 \pm 1.1	0.15 \pm 0.01
	17.5	12.3 \pm 0.8	0.17 \pm 0.01
	20	10.4 \pm 2.4	0.19 \pm 0.01
Corn Mieszko	10	26.2 \pm 3.2	0.20 \pm 0.01
	12.5	19.3 \pm 2.7	0.20 \pm 0.01
	15	15.9 \pm 0.9	0.20 \pm 0.02
	17.5	15.5 \pm 2.6	0.19 \pm 0.02
	20	12.3 \pm 1.4	0.20 \pm 0.02
Oats Borowiak	10	17.8 \pm 2.8	0.18 \pm 0.01
	12.5	16.0 \pm 3.2	0.20 \pm 0.01
	15	13.2 \pm 3.1	0.17 \pm 0.01
	17.5	10.7 \pm 2.4	0.17 \pm 0.01
	20	10.4 \pm 1.9	0.15 \pm 0.01
Triticale Fidelio	10	20.4 \pm 2.6	0.20 \pm 0.02
	12.5	18.5 \pm 1.6	0.22 \pm 0.01
	15	18.4 \pm 1.4	0.20 \pm 0.01
	17.5	14.7 \pm 1.8	0.21 \pm 0.03
	20	9.2 \pm 0.9	0.21 \pm 0.01

Table 16.35. Mean values (\pm St. Dev.) of the elasticity modulus E and the Poisson's ratio ν of rape seeds variety Licosmos at the moisture content of 6-16%

Material	Moisture content (%)	Modulus of elasticity E (MPa)	Poisson's ratio ν
Rape seeds Licosmos	6	9.0 ± 0.6	0.24 ± 0.03
	9	8.7 ± 0.8	0.17 ± 0.02
	12	7.1 ± 0.6	0.16 ± 0.01
	16	6.6 ± 0.9	0.10 ± 0.01

Table 16.36. Mean values (\pm St. Dev.) of the elasticity modulus E and the Poisson's ratio ν of selected seeds

Material	Moisture content (%)	Modulus of elasticity E (MPa)	Poisson's ratio ν
Amaranth. Rawa	8	30.8 ± 1.8	0.27 ± 0.02
White mustard. Borowska	9	13.1 ± 0.5	0.24 ± 0.01
Pea. Piast	10	16.8 ± 2.1	0.26 ± 0.03
Buckwheat. Kora	10	20.6 ± 2.3	0.20 ± 0.02
Lentils.Tina	8	16.3 ± 0.7	0.24 ± 0.01
Soybeans. Aldana	8	32.6 ± 1.4	0.15 ± 0.02

Table 16.37. Mean values (\pm St. Dev.) of the elasticity modulus E and the Poisson's ratio ν of selected food powders

Material	Moisture content (%)	Modulus of elasticity E (MPa)	Poisson's ratio ν
Flour	12.7	18.5 ± 0.7	0.16 ± 0.01
Coarse flour	13.4	16.5 ± 1.5	0.19 ± 0.02
Semolina	12.7	15.3 ± 0.5	0.20 ± 0.01
Wheat groats	13.6	18.9 ± 0.5	0.21 ± 0.01
Pearl barley groats	13.2	14.9 ± 1.2	0.23 ± 0.03
Oat meal	11.0	7.7 ± 1.2	0.23 ± 0.01
Icing sugar	0.4	28.2 ± 4.8	0.20 ± 0.01
Table sugar	0.4	30.8 ± 1.6	0.21 ± 0.01
Potato starch	18.2	21.7 ± 1.3	0.24 ± 0.01
Powder milk	4.4	22.1 ± 1.1	0.18 ± 0.01
Granulated milk	7.9	18.4 ± 0.8	0.17 ± 0.01
Table salt	0.2	31.9 ± 2.3	0.23 ± 0.04
Corn meal	11.7	12.1 ± 1.1	0.21 ± 0.01
Soybean meal	8.5	10.0 ± 2.1	0.26 ± 0.02

Address of Authors

Marek Molenda

Józef Horabik

Institute of Agrophysics, Polish Academy of Sciences

ul. Doświadczalna 4, 20-290 Lublin, Poland

tel. +48 81 7445061 fax +48 81 7445067

e-mail: m.molenda@demeter.ipan.lublin.pl